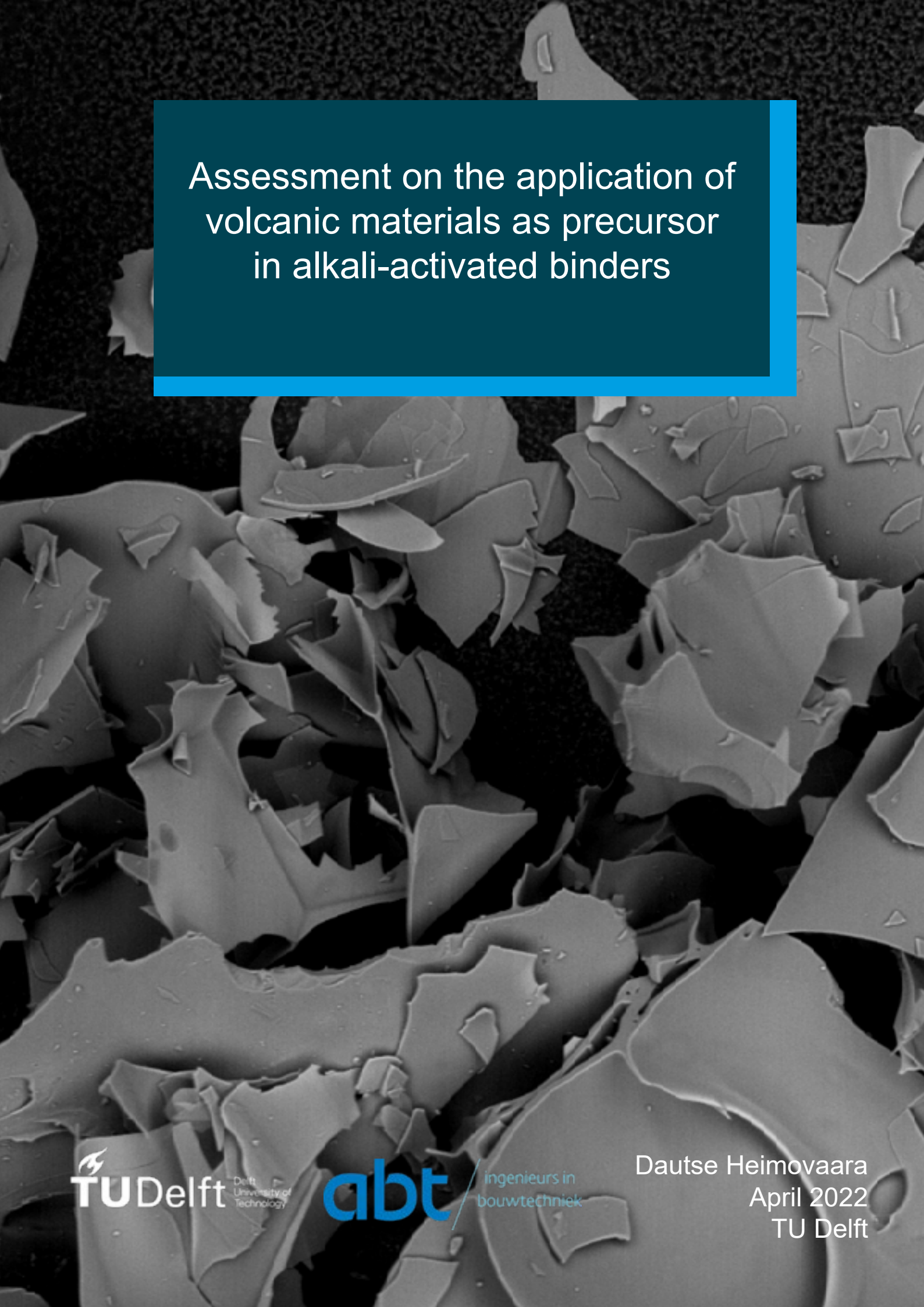

Assessment on the application of volcanic materials as precursor in alkali-activated binders

Dautse Heimovaara
April 2022
TU Delft

Assessment on the application of volcanic materials in alkali-activated binders

by

D. Heimovaara

to obtain the degree of Master of Science in Structural Engineering
at the Delft University of Technology,
Faculty CiTG - Department materials and environment,
to be defended publicly on Wednesday April 6, 2022 at 10:00 AM.

Student number:	4367847	
Thesis committee:	Dr. G. Ye,	TU Delft, chair
	L. Miranda de Lima Junior,	TU Delft
	Dr. ir. G. Meesters,	TU Delft
	Ir. J. Bovend'eerdt,	ABT

An electronic version of this thesis is available at `http://repository.tudelft.nl/`.

TU Delft

Preface

Dear reader,

In front of you is my thesis, which ends my study time at TU Delft. Since I started this time with a bachelor's degree in architecture, the topic of concrete technology has been an unexpected one, but no less fun for that. During my studies, I covered all scales of the built environment and that is ultimately what I like about concrete: its multi-scale character.

This thesis would not have been possible without a number of people. First, the technicians who helped me with testing and consultations when things got a little more complicated. John, Arjan, Maiko and Ton: thanks for all the help. Ruud from the X-ray department, thank you for always providing all the results quickly.

Then thanks to my supervisors. Gabrie Meesters for the useful input during our meetings and the sharp look at everything that has to do with grain size. Joop van Bovend'eerdt for our weekly meetings, in which I sometimes had to be asked about my schedule, but in which I was mainly encouraged to look at the bigger picture. Guang Ye for the expertise brought in during our meetings, which helped me understand the subject even better. Luiz Miranda de Lima for all the time you put in, for the coffee and appelflappen when I was feeling down and for the fun days in the lab. Without you, this thesis would not have been half as good.

Thanks to my parents for all the expert input, to my sisters for hearing my stories, to my friends and roommates for all the coffee rounds and walks, and to Timo for the endless support.

D. Heimovaara
Delft, April 2022

Abstract

In 2016 the Paris agreement was adopted by 196 parties. The main goal of this agreement is to obtain a climate-neutral world in 2050. The CO_2 emissions should decrease as soon as possible to achieve this goal. Concrete is the world's most used building material, and with good reason, it provides cheap, solid and reliable products used for over 200 years. However, concrete is responsible for 5-10 % of the yearly CO_2 emissions worldwide. These emissions are mainly because of cement production, the binding agent of concrete. Therefore, to lower the CO_2 emissions from concrete, it is most effective to opt for an alternative binder. This research focuses on alkali-activated materials (AAMs), where an alkali-activated binder has replaced cement. This binder consists of a precursor and an alkaline activator. The materials most commonly used as precursors are blast furnace slag and fly ash, waste products. The production of these materials is not nearly enough to replace cement. Therefore, there is a need for alternative precursors. Volcanic materials can be an alternative precursor, and some have been successfully applied in AAMs before. However, since volcanic materials come in different forms, validation of a wide range of volcanic materials.

This research has investigated four European aluminosilicate volcanic materials: trass, phonolite, perlite and pumice. Each of these materials has been assessed on their particle size, chemical composition and microstructure to determine whether they exhibit (pozzolanic or latent hydraulic) reactivity. All four materials classify as inert. For trass and phonolite, the lack of reactivity is most likely because of their lack of amorphous phases (around 30% and 5%, respectively). For perlite and pumice, it is because of the too coarse particles.

The reactivity of trass and phonolite is enhanced by calcination, and the reactivity of perlite and pumice is enhanced by grinding. Determination of the reactivity shows that calcination had no or a negative effect on the reactivity of trass and phonolite. Most likely because of the lack of calcium and magnesium in these materials. Ground pumice does show an increase in reactivity. However, not sufficient to be classified as reactive. Ground perlite does show reactive behaviour and is classified as pozzolanic, less reactive.

Ground perlite and BFS are used as precursors in mortar to assess the contribution of perlite to compressive strength development. It shows that perlite contributes to the strength of mortar when combined with a sodium silicate and sodium hydroxide activator. Likely, the sodium silicate is necessary to delay the alkalinity of the mixture. This alkaline delay makes that perlite does not form a layer of hydration products over the particles, making it impossible for perlite to react further and contribute to the compressive strength. TGA measurements found that because of the silicates that perlite contributes to the mixture, the hydration products become denser, which seem to cause higher strength. However, it is also found that silicates from sodium silicate solution are more effective in providing silicates than perlite is.

Of all four materials, only perlite seems to be reactive enough to contribute to the strength of alkali-activated binders as precursors. Volcanic materials cannot be considered one material, and each one has to be assessed individually.

Contents

List of Figures

List of Tables

Acronyms

A Alumina. xv

AAM Alkali-activated materials. xv

ASR Alkali-silica reaction. xv

BFS Blast furnace slag. xv

BO Bridging oxygen's. xv

C Calcium. xv

C2S dicalcium silicate (belite). xv

C3A Tricalcium aluminate. xv

C3S tricalcium silicate (alite). xv

C4AF Tetracalcium aluminoferrite. xv

CAH Calcium alumina hydrate. xv

CASH Calcium alumina silicate hydrate. xv

CH Calcium hydroxide. xv

CO2 Carbondioxide. xv

DTG Derivative thermogravitmetry. xv

F Ferrite. xv

FA Fly ash. xv

GGBFS Ground granulated blast furnace slag. xv

GWP Global warming potential. xv

H Hydrogen. xv

ICP Inductively coupled plasma. xv

LCA Life cycle analysis. xv

LDA Laser diffraction analysis. xv

MIP Mercury intrusion porosimetry. xv

NASH Sodium alumina silicate hydroxide. xv

NBO Non-bridging oxygen's. xv

OPC Ordinary Portland cement. xv

P Perlite. xv

S Silica. xv

SF Silica fume. xv

SS Sodium silicate. xv

TGA Thermogravimetric analysis. xv

XRD X-ray diffraction. xv

XRF X-ray fluorescence. xv

1 Introduction

1.1. Background

Concrete is the most commonly used building material worldwide, it is defined as a mass or product made using a cementing medium. Concrete consists typically of a binder and water, which together form the cementing medium, and sand and aggregates. The cementing medium forms a paste which acts as glue for the sand and the aggregates. The most used binder is known as ordinary Portland cement (OPC) [1]. More than 98% of the concrete used this day is produced with OPC. One can easily explain the frequent use of OPC since it gives cheap, reliable, high-quality concrete and has been used successfully for almost 200 years [2].

OPC must show hydraulic properties, meaning that it hardens when it comes into contact with water [1, 3]. The hydraulic concept is more elaborately explained in section 2.3.2. To exhibit hydraulic properties, anhydrous calcium species are necessary. To obtain these properties, OPC is made by mixing and heating materials that bear calcium-, silica-, alumina-, and iron oxide. This process produces clinker, OPC is made by adding gypsum. In OPC, clinker is responsible for the hydration and gypsum is responsible for the reduction of the setting time. More on OPC is discussed in section 2.2. These calcareous materials are limestone, clay shales or chalk. OPC is produced as follows [1, 4]:

1. The raw calcareous materials are ground into a fine powder.
2. The materials are mixed in the proper proportions.
3. The fine powder is burned in a rotary kiln at about 1450°C. In this process, fused clinker is produced.
4. The clinker is cooled down and ground into a powder.
5. Gypsum is added to the clinker powder, resulting in OPC.

During cement production, the initial reaction taking place in the kiln is:

$$CaCO_3 \rightarrow CaO + CO_2 \tag{1.1}$$

As seen in the reaction above, CO_2 is released during cement production. Per ton of CaO produced, 0.78 tons of CO_2 is released [4]. More than 4 billion tonnes of cement are produced each year, making cement production responsible for 5-10% of the CO_2 emissions worldwide [2, 5]. The prospects are that the emissions coming from concrete will only increase in the coming years. Researchers expect this increase because of the foreseen development of the building industry in developing countries [2, 6].

To keep the world's temperature rise well below 2°C, 196 parties adopted the Paris Agreement in 2016. The greenhouse gas emissions should peak as soon as possible to obtain the goal, reaching a climate-neutral world in 2050. There is an urgent need to reduce the environmental impact of cement, considering the significant contribution of cement to global warming. There are several ways of doing so, and this report addresses one of the possible options: considering the production and application of an alternative binder in concrete. Figure 1.1 shows an overview of the process CO_2 emissions from several alternative binders compared to OPC. This figure includes the process emissions from the clinker composition of these binders, more on clinker can

be found in section 2.2. As shown in the figure, one of the options reaching the highest decrease in emissions is the use of alkali-activated binders [2]. Alkali-activated binders are widely studied and generally considered one of the best options to lower the environmental impact of concrete [4]. Therefore, this research will focus on alkali-activated binders.

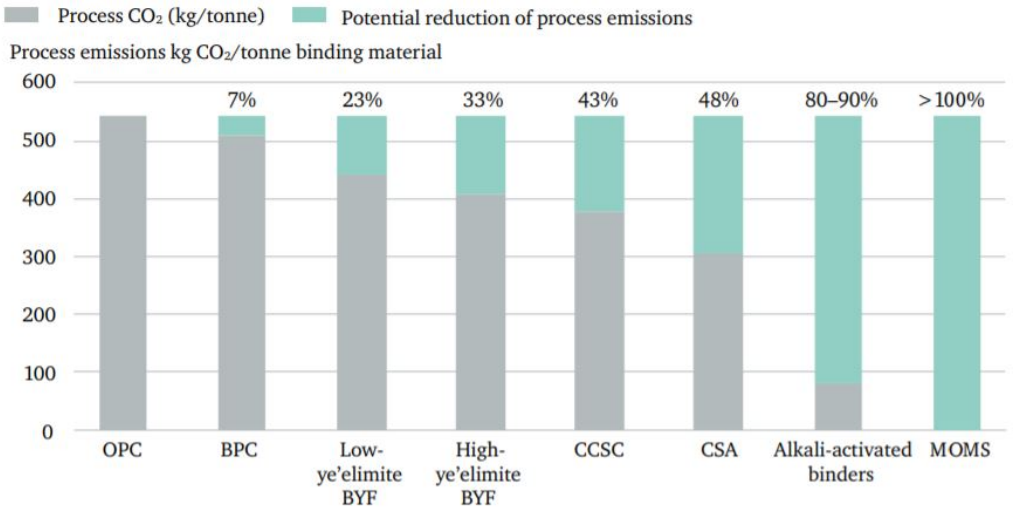

Figure 1.1: Process CO_2 emissions from clinker composition of alternative binders compared to OPC, from [2] (OPC = ordinairy portland cement, BPC = blended portland cement, BYF = belite ye'elimite ferrite, CCSC = carbonatable calcium silicate clinkers, CSA = calcium sulphoaluminate, MOMS = magnesium oxides derived from magnesium silicates).

In alkali-activated binders (often called geopolymers), an aluminosilicate precursor replaces OPC. This precursor hardens in an alkaline environment, resulting in a hardened paste, similar to cement [7]. The most commonly used precursors in alkali-activated binders are blast furnace slag (BFS), coal fly ash (FA) and calcined clays, such as metakaolin [8]. A more detailed explanation on alkali-activated systems is given in chapter 2.3.

1.2. Problem

In the Netherlands, BFS, a by-product from the steel industry, is commonly used to produce blended cement (CEMIII/B). Using blended cements already lowers the environmental impact of concrete, shown as BPC in Figure 1.1. The utilization of BFS in the Netherlands is quite common, but applying BFS in blended cement is not standard in other countries [2]. The need for a more sustainable concrete type is increasing, leading to a rise in countries implementing BFS to decrease the cement content and therefore the CO_2 emissions. All this leads to an increase in the demand for BFS. However, the current production of BFS is limited (170-250 Mt/year, globally), especially when compared to the global OPC production (3-4 trillion tons/year, globally)[9]. Which means that the production of BFS is already insufficient to supply the entire world [10, 11, 12], but the steel production is also expected to change to be more sustainable, which might influence the slags' quality. Therefore, a shortage in suitable BFS is predicted [3, 9, 13].

The other most used material in blended cement is fly ash (CEMII/B), a by-product of the coal industry. The global production of FA stands currently at 500-700 Mt/year [9]. Fly ash production is expected to decrease because of the necessary closure of coal-fired power plants. [11, 12]. The shortage of this material is expected to increase, leading to an urge to search for alternative materials to use as supplementary cementitious materials (SCMs) in blended cements, and as a precursor in alkali-activated binders [3, 14].

Possible alternative aluminosilicate resources could be volcanic materials. In this research, volcanic materials are described as 'soils derived from volcanic ash'. Volcanic materials are an interesting source since this material is widely available. These natural pozzolans account for approximately 0,84% of the world's total soil and are well distributed over the world [9]. Volcanic materials are already more often used in concrete as supplementary cementitious materials, but research regarding their implementation in alkali-activated binders is still scarce.

1.3. Research goal and objective

This research aims to assess the potential of volcanic materials as an alternative precursor in alkali-activated binders. Eventually, the main goal is to determine if volcanic materials are sufficiently reactive to contribute to the properties of alkali-activated binders. The hypothesis for this research is:

Volcanic materials can be sufficiently reactive to be used as precursors in alkali-activated binders, preserving adequate mechanical properties without compromising the reduction of CO_2 emissions.

In order to test this hypothesis, several research questions are stated. The questions are the following:

1. What properties are relevant in determining the reactivity of materials to be applied in alkali-activated binders?
2. Is the reactivity of volcanic materials originating from Europe sufficient to apply as precursor in alkali-activated binders?
3. Can the reactivity of volcanic materials be improved, to be able to be successfully applied as precursor in alkali-activated binders?
4. How does the application of volcanic materials influence the mix design of alkali-activated materials?
5. What is the contribution of volcanic materials to the mechanical strength development of alkali-activated mortars?
6. What is the CO_2 footprint from alkali-activated binders with volcanic materials as precursor?

By finding answers to these research questions, the hypothesis can be accepted or rejected.

1.4. Scope

This research will assess four types of volcanic materials to ensure feasibility of the thesis. The four materials are trass, phonolite, pumice and perlite, and are all available in Europe. Trass is a natural pozzolan consisting of volcanic ash and minerals [15], phonolite is a rock formed by the cooling of magma [16], perlite is a volcanic glass formed from rapidly cooled lava [17] and pumice is formed by the cooling of silica rich lava and the releasing of gases [18]. Pictures of the four materials are shown in appendix C. To ensure feasibility of this research, the following limitations are stated:

- Only four volcanic materials shall be assessed.
- The mechanical strength will be tested on mortar-level.
- Only one of the four materials will be assessed as precursor in alkali-activated mortar samples.
- The curing time of mortar samples will be up to 7 days.
- The compressive strength is tested, flexural strength and durability are outside the scope of this research.

1.5. Outline thesis

This research is divided into three phases:

1. Phase 1: Assessing the reactivity of raw volcanic materials.
2. Phase 2: Assessing the reactivity of pre-treated volcanic materials.
3. Phase 3: Assessing the properties of alkali-activated mortar produced with volcanic materials.

First, literature review is conducted to answer research question 1. In phase 1, all four volcanic materials will be assessed in their raw state. The important properties will be examined, and their reactivity. Phase 1 will evaluate research question 2. If it is necessary, the materials will be treated and their reactivity is again analyzed in phase 2, focusing on research question 3. Phase 3 will test one material as precursor in alkali-activated mortar. Several mortar mixes will be tested and the contribution of the material to the strength development of the mortar is assessed. Phase 3 will answer research question 4 in chapter 5 and question 5 and 6 in chapter 6. Figure 1.2 presents the outline of this thesis.

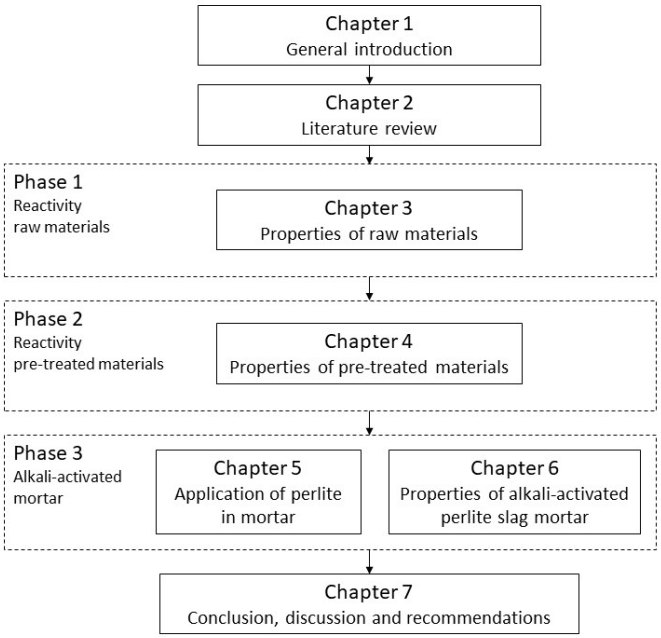

Figure 1.2: Outline thesis

2

Literature review

2.1. Introduction

The literature review gives an overview of cement hydration and the state-of-the-art of alkali-activated binders and volcanic materials. The report addresses the reaction mechanisms and relevant properties of precursors and activators and current studies on the application of volcanic materials in alkali-activated systems.

2.2. Cement

OPC consists of clinker and gypsum, with clinker being responsible for the hardening of cement once it comes into contact with water (called cement hydration) and gypsum being responsible for reducing the setting time of cement [1, 19]. Section 1.1 describes the production of OPC. The four main components of the produced clinker are:

Table 2.1: Overview of the components from clinker, after [1] (C = Cao, S = SiO_2, A = Al_2O_3, F = Fe_2O_3).

Name of component	Oxide composition	Abbreviation
Tricalcium silicate (alite)	$3CaO.SiO_2$	C_3S
Dicalcium silicate (belite)	$2CaO.SiO_2$	C_2S
Tricalcium aluminate	$3CaO.Al_2O_3$	C_3A
Tetracalcium aluminoferrite	$4CaO.Al_2O_3.Fe_2O_3$	C_4AF

The calcium silicates alite and belite are considered the main compounds since they are mainly responsible for the strength of the hydrated cement paste. Tricalcium aluminate and tetra calcium aluminoferrite react with gypsum and may benefit the hydration of alite and belite [1, 19].

The hydration process of cement begins when the cement particles come in contact with water. Silicates and aluminates form hydrates, which eventually form a solid mass. The main products of these reactions are calcium silicate hydrates (C-S-H-gel) and calcium hydroxide (CH), also known as portlandite. The hydration reactions that take place are (roughly) as follows [1, 19]:
C_3S:

$$2C_3S + 6H_2O \rightarrow C_3S_2H_3 + 3Ca(OH)_2 \tag{2.1}$$

C_2S:

$$2C_2S + 4H_2O \rightarrow C_3S_2H_3 + Ca(OH)_2 \tag{2.2}$$

C-S-H-gel constitutes for 60-70% volume of the hydrated cement paste of OPC and is therefore mainly responsible for the mechanical strength of concrete [20, 21]. The other main hydration product is portlandite, which makes up 20-25% of OPC hydrated cement paste volume [5]. The CH crystals are relatively large compared to C-S-H, leading to a significantly smaller surface area. Due to this smaller surface area, portlandite is less dense than C-S-H-gel and it contributes less to the mechanical strength of concrete [20].

2.2.1. Blended cement

Blended cement consists of OPC and a percentage of supplementary cementitious materials (SCMs). The addition of SCMs to OPC has been shown to specifically improve the durability of concrete and lower the environmental impact of concrete [3, 22]. Because the environmental impact is reduced without compromising the structural integrity of concrete, SCMs are often implemented [1, 3].

SCMs are materials that generally show pozzolanic or (latent) hydraulic properties, as both of these properties lead to the nucleation of reaction products. The reaction mechanism is classified as hydraulic if the material hydrates once it comes into contact with water. If this reaction is slow, the material is classified as latent hydraulic. Alkaline conditions can accelerate the hydration of latent hydraulic materials under alkaline conditions. If portlandite ($Ca(OH)_2$) is consumed during the hydration process, the reaction mechanism classifies as pozzolanic [2, 3, 22]. The pozzolanic reaction in cement is as follows ($A = Al_2O_3, C = CaO, H = H_2O, S = SiO_2$):

$$AS + CH + H \rightarrow C-S-H + C-A-H \tag{2.3}$$

As can be seen above, the pozzolanic reaction leads to an increase in C-S-H-gel and C-A-H-gel (calcium alumina hydrates). This increase in reaction products results in a more dense microstructure and better structural integrity.

Supplementary cementitious materials can roughly be divided into natural and artificial SCMs. The artificial SCMs are commonly waste materials, such as BFS and FA, but also silica fume and calcined clay are classified as artificial SCMs. The natural SCMs can be used as they come; often, only grinding or sieving is necessary. Natural SCMs are of sedimentary or volcanic origin [3, 22].

Different types of cement are classified by the type of SCM and the percentage OPC/SCM. Appendix A contains an overview of the several cement types. In the Netherlands, CEMIII/B is the most used cement type. Using CEMIII/B instead of OPC achieves a significant reduction of CO_2 emissions. Volcanic and sedimentary rocks are categorized under *natural pozzolans* and are used in CEMIV.

2.3. Alkali-activated systems

The introduction discusses the environmental impact of concrete. To lower the CO_2 emissions from concrete, reducing the cement content is the most effective option. One option to lower the cement content is the implementation of alkali-activated binders [4]. Calculations of Duxson et al. showed CO_2 savings in the order of 80%, comparing alkali-activated fly-ash and metakaolin binders with OPC [23]. Alkali activation describes the reaction of an aluminosilicate or calcium precursor in an alkaline environment, forming a hardened binder similar to cement [7]. The precursor dissolves in the alkaline environment, releasing ions that are available for the formation of hydration products. More on the dissolution and condensation mechanisms is discussed in the next section (2.3.1).

Precursors that are commonly used in alkali-activated binders are often also used as SCMs, such as BFS and FA. Precursors are more thoroughly discussed in section 2.3.2. An alkaline activator causes an alkaline environment necessary for the dissolution. Often, hydroxides in combination with silicates are used. More on this in section 2.3.3.

Alkali-activated materials are shown to have properties similar to OPC and even superior to OPC. These superior properties are mostly related to durability [24]. Challenges regarding alkali-activated binders are in the lack of standardization. There are no consistent guidelines because there are many parameters regarding mix designs of alkali-activated binders [4, 24].

2.3.1. Dissolution and condensation

In alkali-activated binders, the activator ensures an alkaline environment in which the precursor can dissolve. This dissolution process takes place according to the following steps, shown in Figure 2.1:

- First Na^+ and Ca^{2+} dissolve from the precursor surface through the exchange for H^+. These are the first ions to dissolve because they have weaker bonds to the network.
- The hydrolysis of Al-O-Si bonds starts. Since the Al-O bonds are weaker than the Si-O bonds, aluminate species dissolve first. The initial tetrahedrally coordinated Si becomes partially coordinated once aluminate species dissolve, leading to a faster dissolution of the silicate species [25].
- More ions will split from the network, leading the depolymerized glass network to break down.

- Alumina and silica species break free from the framework into the solution. The species are now free to form new bonds and create a new network.

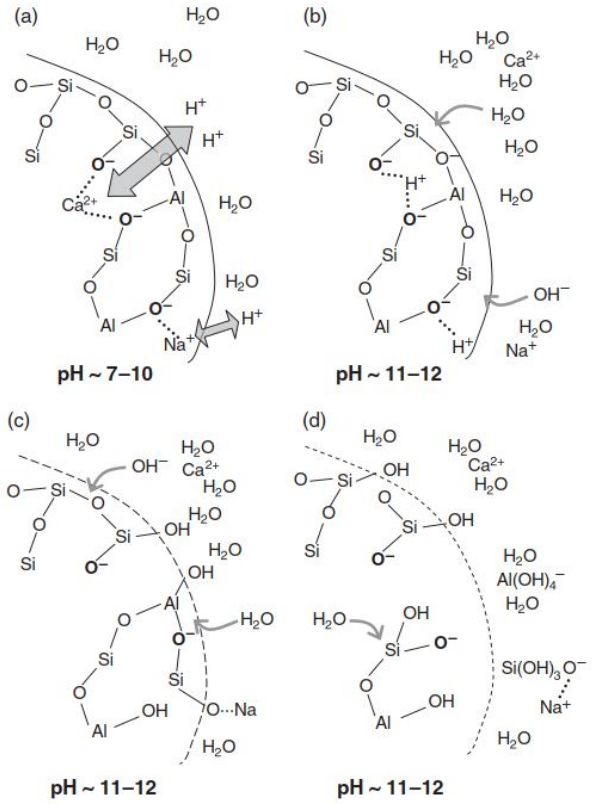

Figure 2.1: Dissolution mechanism of an aluminosilicate glass during the early stages of reaction of a geopolymer mix, from [8]. (a) Dissolution of Na^+ and Ca^{2+} through exchange for H^+. (b) Hydrolysis of $Al-O-Si$ bonds. (c) Continuation of the down breaking of the network. (d) Dissolution of the alumina and silica species.

The dissolution and hydrolysis of alumina and silica of aluminosilicate precursors in an alkaline solution can be described by the following reactions:

$$Al_2O_3 + 3H_2O + 2OH^- \rightarrow 2[Al(OH)_4]^- \tag{2.4}$$

$$SiO_2 + H_2O + OH^- \rightarrow [SiO(OH)_3]^- \tag{2.5}$$

$$SiO_2 + 2OH^- \rightarrow [SiO_2(OH)_2]^{2-} \tag{2.6}$$

The ratio of $[SiO(OH)_3]^-$ to $[SiO_2(OH)_2]^{2-}$ decreases with an increase of the pH of the pore solution [26]. It is found that the reaction between alumina and silica happens more rapidly than silica-silica reactions [27]. This means that condensation mainly consists of the reaction of $[Al(OH)_4]^-$ with $[SiO(OH)_3]^-$ or $[SiO_2(OH)_2]^{2-}$, considering the species from reactions 2.4, 2.5 and 2.6. The condensation between $[Al(OH)_4]^-$ and $[SiO(OH)_3]^-$ forms longer and more stable networks than the condensation between $[Al(OH)_4]^-$ and $[SiO_2(OH)_2]^{2-}$. This way, the alkalinity of the pore solution influences the condensation products [27].

AAMs can be classified into three different systems, depending on the calcium content of the precursor: high-calcium based systems, such as BFS; low-calcium based systems, such as FA, and blended systems.

The main reaction product of high-calcium based systems is a C-(N-)A-S-H type gel, which has a two-dimensional, layered structure, similar to C-S-H-gel, shown in Figure 2.2. Besides the primary reaction product, crystalline, secondary reaction products are formed, such as hydrotalcite ($Mg_6Al_2CO_3(OH)_{16}.4H_2O$). The secondary reaction products also depend on the alkaline activator [28, 29, 30].

The main reaction product of low-calcium based systems is an aluminosilicate N-A-S-H gel. The structure of this gel is three-dimensional in which Si and Al are tetrahedrally coordinated, shown in Figure 2.2. The curing time, curing temperature and the alkaline activator influence the nature of the N-A-S-H gel. Secondary reaction products accompany the N-A-S-H gel, such as zeolites and hydroxy sodalite [4, 31].

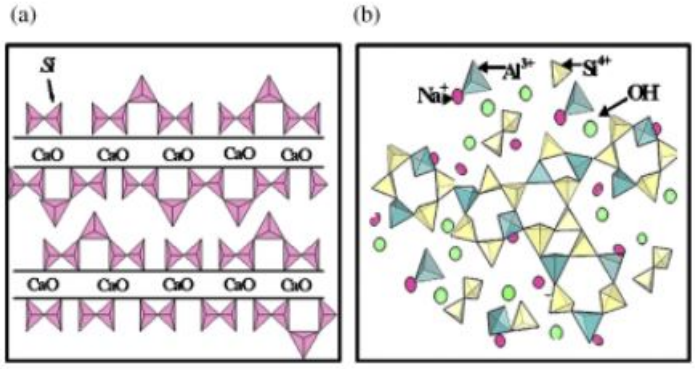

Figure 2.2: (a) Schematic overview C-(N-)A-S-H gel (b) Schematic overview N-A-S-H gel, from [32].

2.3.2. Precursors

To be a suitable precursor in alkali-activated binders, the precursor must present reactive behaviour from either hydraulic or pozzolanic properties since both types of properties lead to the nucleation of species [3]. Whether or not a material displays these properties is determined by several factors. There is a distinction between these factors of intrinsic material properties and extrinsic system properties [13]. Intrinsic properties are properties the material presents. Extrinsic system properties refer to the environment in which the reaction takes place. Examples of the extrinsic properties are temperature, humidity and alkalinity of the environment. This section focuses on the intrinsic material properties.

The microstructure is one factor that influences the reactivity of a material. Regarding precursors, a distinction is made between crystalline and amorphous structures. If the structure is crystalline, the atoms have formed a highly ordered pattern, the so-called crystal lattice. This lattice results in a lower reactivity because it is difficult to break down the network. The atoms have a random pattern if the structure is amorphous (also called glassy). Because the atoms are more loosely placed in the structure than when they have formed a grid, it is easier to break the structure. Since amorphous structures are more easily broken down, they show higher reactivity. The difference between these two types of microstructure is visualized in Figure 2.3. The rapid cooling of high-temperature materials can lead to an amorphous microstructure. By cooling quickly, the atoms do not have the time to organize themselves in the crystal grid, and they 'freeze' in an amorphous structure [13, 22].

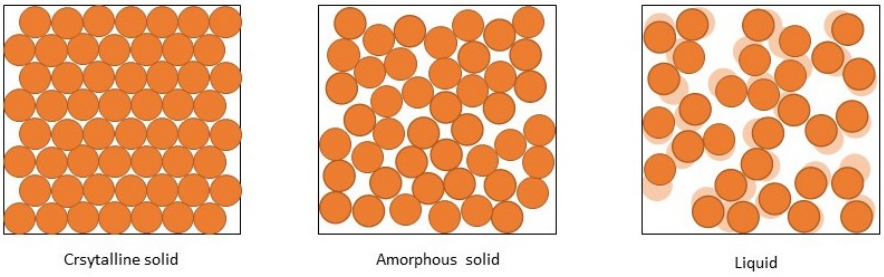

Figure 2.3: Illustration of the structure of atoms in a crystal grid (left), an amorphous structure (middle) and in a liquid (right), after [33]

The chemical composition of the amorphous content of the material is another factor that influences the reactivity of a material. A sufficient amount of reactive alumina or silica should be present to exhibit pozzolanic properties. Anhydrous calcium silicates must be available to display hydraulic properties [14, 34]. This way, the chemical composition of the amorphous phases and the amorphous phase content indicate the material's reactivity.

The network's ions are connected by oxygens. A distinction is made between bridging oxygens (BO) and non-bridging oxygens (NBO). The BOs connect network forming ions, whereas the NBOs disrupt the network.

A distinction is made between network forming ions and network modifying ions in the chemical composition. Network forming ions (SiO_4, AlO_4) have the ability to form multiple bonds and cause a tetrahedrally coordinated (cross-linked) network. Consequently, an increase in the network forming ions leads to a more extended network. Network modifying ions (CaO, MgO) can form one or two bonds. This way, they disrupt the network. Figure 2.4 presents an aluminosilicate network including the network modifiers, BOs and NBOs. The reactivity of materials strongly depends on the material's potential to dissolve. If the material network has more network forming ions and, therefore, longer network chains, the more difficult it is to break down and consequently, the more difficult it is to dissolve. Network modifying ions cause a lower degree of cross-linking, resulting in higher reactivity [13].

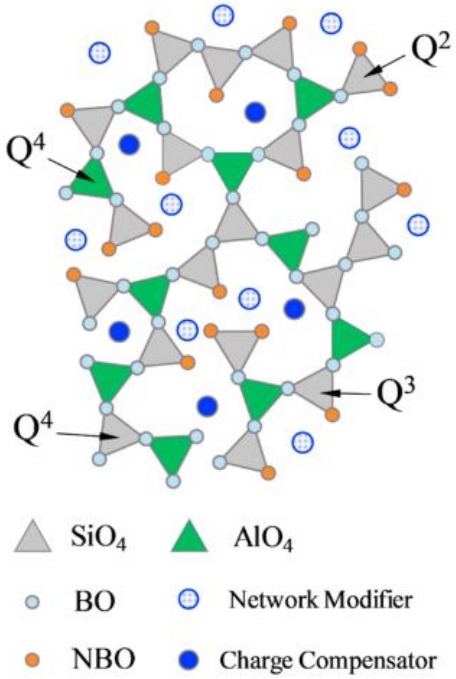

Figure 2.4: Schematic two-dimensional microstructure of aluminosilicate precursors, from [13].

The fineness of the particles plays a role in the reactivity of materials. A smaller grain size leads to a higher relative surface area and higher reactivity. The reactivity increases because a higher relative surface area leads to a higher dissolution rate of the precursor. An increase in surface area causes an increase in nucleation sites for hydrate precipitation and growth [13].

If a material does not meet all of the previously mentioned requirements, manipulation is possible. The particle size can be manipulated by grinding, which reduces the particle size and increases the surface area. Thermal activation (calcination) can improve the microstructure of a material. The most well-known example for calcination is the production of OPC (described in chapter 1), but also meta kaolin is a calcined precursor. During calcination, inorganic materials are thermally treated at temperatures above 700 °C, to release volatile components (such as CaO and MgO) from their mineral phases [35].

As society works towards lowering emissions, the use of blended cements and alkali-activated materials increases. This leads to a rise in the demand for precursors, whereas the production is not increasing or even decreasing [11]. Because of the reduced availability of typical precursors, there is a need to find new precursors that display hydraulic or pozzolanic properties [3, 22, 36].

2.3.3. Activators

In alkali-activated systems, activators create an alkaline environment that can trigger the dissolution process of precursors. Generally, activators are alkali hydroxides or silicates. They are usually applied in dissolved form because the dissolution of hydroxides or silicates results in high heat production, leading to thermal stresses in the evolving gel [4]. Using a solid activator can increase the setting time of the concrete, leading to

lower early strength and a more variable strength because of the slower availability of the alkalinity [37].

Table 2.2: Overview of the different combinations of solid precursor and alkaline activator which are feasible and desirable, from [4].

	MOH	$M_2.rSiO_2$	M_2CO_3	M_2SO_4	$Other$
Blast furnace slag	Acceptable	Desirable	Good	Acceptable	
Fly ash	Desirable	Desirable	Poor - becomes acceptable with cement/clinker addition	Only with cement/clinker addition	$NaAlO_2$ - acceptable
Calcined clays	Acceptable	Desirable	Poor	Only with cement/clinker addition	
Natural pozzolans and volcanic ashes	Acceptable/ Desirable	Desirable			
Framework aluminosilicates	Acceptable	Acceptable	Only with cement/clinker addition	Only with cement/clinker addition	
Synthetic glassy precursors	Acceptable/ Desirable (depending on glass composition)	Desirable			
Steel slag		Desirable			
Phosphorus slag		Desirable			
Ferronickel slag		Desirable			

Table 2.2 shows an overview of suitable activators for each precursor from the 2014 RILEM report [4]. The 'M' stands for metal and can generally be replaced by Na (sodium) or, less often, K (potassium) [4]. Alkali silicates and hydroxides generate the highest pH, whereas carbonates and sulphates generate moderate pH values. Different activators bring different species into the dissolution and thus influence the nature of the hydration products. For example, waterglass ($Na_2O.(n)SiO_2$) brings dissolved silica species into the dissolution, resulting in higher cross-linking of the hydration products. Sodium hydroxide ($NaOH$) generates a high pH, beneficial for the dissolution of the precursor and bringing sodium species into the dissolution. Sodium species cannot form multiple bonds and therefore result in lower cross-linking of the hydration products [30, 37].

Choosing a suitable activator is of great importance when designing an alkali-activated concrete mixture. The right choice is not straightforward but depends on the specific conditions and requirements.

2.4. Precursors in alkali-activated systems

The most commonly used precursors in alkali-activated systems are fly ash and blast furnace slag. This section discusses both these precursors and volcanic materials, an alternative option for precursors.

2.4.1. Fly ash

Fly ash (FA) is an industrial waste product from the coal consumption process in thermal power plants [38, 39]. FA consists of a heterogeneous mixture of crystal and amorphous phases. It is known for its' spherical particle shape. The chemical composition can be described as a fero-aluminosilicate containing toxic metals ($As, Ba, Hg, Cr, Ni, V, Pb, Zn, Se$).

The properties of FA depend on the type of coal, the handling and the storage. There are four types of coal: anthracite, bituminous, sub-bituminous and lignite. The type of coal determines the chemical composition. FA is divided into class C, and class F. Lignite or sub-bituminous coal results in class C FA, Anthracite or bituminous coal results in a class F FA [38]. ASTM C618 describes the classification of FA. Table 2.3 shows typical chemical compositions of FA.

Because of the metals present, FA could be a harmful material once these elements migrate from FA through water when it is put into landfills. This migration leads to soil and groundwater pollution, negatively

Table 2.3: Typical chemical compositions of FA, based on the type of coal, from [39]

[wt.%]	Bituminous	Sub-bituminous	Lignite
SiO_2	20-60	40-60	15-45
Al_2O_3	5-35	20-30	10-25
Fe_2O_3	10-40	4-10	4-15
CaO	1-12	5-30	15-40
MgO	0-5	1-6	3-10
SO_3	0-4	0-2	0-10
Na_2O	0-4	0-2	0-6
K_2O	0-3	0-4	0-4
LOI	0-15	0-3	0-5

influencing the environment and human health [38, 39, 40]. Therefore, it is better to utilize FA. Currently, in Europe, almost all produced FA is used. However, plenty of FA could be utilized in India, China, and the UK instead of landfills.

The use of FA as cement replacement is well known. The spherical particles of which FA is made result in a ball-bearing effect, decreasing the water demand for cement. FA is a pozzolanic material; adding it to a cement mixture will consume portlandite (CH) and produce a C-S-H-gel, resulting in higher strength concrete over a long period [39].

Because FA is a waste material, utilizing it has economic, environmental and health benefits. Due to the energy transition, coal consumption in Europe and America has decreased for many years now. However, the global coal consumption still rose in 2018 by 0,9%, namely because of the increase in coal consumption in Asia (i.e. China, India, Turkey and Russia) [40]. However, there is an expected decrease in coal combustion plants. Therefore, researchers expect the amount of FA produced to decrease in countries where all FA is utilized, which leads to a shortage of FA [40].

2.4.2. Blast furnace slag

Blast furnace slag is the non-metallic product developed during the production of iron in a blast furnace, and it consists mainly of alumina, silicates and calcium [41]. High-pressure water jets quench the slag directly from the furnace, ensuring the amorphous phases and producing ground blast furnace slag (GBFS). BFS in concrete is most beneficial when the grain size is smaller than cement. To achieve this, the GBFS is ground to a particle size of preferably 375-425 m^2/kg, called ground granulated blast furnace slag (GGBFS) [42, 43].

If BFS is rapidly cooled by water, it can become almost entirely amorphous. Because of the presence of calcium, it exhibits latent hydraulic properties. The amorphous content is most significant for the reactivity of slag. An amorphous content of above 90% is preferred for optimal reactivity [41, 42]. Table 2.4 shows typical chemical compositions for BFS, Figure 2.5 shows a typical XRD pattern. In the pattern, one can identify a clear hump between 20 and 40 $^\circ 2\theta$, indicating the amorphous phases present.

Table 2.4: Typical chemical compositions of GGBFS from different countries, from [43]

[wt.%]	USA	South Africa	Turkey
CaO	29-50	30-40	34-41
$SiO2$	30-40	30-36	34-36
Al_2O_3	7-18	9-16	13-19
Fe_2O_3	0,1-1,5	-	0,3-2,5
MgO	0-19	8-21	3,5-7
MnO	0,2-1,5	-	1-2,5
S	0-2	1-1,6	1,2
SO_3	-	0	-

Because of the latent hydraulic properties, BFS is an excellent SCM. For many years CEM-III(A/B/C) has been available, which contains up to 70% BFS [1]. The use of BFS in concrete mixtures affects the properties of concrete. The workability of the concrete increases because of better particle dispersion and fluidity. Because of the latent hydraulic properties, the short term strength development decreases. However, the BFS reacts with the developed CH to form C-S-H, which leads to a long term strength increase [41]. The newly formed

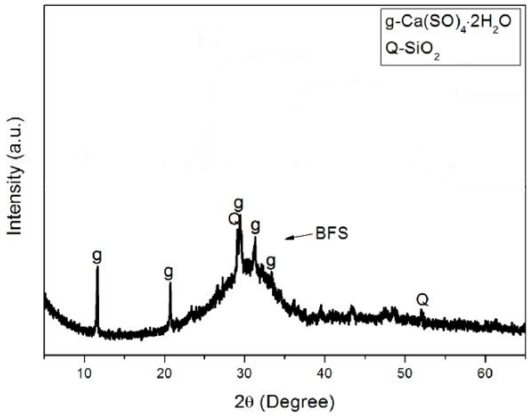

Figure 2.5: XRD pattern BFS, showing a hump between 2 and 40 °2θ after [44].

C-S-H particles form in the voids, which leads to a reduction in pore volume and better durability properties.

The use of BFS in concrete mixtures has many benefits, besides improved concrete properties. For instance, the use of BFS in blended cements decreases the CO_2 emissions compared to OPC. Because BFS is a waste product, no raw materials are used in the production of BFS, and resource depletion decreases as well [43]. As mentioned before, the demand for BFS is expected to increase, whereas the current global production of BFS is already limited. Therefore, availability is one of the biggest challenges regarding the use of BFS [13].

2.4.3. Volcanic materials

Because of the chemical composition and possible amorphous phase content, volcanic ashes can be considered a potential precursor in alkali-activated binders. An overview of the chemical composition of volcanic materials compared to well-known precursors is given in Figure 2.6. The chemical composition of volcanic materials is within FA and silica fume range. It must be noted that volcanic materials are present within an extensive compositional range, depending on the origin of the volcanoes, which makes it essential to define the chemical composition of specific volcanic material [3].

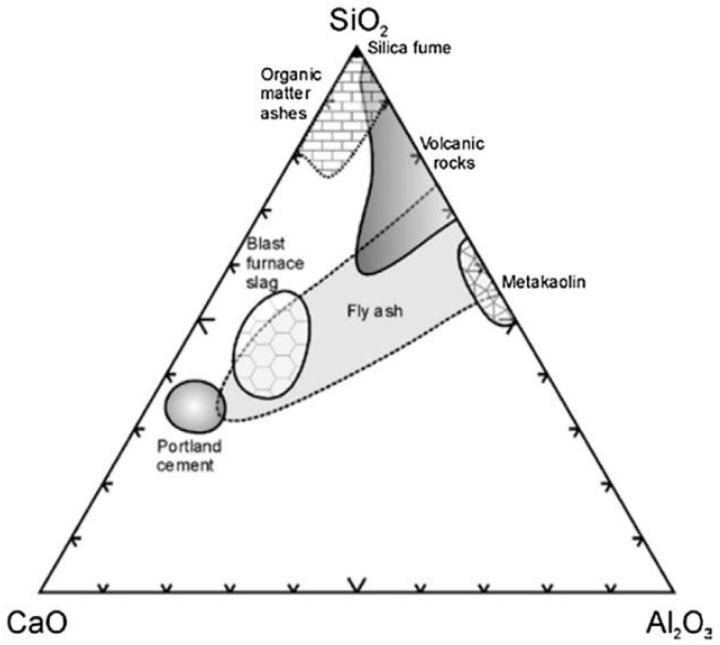

Figure 2.6: Ternary CaO-SiO2-Al2O3 diagram (wt. % based) situating the chemical composition of several SCMs, from [3].

Djon Li Ndjock et al. classify volcanic materials into two categories: one category contains a SiO_2 content

of 40-55%, the other category contains 60-75% SiO_2 [45]. Note that the chemical composition refers to the chemical composition of the amorphous phase content. The SiO_2/Al_2O_3 ratio impacts the reactive nature of the material. Because Si-O-Si bonds are stronger than Si-O-Al or Al-O-Al bonds, a higher ratio leads to lower reactivity [46]. Therefore, if more alumina is present, the network will be more easily disrupted, leading to an accelerated dissolution of the material. The reaction can also be accelerated by ensuring a higher alkaline environment or adding active calcium since this modifies the network. The SiO_2/Al_2O_3 ratio also influences the activation temperature of the material. A ratio lower than three results in a relatively low activation temperature. A SiO_2/Al_2O_3 ratio larger than 4 results in an relatively high activation temperature (80-100°C).

An advantage of the use of volcanic materials is their availability. Since volcanoes are widespread, one can apply volcanic materials in alkali-activated binders worldwide. Natural volcanic pozzolan deposits account for approximately 0,84% of the 124 million hectares of the world's soils [9]. Volcanic materials are derived from hot magma that rises to Earth's surface and takes on a glassy structure if the lava is cooled down rapidly enough [22]. For the Netherlands, the nearest source of volcanic materials is the Eifel region in Germany.

The four volcanic materials discussed in this report are trass, phonolite, perlite and pumice. All four materials will be examined based on the available literature, after which a comparison will be made.

2.4.4. Trass

Trass is a natural pozzolan that consists of volcanic ash and minerals. The pozzolanic nature of trass is due to its' siliceous ingredients [15]. Trass can be found in Iran, Indonesia and Germany, among others [15, 47, 48, 49]. Trass originating from Germany, the Eiffel region, is a material that has been commonly applied in the Netherlands by Romans. It was widely used in masonry mortars, especially in hydraulic engineering works. The heyday of trass in the Netherlands was in the 17th century, in trass-lime mortars. Later, in the 19th and 20th centuries, the use of trass in the Netherlands started to decrease, mainly due to trass quality problems, which was often mixed with loose volcanic material and tuff from other sources [50].

Although not widely researched, several studies have been conducted on the properties of binders that implemented trass. An overview of the chemical compositions from the trass samples used in these studies is shown below in Table 2.5. The fifth column shows the yearly average values of the chemical composition from trass samples from the Eiffel region [49].

Table 2.5: Overview of the chemical compositions of trass samples.

[wt.%]	Trass 1 (Indrawati and Manaf)	Trass 2 (Risdanareni et al.)	Trass 3 (Joshaghani et al.)	Trass 4 (Trasswerke Meurin)
LOI				5,2
SiO_2	59,65	87,5	24,24	52
Al_2O_3	20,64	0,2	4,25	17
CaO	3,32	1,7	58,8	8
MgO	1,02	0,5	3,8	-
Fe_2O_3	5,51	1,9	3,8	-
TiO_2	-	0,9	-	-
K_2O	1,64	0,41	0,7	6
Na_2O	1,5	0,8	0,6	-
SO_3	0,15	6,2	3,8	0,1

As shown in Table 2.5, the trass samples from the Eiffel region (trass 4) are, in terms of chemical composition, most similar to the trass samples used in the research of Indrawati and Manaf (trass 1). The trass samples obtained from the north of Iran (trass 3) differ most from the German trass because of their relatively high calcium content. Therefore, this report will not discuss the research performed by Joshaghani et al. This overview shows the inconsistency of the chemical composition of trass throughout the world. Consequently, it is essential when investigating the suitability of a trass-based binder to obtain the chemical composition and the microstructural analysis. Trass from Trasswerke Meurin belongs to the aforementioned first category of Djon Li Ndjock et al.. It has a SiO_2/Al_2O_3 ratio of approximately 3, which indicates that the powder could react relatively fast with an activation temperature of 30°C [51]. The specific surface area of trass 4 has a yearly average value of 7600 cm^2/g [49].

The reactivity of trass is debatable. Indrawati and Manaf performed research in 2008 on the mechanical properties of pozzolanic-lime obtained from trass reacting with lime [47]. They found that mortars with 70% trass and 30% lime would reach a maximum compressive strength of merely 11 MPa. A similar analysis was performed by Risdanareni, Ekaputri and Triwulan, assessing the use of trass in an alkali-activated binder [48]. They found that a FA bases binder would reach mechanical strengths of almost 50 MPa, whereas a binder containing trass and FA would reach 30 MPa. The reduction in strength indicates that the addition of trass lowers the mechanical strength. Neither of the researchers discussed durability aspects.

2.4.5. Phonolite

Phonolite is an extrusive igneous rock, meaning that it originates from magma, erupts out of the earth crust as lava and then cools down and solidifies outside of the earth crust. Phonolite contains 45% zeolites and has a texture ranging from fine-grained to fine and coarse-grained. The material has a glassy or finely crystalline core mass [16].

The application of phonolite in concrete mix design is not a widely discussed subject. In 2006, at the International Conference on the Occurrence, Properties and Utilization of Natural Zeolites, research on the applications of natural zeolites in concrete was presented by F. Hauri [52]. The mechanical strength of a hybrid cement binder, consisting of 48,5% clinker, 48,5% phonolite and 3% gypsum, was tested at seven days and 28 days. Compared to a mix with 100% OPC, the strength of the hybrid binder was significantly lower at seven days. However, due to the ongoing pozzolan reaction in the hybrid binder, the strength at 28 days is almost equal (58,2 MPa for the OPC-based mix and 53,0 MPa for the hybrid binder mix) [52].

The phonolite available in the Netherlands comes from Brenk, in the Eiffel region. Volcanic activity in the Eiffel region started around 700.000 years ago, and the last eruption occurred over 11.000 years ago [53]. The mineral deposit is homogeneous and available in grain sizes ranging from 0-3 mm and 0-0,09 mm [54]. Table 2.6 shows the chemical composition as offered by the supplier. Due to the SiO_2 content of approximately 55%, phonolite belongs to the first category of Djon Li Ndjock et al.. It has a SiO_2/Al_2O_3 ratio lower than 3, indicating a relatively fast reaction and low required activation temperature [51].

Table 2.6: Chemical composition of phonolite obtained from AG Steinindustrie.

	Mass share [%]
LOI	3,0
SiO_2	54,4
Al_2O_3	22,1
CaO	1,3
MgO	0,3
Fe_2O_3	3,1
TiO_2	0,3
K_2O	9,8
Na_2O	7,6

The material phonolite shows potential as a supplementary cementitious material. Limited literature on the application of phonolite in concrete mixtures is available. However, the chemical composition is encouraging. A meaningful subject to address is the reactivity of phonolite since this is an essential property for a successful precursor in AAMs. Therefore, research should assess the microstructure of phonolite to obtain an indication of the reactive properties of the material.

2.4.6. Perlite

Perlite is a natural volcanic glass formed from silicate-rich lava which has been cooled down rapidly. The cooling down occurs when the lava meets cold water and hardens [55]. The current perlite reserves are estimated at approximately 6700 million tons and are globally available, with the primary deposits in Turkey, Greece, the US and Japan [17]. Perlite has the unique ability to expand when exposed to high temperatures, resulting in a highly porous material with a density of 75-80 kg/m^3 [56]. Expanded perlite is commonly known as an efficient heat insulating material due to its' high thermal resistance, high availability, ecological friendliness and simplicity of manufacturing [57]. Perlite is also used as lightweight aggregate in concrete mixtures and in agriculture to improve the air content of the soil [17].

Several studies on the applications of perlite in a concrete mix have already been performed. Table 2.7

gives an overview of obtained chemical compositions.

Table 2.7: Overview of the chemical composition of perlite samples.

[wt.%]	Perlite 1 (Yu et al.)	Perlite 2 (Erdem et al.)	Perlite 3 (Zhang et al.)	Perlite 4 (Fodil & Mohamed)	Perlite 5 (Çeliktен et al.)
LOI	0,64	-	-	-	3,21
SiO_2	76,89	76,57	71,46	76,40	72,84
Al_2O_3	10,51	9,99	16,79	13,43	13,34
CaO	0,12	0,51	1,52	3,16	0,93
MgO	0,06	0,03	0,35	0,37	0,14
Fe_2O_3	2,48	0,96	-	2,92	0,67
TiO_2	0,07	-	-	-	0,07
K_2O	8,25	5,58	4,54	4,33	5,53
Na_2O	0,80	0,00	4,33	0,82	3,28

One can conclude that the chemical composition of perlites does not differ significantly. Perlite belongs to the second category of Djon Li Ndjock et al. and contains a SiO_2/Al_2O_3 ratio higher than 4, indicating that the reaction happens relatively slow and requires an activation temperature of 80-100°C [51]. Erdem et al. performed an XRD test on two perlite samples. Both patterns showed blunted peaks, shown in Figure 2.7, indicating the amorphous nature of the material [58, 59].

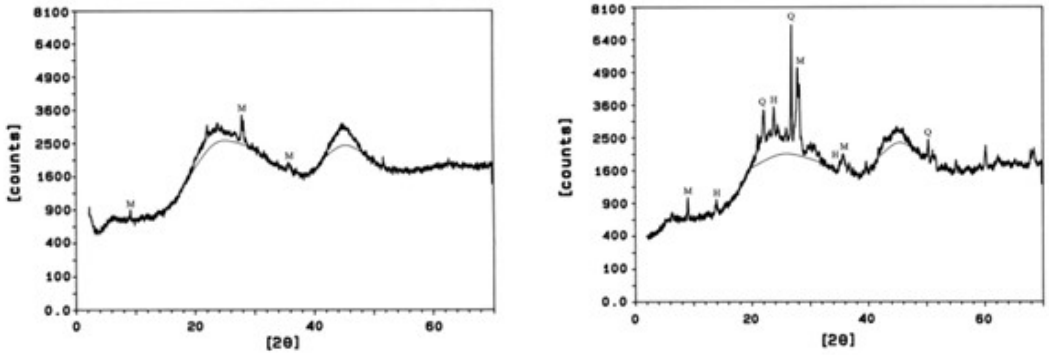

Figure 2.7: X-ray diffraction pattern of two perlite samples (M: muscovite, Q: quartz, H: hauyne, from [59].

Numerous researchers tested the mechanical properties of a concrete mix design containing perlite. Fodil and Mohamed state that a 10% replacement of Portland cement by perlite has a beneficial effect on the compressive strength of the concrete [60]. Ramezanianpour et al. studied the impact of calcined perlite powder as a supplementary cementitious material. The authors concluded that replacing 30% OPC with perlite would reduce the compressive strength by 8-12% [61]. Yu et al. replaced Portland cement partly with perlite powder and tested the compressive strength at 28 and 91 days. Especially at 91 days, the samples with added perlite powder reached higher strengths than the OPC samples [62]. Erdem et al. tested the compressive strength of blended cement containing perlite and OPC. The researchers conclude that the addition of perlite may cause strength losses, especially at an early age. However, due to the ongoing pozzolanic reactions, the compressive strength of the blended mixtures increases over time and might even exceed the strength of Portland cement [59]. Considering all studies, it can be concluded that perlite can be a successful supplementary cementitious material.

Finally, Erdogan tested the compressive strength of alkali-activated raw perlites using sodium hydroxide and waterglass as activators. At room temperature, $NaOH$ activation did not provide samples with sufficient strength. However, waterglass activated samples reached a compressive strength of 30-40 MPa at 28 days. At elevated curing temperatures (100°C), mixtures with a compressive strength of 40-50 MPa were obtained using either of the activators [63]. The perlite Erdogan used for his research is raw, not the commonly available expanded form.

Tsaousi et al. discussed the setting time of perlite geopolymer pastes, concluding that an increase in sodium hydroxide slows the setting time of the paste, whereas increasing the curing temperature to 90°C reduces the setting time [64]. These statements are in agreement with the findings of Erdogan (2015).

The durability of concrete mixtures with perlite additives was researched by Fodil and Mohamed, comparing 100% CEM-I based concrete to concretes containing 10%, 20% and 30% perlite. The authors have concluded that adding 10% perlite reduces the corrosion rate in an environment containing 5% NaCl for one year [60]. Bektas et al. found that the use of perlite powder in a concrete mix design showed potential to suppress alkali-silica expansion [65].

Investigation concludes that perlite has beneficial effects as supplementary cementitious material. As a precursor in alkali-activated cement, it has achieved sufficient strength at elevated temperatures. Considering the above statements, perlite shows good potential to be used in alkali-activated cement.

2.4.7. Pumice

Pumice is a light-coloured, natural volcanic material that contains pozzolanic properties. It is produced by the release of gases in melted, silica-rich lava, which then rapidly cools. This proces results in a very light, porous material. Pumice can be found in large quantities in volcanic regions in Germany, Turkey, Greece and Italy, amongst other countries [18, 66]. Because of the porous nature of this material, it is often used for lightweight structural applications, such as lightweight aggregates in concrete. Building structures containing pumice can be found in Europe and the USA, with some ancient structures in Rome still standing today [67, 68].

Because of the pozzolanic properties of the material, pumice is a promising precursor in alkali-activated binders. Several studies have been performed, assessing the use of pumice as a precursor. The pumice samples used in these studies are from different locations worldwide. Pumice 1 and 2 origins from Papua New Guinea, pumice 3 from Iran, Pumice 4, 5 and 7 from Turkey, Pumice 6 was commercially obtained in the USA, and pumice 8 was obtained in Italy. Table 2.8 shows an overview of the chemical compositions of the studied pumice materials.

Table 2.8: Overview of the chemical composition of pumice samples.

[wt.%]	Pumice1 (Hossain et al. 2011)	Pumice 2 (Hossain 2004)	Pumice 3 (Allahverdi et al. 2007)	Pumice 4 (Balun et al. 2021)	Pumice 5 (Safari et al. 2020)	Pumice 6 (Seraj et al. 2017)	Pumice 7 (Özodabas et al. 2013)	Pumice 8 (Occhipinti et al. 2020)
LOI	1,1	1,52	2,15	4,59	4,4	-	-	-
SiO_2	61,2	60,82	61,57	63,6	75,23	69	70	70,85
Al_2O_3	18,1	16,71	18	14,8	14,04	12	14	12,83
CaO	4,9	4,44	6,69	2,66	0,52	0,94	0,9	0,83
MgO	1,8	1,94	2,63	1,02	0,22	0,44	0,6	0,55
Fe_2O_3	7,4	7,04	4,93	6,75	1,95	1,2	2,5	2,37
TiO_2	-	-	-	-	0,11	-	-	0,15
K_2O	2,5	2,25	1,95	4,36-Na_2O	5,05	5,2	4	4,7
Na_2O	3,9	5,42	1,65	4,36-K_2O	2,09	3,8	5	4,46
SO_3	0,11	0,14	0,1	0,02	0,29	0,04	-	-

From the chemical compositions, it can be stated that there are roughly two types of pumice; pumice with a lower silica content and a higher alumina content (1, 2, 3 and 4), and pumice with higher silica and a lower alumina content (5, 6, 7 and 8). Overall, the chemical composition seems to be relatively consistent throughout the world. The SiO_2/Al_2O_3 ratio lies between 3,3 and 5,6. Therefore, pumice will be categorized in the second category of Djon Li Ndjock et al., indicating that a high activation temperature is required [45]. Several researchers performed XRD analysis on pumice samples, and every pattern showed a hump in the interval of 20-40°2θ. This hump suggests that each pumice sample contains a significant amount of similar amorphous phases [69, 18, 66, 70]. The pattern obtained by Balun and Karatas is shown below (Fig. 2.8).
The pumice samples have been assessed as both SCMs and AAMs. Hossain conducted two experiments on pumice as SCM in 2004 and 2011 (pumice 1 and 2). In both experiments, the compressive strength and the

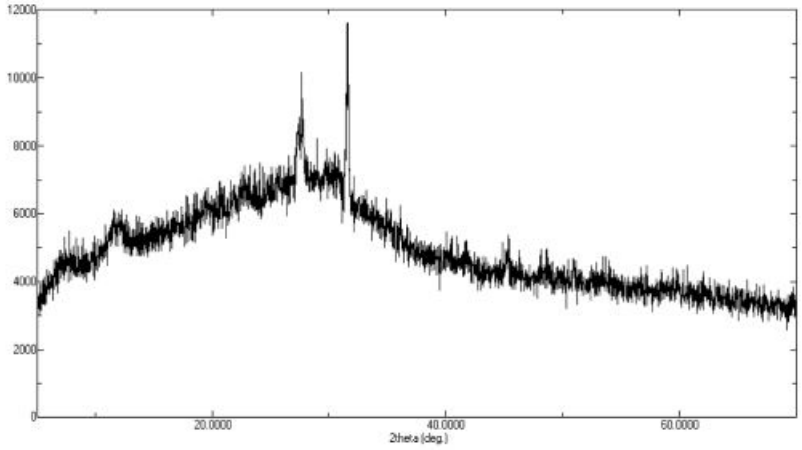

Figure 2.8: X-ray diffraction pattern of pumice sample, from [70].

slump of the mortars decrease as the percentage of pumice increases. However, reasonable strengths of 32 MPa and 28 MPa are achieved using pumice. Hossain concludes that pumice is a good option for SCMs, especially in volcanic regions, as it could decrease the costs [67, 68]. Seraj (pumice 6) has also researched the use of pumice as SCM, specifically the influence of the particle size on the performance of the pumice. All samples consist of 80% PC and 20% pumice. The smaller the particle size of the pumice, the more beneficial it is for the mechanical properties. However, the workability might decrease [18].

Numerous research has been performed on the use of pumice in alkali-activated binders. The pumice samples from Turkey all obtained a mechanical strength of over 35 MPa [66, 70, 71]. By varying the activator and the curing conditions, 100% pumice precursor paste samples could reach mechanical strengths from 37,2 MPa to 70 MPa. Balun and Karatas and Safari et al. found elevated curing conditions could gain optimum strength up to 80°C. Özodabas found that samples with a mixture of BFS and pumice had similar compressive strength as samples using 100% BFS. Therefore, this indicates that pumice from Turkey has sufficient reactivity to act as a precursor in alkali-activated binders [66, 70, 71, 72]. However, research performed by Occhipinti et al. (pumice 8), using pumice from Italy, showed no strength was obtained by activating the pumice samples. The authors stated that the reason for this was the lack of amorphous alumina in industrial pumice. Using an addition of 30% metakaolin, paste samples showed strength up to 14 MPa [69].

Özodabas et al. (pumice 7) assessed the durability of 100% BFS samples and 70% BFS + 30% pumice samples. The authors found that the addition of pumice increased the resistance to sodium sulphate and magnesium sulphate attacks [71].

Pumice shows potential to be a successful precursor in alkali-activated binders, taking all the research discussed into account. One condition is that the pumice is of good quality and contains sufficient amorphous phases. If there is enough amorphous content, pumice shows excellent potential to achieve adequate mechanical strength in alkali-activated binders.

2.5. Conclusion

There is a great need to reduce the environmental impact of concrete. One way to do so is to use an alternative binder. Alkali-activated binders are a promising alternative, which has been shown to achieve a CO_2 reduction of 80%. However, a shortage is predicted in the most commonly used precursors for alkali-activated binders (BFS and FA). Because of this shortage, there is an urge to find alternative precursors in alkali-activated binders. Successful precursors must contain reactive (hydraulic or pozzolanic) properties. The factors that influence the reactivity of materials are:

- Amorphous phase content
- Chemical composition
- Particle size

Volcanic materials could be a successful precursor because of the possibility that they contain amorphous phases. Four volcanic materials were discussed in this chapter: trass, phonolite, perlite and pumice. According to data available, all are reviewed based on their chemical composition, microstructure, particle size distribution and compressive strength when applied in binders. All four materials are aluminosilicates, with perlite and pumice belonging to the second category of Djon Li Ndjock and trass and phonolite to the first category [45]. Noticeable is that the chemical composition of trass is inconsistent throughout the world.

The particle size of all four materials is different; however, this is not a critical property since the grain size is relatively easy to manipulate (e.g., grinding). Research by Seraj et al. concluded that a smaller particle size results in more satisfactory mechanical properties [18]. The amorphous content of perlite is known since this is fundamentally a glassy material and therefore has an amorphous microstructure. Numerous researchers have assessed the amorphous content of pumice, and all research showed a significant amount of amorphous phases. The amorphous trass and phonolite content is unknown and must still be determined.

Perlite and pumice seem to have the most significant reactivity, according to literature. Therefore, they would be most likely to give adequate strength when applied in AAMs, not taking phonolite into account because of the little research performed. However, it is too soon to discard the potential implementation of phonolite and trass in alkali-activated binders since some factors are yet to be determined. A well-considered choice can be made as to which of the materials shows the highest potential for a precursor in an alkali-activated binder, considering the microstructure and the chemical composition of all four available materials.

The implementation of volcanic ashes in alkali-activated binders seems to be the most commercially and industrially viable option for the foreseeable future. However, as is shown in the literature above, volcanic materials are not of a homogeneous composition throughout the world, so verification of the use of volcanic materials in alkali-activated binders is necessary. Studies on the use of volcanic ashes in alkali-activated binders are still scarce. Therefore, it is crucial to perform research to validate the reactivity of volcanic materials and options on how to activate them [9].

I

Phase 1

3

Properties of raw materials

3.1. Introduction

This research focuses on four volcanic materials that are commercially available. Initially, this study will assess the potential reactivity of the raw materials. From literature research, it was found that there are three properties mainly responsible for the reactivity of materials: particle size, mineralogy and content of amorphous material, and chemical composition. Phase 1 will focus on determining these properties of the raw materials, together with classifying the materials based on their reactivity. The evaluation of the aforementioned properties will be performed according to the following methods:

- Particle size distribution and morphology
  - Laser diffraction analysis

    By performing a laser diffraction analysis, the particle size distribution is measured. A small particle size is crucial to exhibit reactive properties.
  - Brunauer-Emmett-Teller (BET) surface area analysis

    The BET measurements determine the specific surface area of materials. A larger specific surface area leads to more space available for the nucleation and growth of reaction products. Therefore, a large surface area is necessary to exhibit reactive properties.
  - Scanning electron microscopy

    By examining materials using microscopy, the shape of the particles is studied. The particle shape can explain the discrepancies between the particle size and surface area, and, also gives an indication on the workability of the material.
- Chemical composition
  - X-ray fluorescence

    By performing x-ray fluorescence analysis the elements present in the material are determined. To show hydraulic or pozzolanic behaviour, calcium, silicates or alumina species should be present.
- Amorphous phase content
  - X-ray diffraction

    By performing X-ray diffraction analyses, the crystalline phases of materials can be identified. By performing a quantitative analysis (QXRD), the amorphous phase content can be determined. Amorphous materials show higher reactivity.
- Classification of raw materials
  - Isothermal calorimetry

    The hydraulic or pozzolanic reaction mechanism is an exothermic reaction. Isothermal calorimetry measures the heat flow during the hydration of pozzolanic or (latent) hydraulic properties. A higher heat flow indicates higher reactivity.

– Thermogravimetric analysis

  The distinction between a hydraulic and a pozzolanic reaction mechanism is determined by the consumption of portlandite during hydration. The portlandite consumption can be determined by thermogravimetric analysis.

Based on the outcome of these tests, one can make an informed decision on potential ways to activate these materials for application in alkali-activated materials. Further analysis of these materials and their activation will occur in phase 2 and 3. Appendix B shows a more detailed description of the tests performed in phase 1. This chapter describes the experimental program.

3.1.1. Materials

The four examined volcanic materials are: trass, phonolite, perlite and pumice. These materials are more extensively described in section 2.4.4, 2.4.5, 2.4.6 and 2.4.7. All four materials are obtained as commercially available. The perlite used in this research origins from Turkey and Greece. Perlite is commercially available in expanded form, so in this research expanded perlite is examined. The used pumice originates from the Mediterranean sea region. The material obtained is not yet ground and, therefore, course and heterogeneous. The phonolite and the trass used in this research originate from the Eiffel region in east Germany. Phonolite and trass are both obtained in ground form. Figure 3.1 gives an overview of the origin of the four volcanic materials. Appendix C contains pictures of all four materials.

Figure 3.1: Origin of the volcanic materials used in this research.

3.2. Methods

3.2.1. Particle size distribution and morphology

The particle size distribution (PSD) is of importance for the reactivity of the material. Smaller particles react more quickly than larger particles because of the relatively larger surface area [13]. The grain size is relatively easy to adjust (e.g. grinding) and significantly influences the reactivity of the materials. Because some materials are known to be porous (expanded perlite), next to the PSD, the particle's specific surface area is determined. Finally all materials are analysed using scanning electron microscopy (SEM), to visualize the particles morphology and explain possible unexpected outcomes.

Laser diffraction analysis (LDA) determines the PSD of the materials in volume [%]. This research uses wet LDA; Appendix B shows more on this test. Each PSD analysis consists of three consecutive measurements, which shows the average as a final result. The material is sampled by quartering a large representative sample before adding it to the equipment. This way, a representative measurement is ensured.

BET surface area analysis measures the surface area of the particles in m^2/kg. The larger the surface area, the more space there is for nucleation and growth of the reaction products and, thus, the more reactive the

material is. For the analysis, the material is put in the glass test tube, then placed in the equipment. Apart from the four volcanic materials, the surface area of BFS is also measured, as reference. The reference glass beads and the height of the tube determine the amount of material used in the measurement. The analysis is performed at an evacuation rate of 400 mm Hg/min, evacuation time of 3 minutes and equilibrium time of 3 seconds. The number of glass beads added in the reference tube was 25, except for perlite, which used 20 beads. Perlite requires fewer beads because the material is very porous and light. Liquid nitrogen is used as an absorption material.

By performing SEM analysis the morphology of the particles can be made visible. The visualization of the particles helps explaining the PSD and surface area results. For the execution of the SEM analysis, a very small fraction of the material was put on a carbon sticker. The morphology of the materials is visualized at 125, 500 and 25000 magnitudes. For trass and phonolite, the raw material is used. For perlite and pumice, the sieved fraction ($< 63\mu m$) is used, otherwise the particles were too large for the image.

3.2.2. Chemical composition

The chemical composition is essential to determine the potential reactivity of the material. As mentioned before, to be a successful precursor, the material must contain a sufficient amount of reactive calcium or silicates [14, 34]. Also the ratio of silicates to aluminates is important.

X-ray fluorescence is used to determine the chemical composition of the raw materials. Note that XRF is an elemental analysis, so the exact minerals present remains unknown. The measurements were performed with a Panalytical Axios Max WD-XRF spectrometer on 2 g of each material. SuperQ5.0i/Omnian software is used for data evaluation. The material should have a maximum particle size of $63\mu m$ to maximize the elements' exposure to ensure a representative result. The PSD is determined by performing the LDA, then can be determined if it is necessary to grind materials for XRF.

3.2.3. Amorphous phase content

By performing an XRD, the presence of crystalline and amorphous phases can be determined. For a material to be reactive, amorphous phases are preferred [22]. By completing a Rietveld refinement analysis and quantitative x-ray diffraction (QXRD) , the amorphous phase content can be quantified and compared.

X-ray diffraction is used to determine the microstructure of the material. The outcome of the XRD is a diffractogram. The peaks in this diffractogram indicate the presence of a crystalline phase, whereas a hump suggests the presence of amorphous material [73]. For QXRD measurements, the material is mixed with an internal standard. 10% of the material should be the reference material, in this case, silicon powder. Therefore, 0,2 g of silicon powder was mixed using a mortar and pestle with 1,8 g of the measured volcanic material. The measurements were performed by depositing approximately 0,5 g in PMMA holder L25. The range that is measured is $8-110^{\circ}2\theta$, the counting time per step is 2 s with a step size of $0,020^{\circ}2\theta$. For XRD, the exposure of the crystal planes must be maximized. Therefore, the material must have a maximum particle size of $\pm 60\mu m$. The LDA determines whether or not the material must be ground.

After the analysis, the quantity of the amorphous phase content has to be determined. Profex software is used for the Rietveld refinement and calculations. With a known addition of silicon powder, one can determine the total amount of amorphous phases. Using data from [74] the chemical composition of the amorphous phase content can then be determined.

3.2.4. Classification of raw materials

The reactivity of the raw materials will be analyzed according to a modified R^3 test, a method proposed by Suraneni et al. [75]. Ramanathan et al. tested and confirmed this method [76]. The exothermic reaction of the hydration of the raw material is the base of this method. The heat released during hydration is measured by performing isothermal calorimetry. par The reactivity test is performed by mixing precursors with $Ca(OH)_2$ in the ratio 1:3, using a mortar and pestle. The SCM-calcium hydroxide blend is mixed for three minutes with a 0,5M potassium hydroxide solution in a water-to-solid ratio of 0,9, after which the ampoule is put in the calorimeter. The calorimetry runs in an environment of 50°C. The heat flow from the samples was recorded for ten days, after which they were removed. For each volcanic material, at least three repetitions are measured. The reference sand sample determines the total weight, which cannot be too large for the ampoule.

Next to the four volcanic materials, FA and BFS samples are also analyzed using calorimetry to compare the volcanic materials with known precursors. This way, the volcanic materials can be classified in compar-

ison to known precursors. If the reactivity is not sufficient compared to FA or BFS, one can decide whether further manipulation of the volcanic materials is necessary (i.e. calcination or grinding).

After the samples were removed from the calorimeter, the reacted materials were examined by thermogravimetric analysis (TGA). The ampoule was broken, after which $35-40\mu g$ was removed and put in the crucible for the study. The TGA is performed in the range of $40-900°C$, with the temperature rising each minute with $10°C$. The weight loss of the material is measured during the temperature rise. The weight loss due to the decomposition of $Ca(OH)_2$ occurs at a temperature range of $400-500°C$, due to the following reaction:

$$Ca(OH)_2 \rightarrow CaO + H_2O \tag{3.1}$$

One can calculate the consumption by knowing the initial $Ca(OH)_2$ content and the loss. The measured $Ca(OH)_2$ from TGA is determined according to [73]. The molecular masses of portlandite ($m_{Ca(OH_2} = 74g/mol$) and water ($m_{H_2O} = 18g/mol$) are used. It is determined as follows:

$$Ca(OH)_{2,measured} = WL_{Ca(OH)_2}\frac{74}{18} \tag{3.2}$$

The initial portlandite content is known, subtracting the measured content from the initial content results in the final portlandite consumption.

3.3. Particle size distribution and morphology

Laser diffraction analysis (LDA) has been performed on all four raw materials. Appendix C presents pictures of these materials. LDA measures the particle size distribution (PSD), which indicates whether a material is finely or coarse-grained. LDA is a good technique for the analysis of more fine-grained particles. The maximum size to be accurately measured by LDA is approximately 1 mm. For materials that contain larger particles, sieving is used to determine the PSD. Sieving is a good technique for more coarse-grained particles. However, the fraction below $53\mu m$ cannot be accurately determined. Note that the obtained PSD from LDA is calculated as a percentage of total volume, and the PSD from sieving is calculated as a percentage of the total mass.

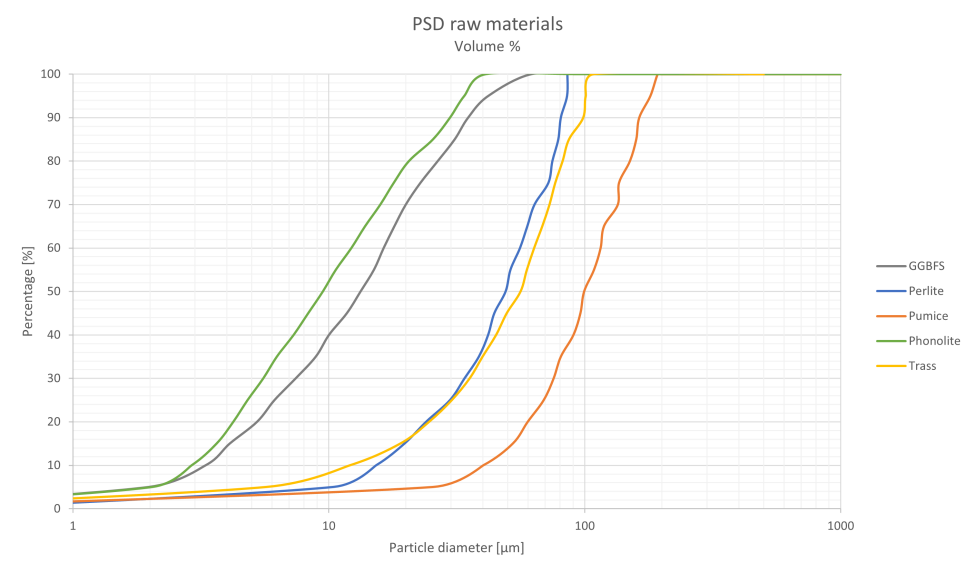

Figure 3.2: PSD of volcanic materials and reference GGBFS, determined by wet LDA. Cumulative undersize [volume %].

The particle size distribution graph shows the LDA results. As a reference, a PSD of GGBFS is given (from:[77]) (Fig.3.2). Because perlite and pumice contain more coarse particles and the LDA technique is not fit to measure particles over 1 mm, the PSD of perlite and pumice is also determined by sieving. The results are shown in Figure 3.3. The two graphs cannot be combined because of the different bases on which the PSDs are normalized. Next to measuring the PSD, the surface area is measured. Table 3.1 presents the D10,

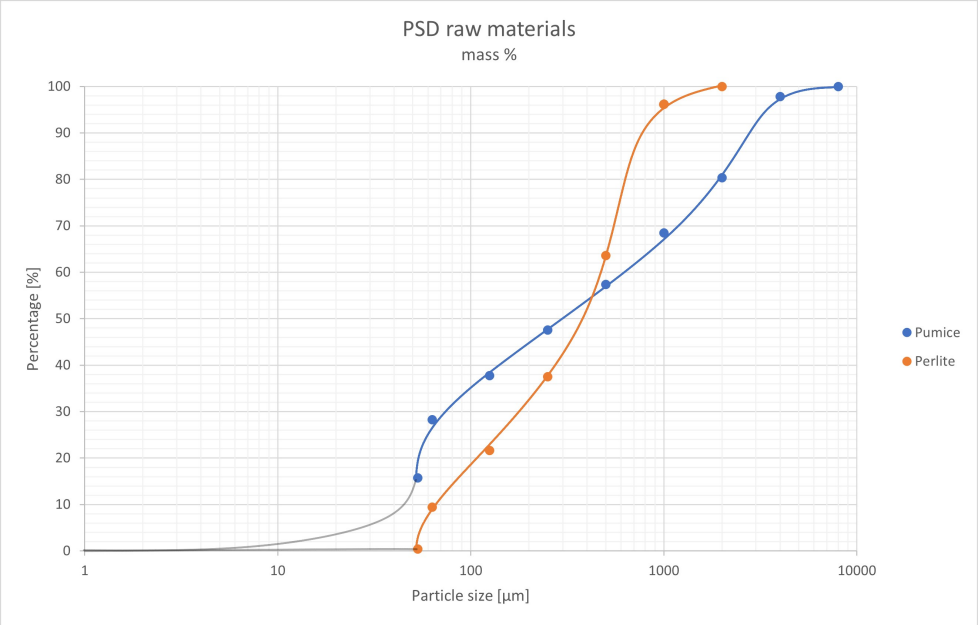

Figure 3.3: PSD of perlite and phonolite, determined by sieving. Cumulative undersize [mass %]. The PSD below 53μm is an estimation since sieving cannot determine these values.

D50 and D90 values and the measured surface area of the materials. Finally, the morphology of the materials is analyzed by scanning electron microscopy (SEM). All SEM images are enclosed in appendix D.

Looking at the pictures of the raw materials (Appendix C), one can see that phonolite and trass are fine powders, perlite seems to be more coarse, and pumice is the most coarse material of all. Graph 3.2 shows unrepresentative PSDs, as evidenced by the lack of a bendline to 100%. This vertical line represents the unmeasured coarser grains. Two reasons why these materials probably were not measured are:

1. Porous materials are very light. Therefore, the larger particles stayed afloat in the equipment and were not measured.

2. Since wet LDA is performed, the particles have to travel through tubes. Coarser particles are too large to pass through these tubes.

The PSD obtained by sieving perlite and pumice confirms that LDA did not measure the larger particles. Because of the non-measured particles by LDA for perlite and pumice, the D10, D50 and D90 values of the sieved PSD are used. Note that one cannot determine the D10 value for pumice because of incomplete information on the particle size below 53μm, which is indicated in the graph as a grey line. For trass and phonolite, the values from LDA are used (Table 3.1).

Table 3.1: D10, D50 and D90 values (perlite and pumice from sieving, phonolite and trass from LDA) and BET surface area raw materials.

Volume	D10 [μm]	D50 [μm]	D90 [μm]	[m^2/kg]
Perlite	65	360	780	1567,9
Pumice	-	300	3000	982,8
Phonolite	3	10	30	3505,2
Trass	13	53	96	7941,8
GGBFS				1540,9

The PSD shows that phonolite is a very fine-grained and homogeneous powder. The material is even finer than GGBFS. The specific surface area of phonolite is relatively large compared to GGBFS, as presented in Table 3.1. The PSD and the specific surface area indicate that the material's particle size is sufficiently small to be reactive. SEM images support these findings, and they show high amounts of small particles and some larger particles with a large surface area, sometimes due to agglomeration (Figure 3.4).

Trass is coarser than phonolite, with the largest particle size smaller than 100μm. The specific surface area of trass is substantial compared to the PSD (Table 3.1). A large surface area is very beneficial for the

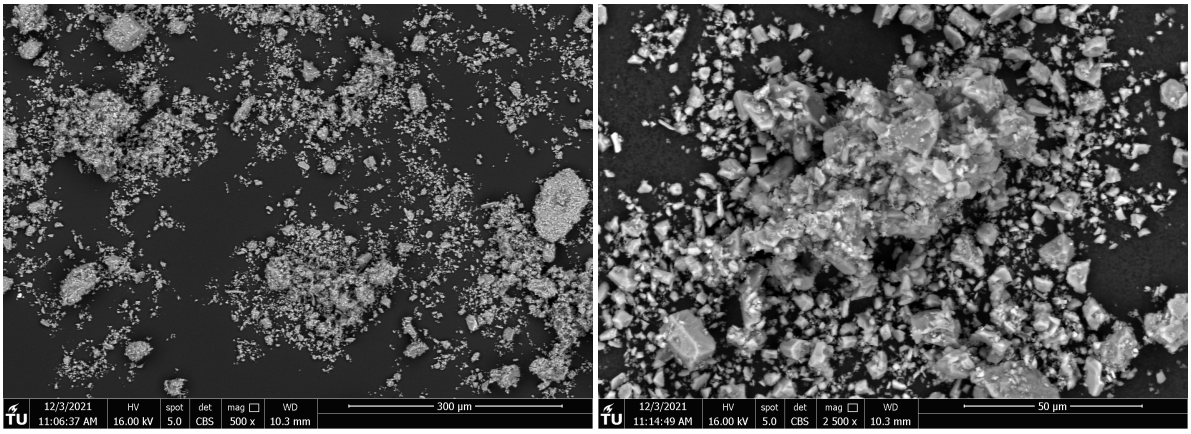

Figure 3.4: SEM images of phonolite, left: overview, right: agglomeration of a larger particle.

precipitation of new phases. The SEM images (Figure 3.5) of trass show that some of the larger trass particles are agglomerates, which explains the large surface area and that the smaller particles are not shown in the PSD. The PSD from trass is therefore not representative. Considering the large surface area, one can conclude that trass is sufficiently fine to be reactive.

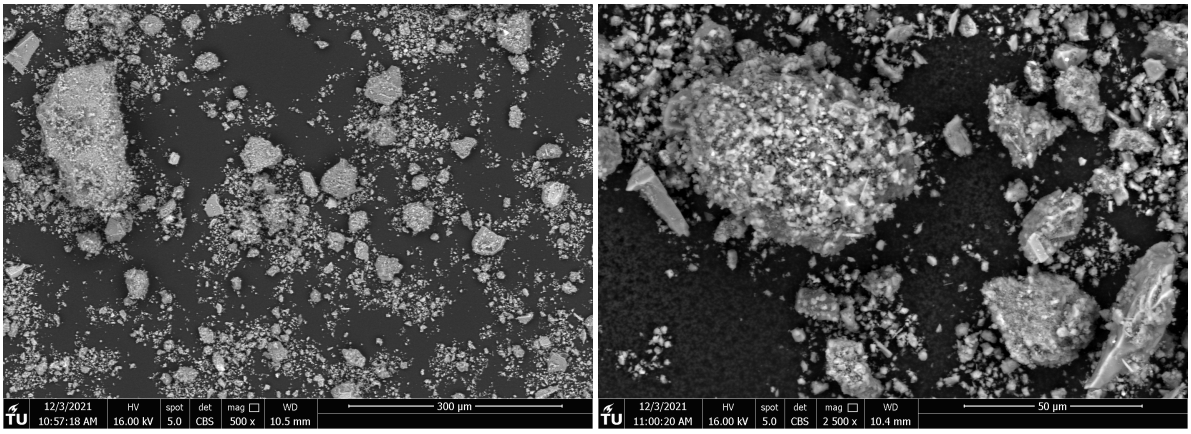

Figure 3.5: SEM images of trass, left: overview, right: agglomeration of a larger particle.

Perlite seems to have a similar PSD as trass. However, the LDA equipment did not measure larger perlite particles, indicated by the top of the perlite line, which goes straight up instead of continuing in the same slope. Sieving the material results in a more representative PSD, including these large particles. Figure 3.3 presents the results of the PSD of perlite obtained by sieving. The specific surface area of perlite is approximately 1500 m^2/kg, which is similar to the GGBFS sample. However, it is known that perlite is expanded, which results in porous material. The BET analysis also measures the internal surface area [73], which will not participate in the reaction mechanism. Consequently, the measured surface area is an overestimation of the surface area that is useful. Considering the specific surface area and the D10, D50 and D90 values of the sieved PSD, perlite is too large to show reactive behaviour. The SEM images of perlite (Figure 3.6) show that this material is flake-like. The morphology of perlite results in an inadequate PSD since the LDA is based on sphere-like particles, which perlite is not. Considering the shape of the perlite particles, the measured PSD from LDA is an overestimation. Taking the larger particles that were not measured by the equipment, one can assume that the finer particles are smaller than shown in the PSD from LDA, and the coarser particles are larger than measured by LDA. Based on the sieved PSD and the specific surface area, this material is probably not sufficiently small to react successfully. Also, the angular shape of the particles suggests that the workability of paste made with this material is low.

Pumice is the most coarse material, and the material seems heterogeneous. The LDA equipment did not measure the largest particles because they were too large for the equipment. To still have an accurate idea of the PSD of pumice, the PSD has been determined by sieving, shown in Figure 3.3. The SEM images (Figure 3.7)

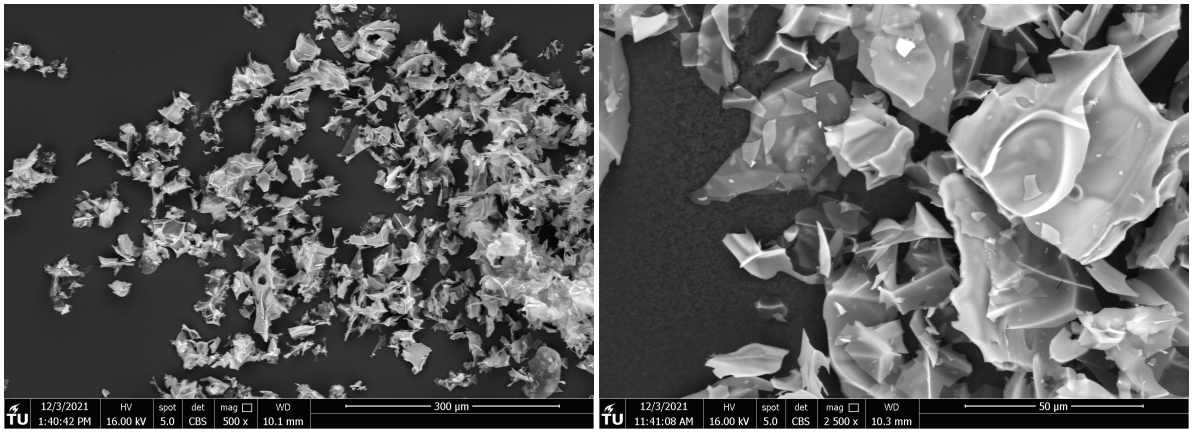

Figure 3.6: SEM images of fraction [$< 63\mu m$] of perlite, left: overview, right: flake-shaped particles.

show that pumice particles hardly agglomerate, except for the smaller particles that get into larger particles' pores. One can conclude that the particles are too large and must be ground to be successfully reactive.

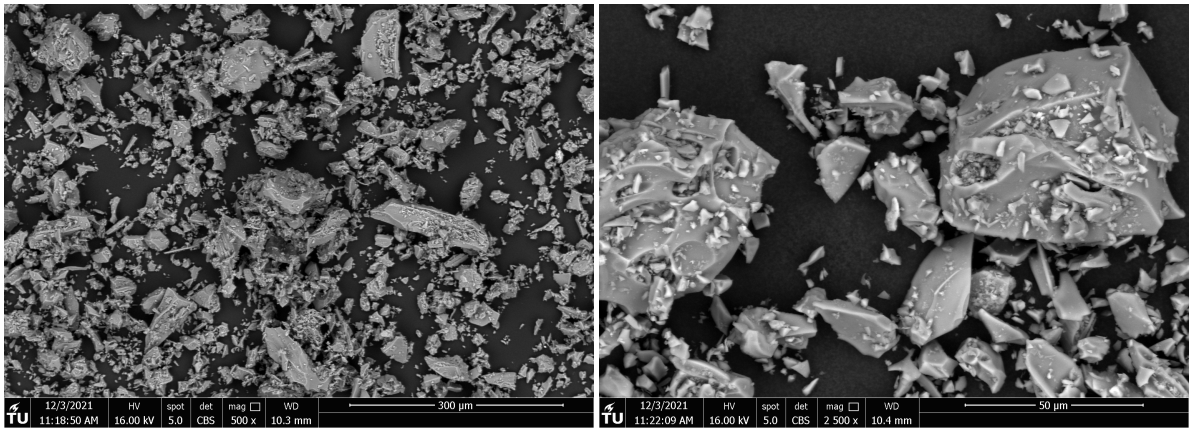

Figure 3.7: SEM images of fraction [$< 63\mu m$] of pumice, left: overview, right: larger particles containing pores.

3.4. Chemical composition

The chemical composition of the four materials has been determined by performing XRF analysis. Table 3.2 shows the obtained chemical compositions.

The chemical composition of perlite and phonolite is similar to what is found in the literature. The compositions of trass and pumice found in the literature vary. The compositions found from the XRF in this research were similar to those found by Indrawati and Manaf, Safari et al., Occhipinti et al. and Ozodabas et al. [47, 49, 66, 69, 71]. Phonolite and trass have a SiO_2/Al_2O_3 ratio lower than 3, and perlite and pumice have a SiO_2/Al_2O_3 ratio higher than 4. According to Djon Li Ndjock et al., the activation temperature would be around 30°C for phonolite and trass and above 80°C for perlite and pumice [45]. An important note is that these statements concern the chemical composition of the amorphous phase, which still has to be determined (section 3.5). Figure 3.8 shows the volcanic materials compared with OPC, BFS and FA. It indicates that volcanic materials contain lower calcium than the more commonly known precursors. The lack of calcium strongly influences the reactive behaviour of the materials, and it is expected that these materials show pozzolanic behaviour.

All four materials contain a significant amount, over 7%, of alkalis (Na & K). These alkalis might influence the microstructure and composition of the hydration products. In Ca-rich alkali-activated binders, alkalis can be incorporated into the reaction products (C-S-H-gel). They are considered network modifying ions and therefore disrupt the network (as mentioned in section 2.3.2). This disruption causes the presence of alkalis to reduce the chain length of the C-S-H gels formed [4, 78]. There is a maximum of alkalis that can

Table 3.2: Overview chemical composition of the four volcanic materials.

[wt.%]	Phonolite	Trass	Pumice	Perlite
SiO_2	55,082	58,492	74,946	76,315
Al_2O_3	23,197	20,840	13,091	13,462
Na_2O	7,956	3,953	3,987	5,170
K_2O	7,190	5,029	3,827	2,174
Fe_2O_3	3,221	5,097	1,461	0,770
CaO	1,394	3,469	1,640	1,647
MgO	0,479	1,567	0,434	0,139
TiO_2	0,340	0,700	0,127	0,097
Cl	0,299	-	0,306	-
CO_3	0,277	0,156	-	-
MnO	0,238	0,186	-	-
P_2O_5	-	0,217	-	-

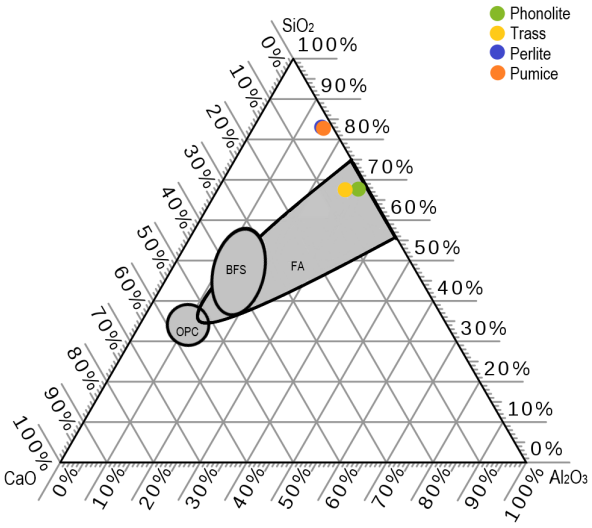

Figure 3.8: Ternary plot of the chemical compositions of the volcanic materials with ordinary portland cement, blast furnace slag and fly ash as references, after [9]. Note that perlite is visible behind the pumice point, both have very similar chemical compositions.

be incorporated in the network, depending on the amount of calcium and silicates. The alkalis that are not incorporated in the network can be either physically absorbed on the surface of hydration products or free in the pore solution [4, 79]. The presence of alkalis also could influence degradation mechanisms such as alkali-silica reaction (ASR). ASR is the reaction between silica from cement (or the alkali-activated binder) with reactive silica in the aggregates. Due to this reaction, a gel is formed, which absorbs water and starts to expand, which causes stresses in the concrete and consequently cracking [1, 4]. Studies have shown that alkalis incorporated in the reaction products reduce the risk of ASR [80]. Also, silica and alumina and a reduction of calcium present lessen the risk [81].

All four materials seem to have the ability to be reactive because of the presence of silica and alumina, taking only the chemical composition into account, not the amorphous phase content. Phonolite and trass have the highest potential to react because they are assumed to dissolve more quickly because of the lower SiO_2/Al_2O_3 ratio. However, it is essential to note that the amorphous phase content is significant, which is determined by QXRD analysis. The considerable amount of alkalis present in the materials could influence the hydration products and cause a reduction in the chain length. The alkalis could also cause a higher risk of ASR, depending on whether or not they are incorporated in the reaction products.

3.5. Amorphous phase content

XRD determines the microstructure of the materials. Most important is the determination of the amorphous phase content. The obtained XRD patterns of the four materials are shown below.

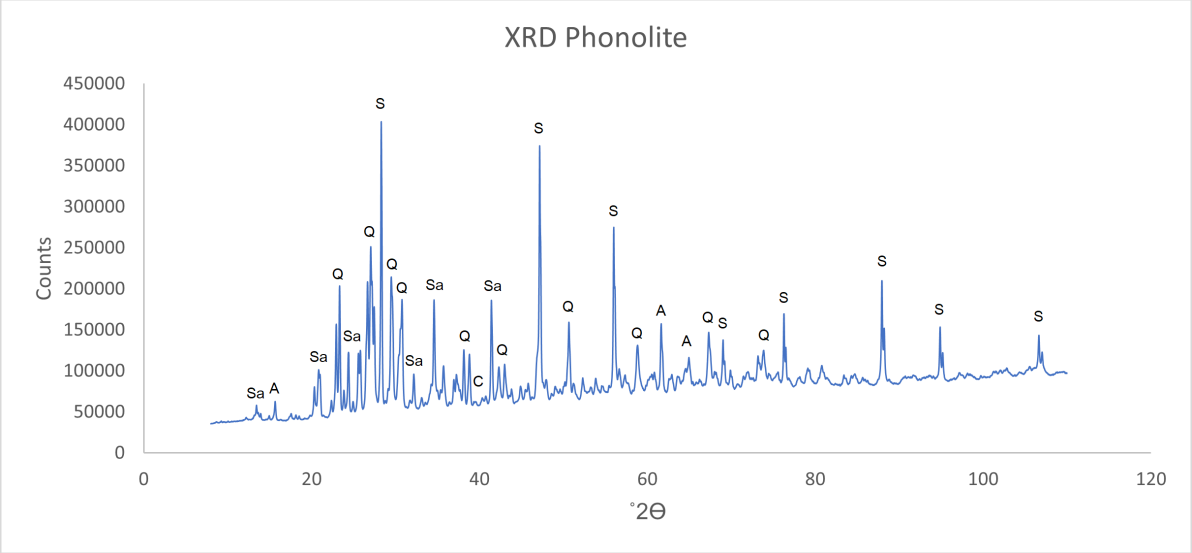

Figure 3.9: XRD pattern phonolite (A = Analcime, C = Calcite, S = Silica, Sa = Sanidine, Q = quartz).

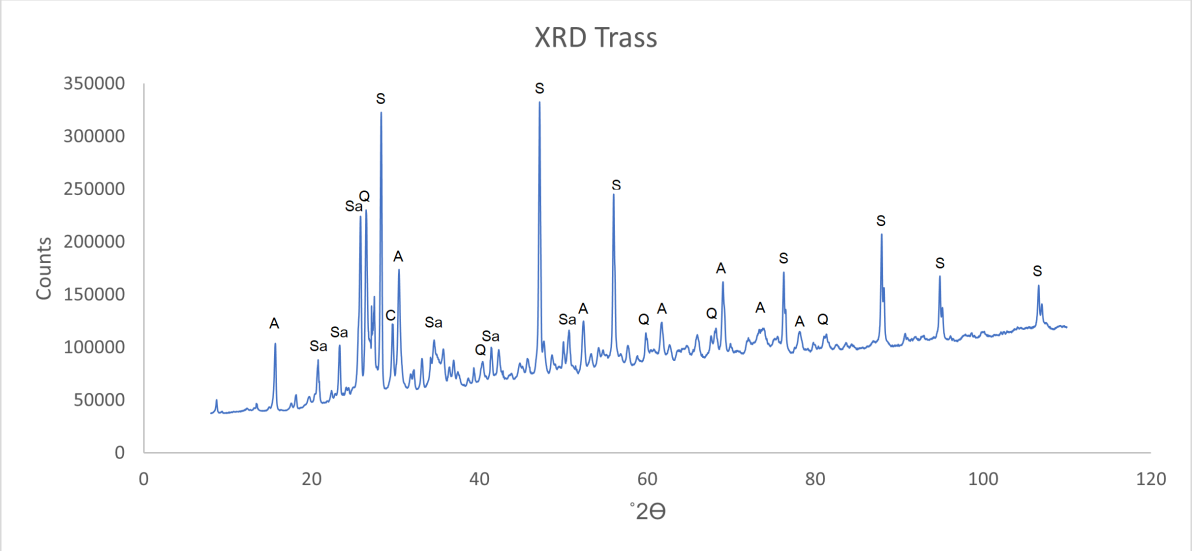

Figure 3.10: XRD pattern trass (A = Analcime, C = Calcite, S = Silica, Sa = Sanidine, Q = quartz).

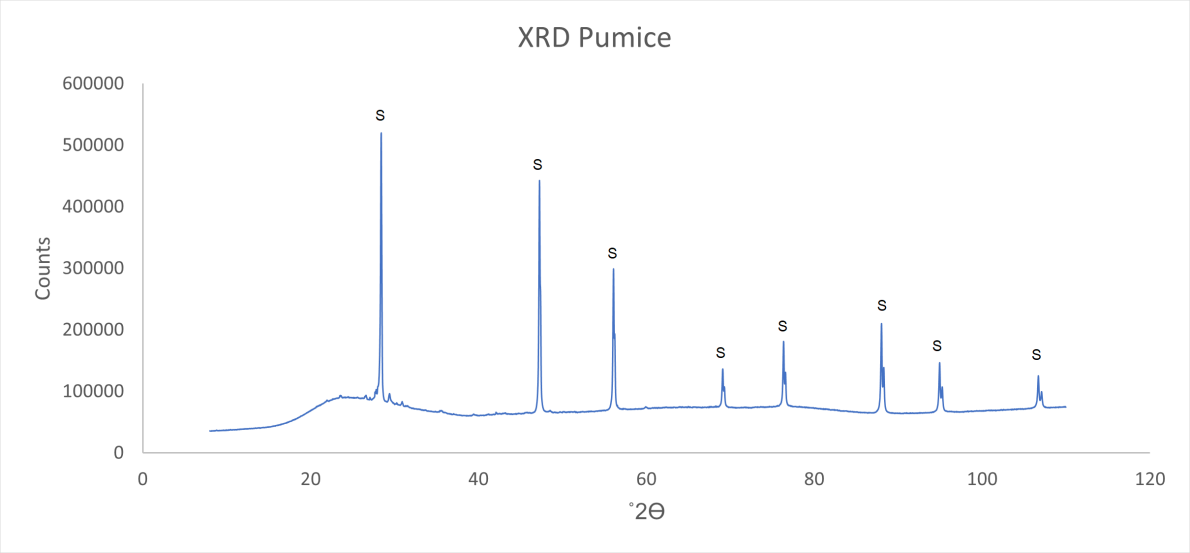

Figure 3.11: XRD pattern pumice (S = Silica).

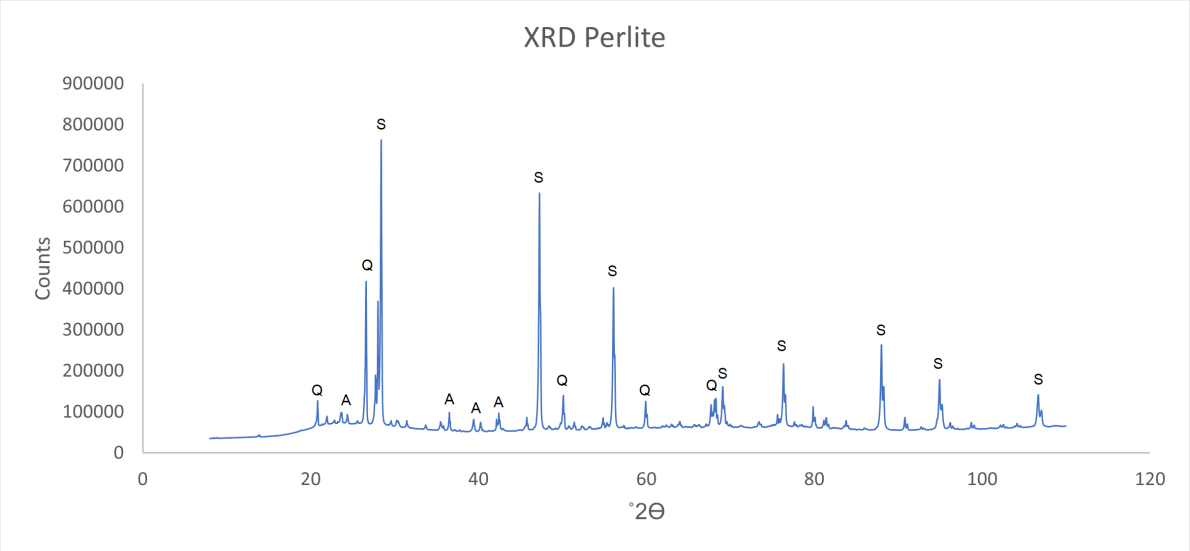

Figure 3.12: XRD pattern perlite (A = Albite, S = Silica, Q = Quartz).

The crystalline phases are shown as a sharp peak in the XRD patterns. The identified crystalline phases are highlighted and shown in the legend in all four patterns. Amorphous phases cannot be identified but are shown in the pattern as hump. All four materials show sharp peaks with high intensities at 28, 47, 56, 69, 76, 88, 95 and 106 °2θ. As is shown in the legend, these peaks refer to the added silicon powder. This powder was added as 10% of the total sample as reference material for amorphous phase quantification (QXRD). The obtained minerals and their chemical formula are shown below in Table 3.3

Table 3.3: Overview of the measured minerals and their chemical formula, after [74].

Mineral	Formula	Mineral	Formula
Muscovite	$KAl_3Si_3O_{10}(OH)_{1.8}F_{0.2}$	Calcite	$CaCO_3$
Analcime	$NaAl(Si_2O_6).(H_2O)$	Nepheline	$Na_{0.75}K_{0.25}Al(SiO_4)$
Quartz	SiO_2	Albite	$Na_{0.95}Ca_{0.05}Al_{1.05}Si_{2.95}O_8$
Sanidine	$K_{0.75}Na_{0.25}AlSi_3O_8$	Dolomite	$CaMg(CO_3)_2$

Looking at the obtained patterns, it can be clearly stated that phonolite and trass are crystalline materials, showing mostly sharp peaks. The crystalline nature of trass and phonolite is not unexpected since they originate from the Eiffel region, which has been inactive for more than 11.000 years [53]. During this time, the amorphous phases that might have been present have reacted and become crystalline. The identified phases of phonolite and trass correspond to the earlier obtained chemical composition, their main elements being silicates and aluminates. Sanidine is the main crystalline phase in both materials. Figure 3.13 shows the results from the QXRD of both trass and phonolite. From quantification of amorphous phases, it is determined that the amorphous phase content of phonolite is 5,58% and of trass is 43,491%. The amorphous phase content of phonolite is very low, suggesting that the reactivity of this material is probably low. Trass has a higher amorphous phase content but is insufficient to be a promising precursor. The chemical composition of the amorphous content cannot be accurately determined, considering the low amorphous content and the margin of error that is included when performing Rietveld refinement analysis.

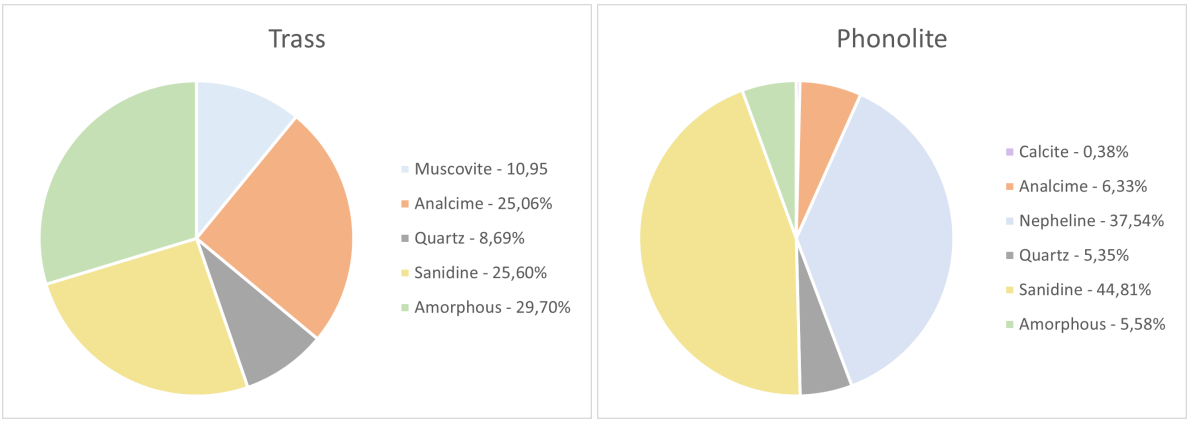

Figure 3.13: Composition of phases obtained from QXRD, left: trass, right: phonolite.

The XRD pattern of pumice shows a large hump in the range $15-35°2\theta$. Apart from the silica, some crystalline phases are identified, but they all have relatively low intensity. Primarily albite is identified, shown in Figure 3.14. The lack of crystalline peaks indicates the presence of primarily amorphous phases. Quantification of the amorphous phases confirms this hypothesis. The amorphous phase content calculated is 94,98%. The high amorphous phase content of pumice is promising for the material's reactivity.

The perlite XRD patterns also show a hump in the range of $15-35°2\theta$. These humps are similar to what is found in the pumice sample but with a lower intensity. However, more and more intense crystalline peaks are identified in the perlite sample. The hump implies the presence of amorphous phases, although less than in the pumice sample. Quantification of the amorphous phases confirms this hypothesis. The amorphous phase content calculated is 81,94%, shown in Figure 3.14. The content is lower than pumice, but still a promising result and corresponding to the findings from the literature [59]. Two crystalline phases are identified: albite and quartz, both primary consisting of silica. With the known chemical composition of both materials and the known crystalline phases present, the amorphous phase content's chemical composition

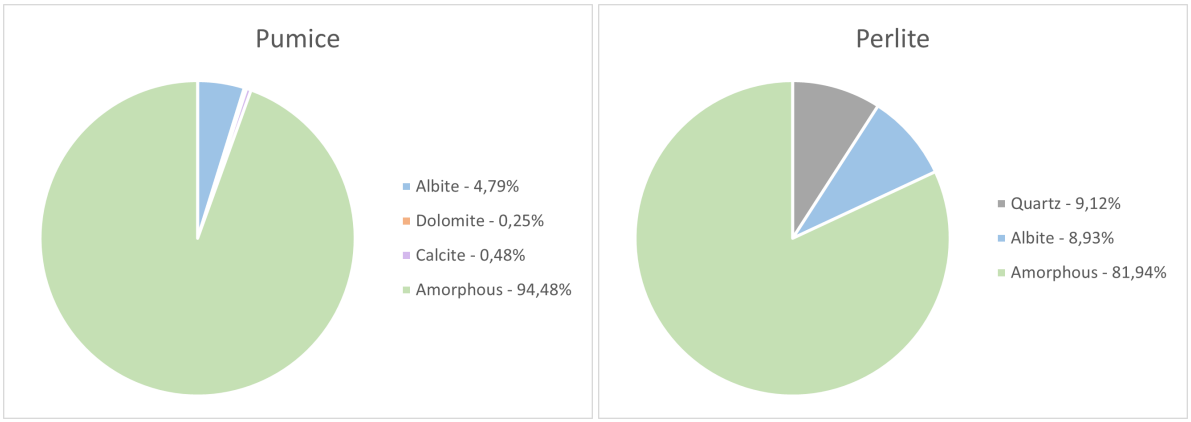

Figure 3.14: Composition of phases obtained from QXRD, left: pumice, right: perlite.

can be determined and shown below (Tab.3.4). The chemical composition of the amorphous phases of both materials is reasonably similar. A slight difference is that perlite contains more alumina, which benefits the SiO_2/Al_2O_3 ratio. However, one cannot conclude that perlite is the more reactive material from this analysis. It is such a subtle difference that it might be due to the marginal error in the Rietveld refinement, and the reactivity also depends on the fineness of the material.

Table 3.4: Chemical composition of the amorphous phases of perlite and pumice.

[wt.%]	Perlite	Pumice
SiO_2	74,64	75,91
Al_2O_3	15,21	12,82
Na_2O	5,09	3,65
K_2O	2,65	4,05
CaO	1,89	1,32
Fe_2O_3	0,94	1,55
MgO	0,17	0,41

3.6. Classification of raw materials

A modified R^3 test assesses the reactivity of the materials after research from Suraneni et al. [75]. The heat release from the volcanic material and two reference samples were measured. The hydraulic or pozzolanic reactions that are expected to take place are rough as follows (the exact response depends on the SCM that is measured [3, 22]($A = Al_2O_3, C = CaO, H = H_2O, S = SiO_2$):

$$AS + CH + H \rightarrow C-S-H + C-A-H \tag{3.3}$$

The reaction products that are formed primarily constitutes C-S-H. Dissolved alumina can be incorporated in the C-S-H gel or can form calcium-alumina-hydrates (C-A-H) [3]. The pozzolanic reaction is exothermic, meaning heat will be released when these reactions take place. The higher the measured heat flow, the more reactive material is. The total heat release is determined by calculating the area underneath the heat flow graph. The results are shown in Figure 3.16. Slag and fly ash are used as references. The materials can be classified by their total heat release: inert for <125 [J/g], less reactive for >125 [J/g] and <375 [J/g] and more reactive for >375 [J/g]. After measuring the heat release, the calcium hydroxide consumption was measured by performing TGA measurements on the reacted samples. The results of the heat release measurements are shown in Figure 3.15.

Noticeably, the slag sample shows a second shoulder, whereas the other materials do not display this shoulder. This second shoulder indicates that the reaction of slag continues for a longer time than the other materials, leading to a higher total reactivity even though the initial peak of slag is not as high as that of different materials. Fly ash shows similar behaviour; it does not show this second peak as clearly as BFS, but because the reaction goes on for a longer time, the total reactivity is relatively high compared to the other materials.

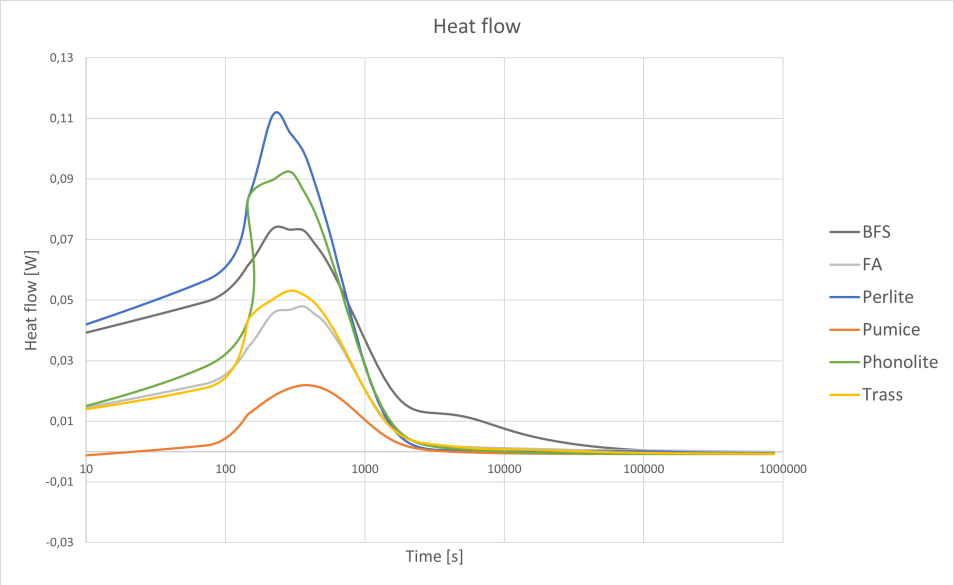

Figure 3.15: Average heat flow of volcanic materials, with blast furnace slag and fly ash as references. It is measured by isothermal calorimetry (ten days).

Figure 3.16 shows the total heat release, derived from Figure 3.15. The first thing that stands out is that all four volcanic materials have significantly lower heat release than slag and fly ash and are classified as inert by Suraneni et al. [75]. Of all volcanic materials, perlite seems most reactive, whereas pumice seems least reactive. The higher reactivity of perlite agrees with the previously found results; the material contains amorphous alumina- and silica-oxides. However, the reactivity is still insufficient, and the material is classified as inert. The inert nature could be because of the particle size of the perlite sample. As mentioned before, grinding the material is necessary. Pumice shows the lowest heat release of all the materials. The low heat release is most likely because pumice is the most coarse of all materials.

Phonolite and trass both show low heat release at ten days, presumably because of the microstructure of both materials, which are both predominantly crystalline. Both materials have a similar chemical composition, shown in the total heat release. The main difference between the two materials is the PSD, where phonolite has the smaller PSD and trass the larger specific surface area.

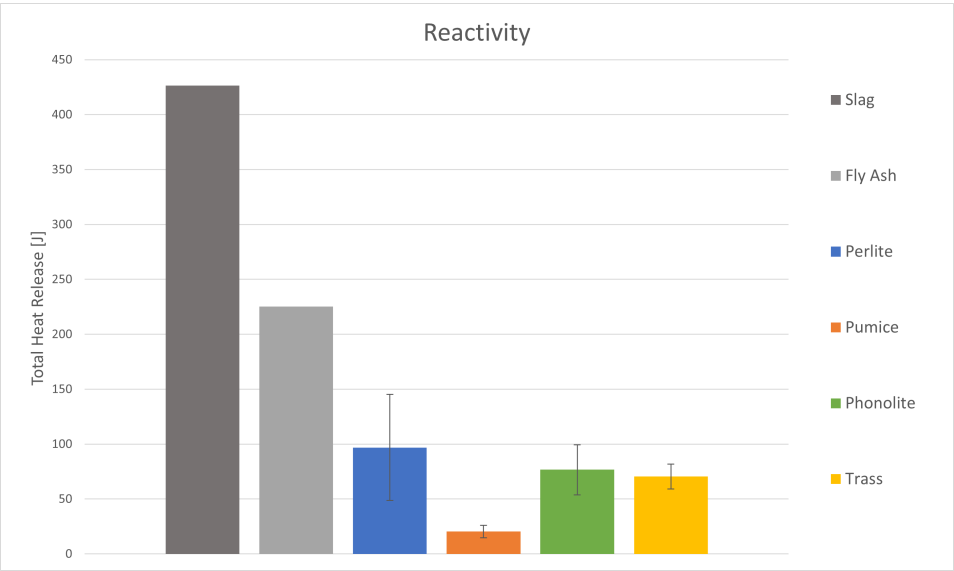

Figure 3.16: Total heat release volcanic materials with blast furnace slag and fly ash as references. The area under the heat flow curve is determined from isothermal calorimetry (ten days).

The results of the calcium hydroxide consumption measurements are shown below. In Figure 3.17 the mass loss in percentages is shown. Figure 3.18 shows the rate of mass loss. The loss in calcium hydroxide is identified in the second drop/peak from 400-500°C. The more significant the drop in Figure 3.17, and the larger the peak in Figure 3.18, the more $Ca(OH)_2$ is lost during the TGA measurement. The higher the loss during the TGA measurements, the less $Ca(OH)_2$ the precursor consumes. The final loss of $Ca(OH)_2$ is determined according to [73], which is more extensively discussed in section 3.2.4.

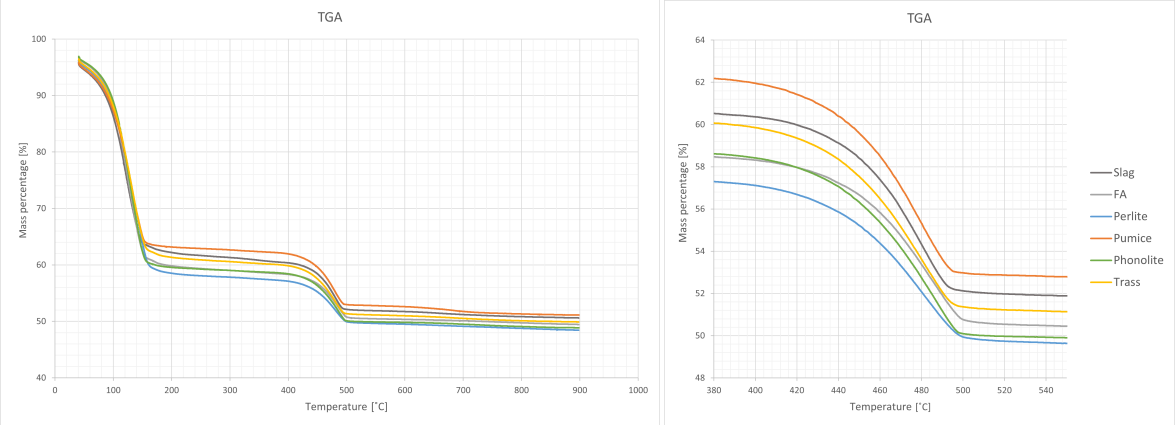

Figure 3.17: Mass loss [%] plotted to increasing temperature for the volcanic materials with blast furnace slag and fly ash as references, measured by thermogravimetric analysis. left: 0 - 1000 °C, right: 380 - 550 °C.

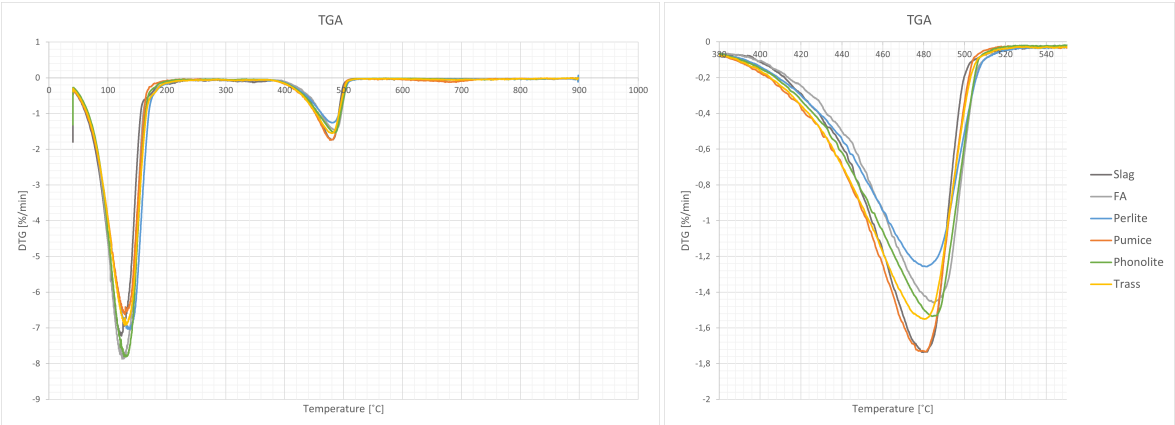

Figure 3.18: Rate of mass loss [%/min] plotted to increasing temperature for the volcanic materials with blast furnace slag and fly ash as references, measured by thermogravimetric analysis. left: 0 - 1000 °C, right: 380 - 550 °C.

The DTG graph (Fig.3.18) shows that perlite has the lowest peak, meaning high $Ca(OH)_2$ consumption of the material, corresponding with the relatively high reactivity of perlite measured during the calorimetry. Slag has a higher peak, meaning little $Ca(OH)_2$ consumption of the material, even though it is the most reactive of all measured materials. The low $Ca(OH)_2$ consumption is because of the amorphous calcium that slag contains, making it a latent hydraulic material instead of pozzolanic. Fly ash is a pozzolanic material but still consumes less portlandite than perlite while showing a higher reactivity. This can also be explained by the chemical composition of fly ash, which, even though less than slag, still contains a more significant amount of calcium than the four volcanic materials.

The total calcium hydroxide consumption is plotted in Figure 3.19. Since the distinction between latent hydraulic and pozzolanic properties is determined by the calcium hydroxide consumption, the materials can be classified taking both heat release and $Ca(OH)_2$ consumption into account. The heat release is responsible for the classification of the reactivity (inert, less reactive, more reactive) and the $Ca(OH)_2$ consumption for the reactive behaviour (latent hydraulic or pozzolanic). Plotting the heat release to the $Ca(OH)_2$ consumption, the materials are classified, shown in Figure 3.20. All four raw volcanic materials are classified as

inert. The reactivity of these materials should be increased to be able to apply these materials as precursor in alkali-activated binders successfully.

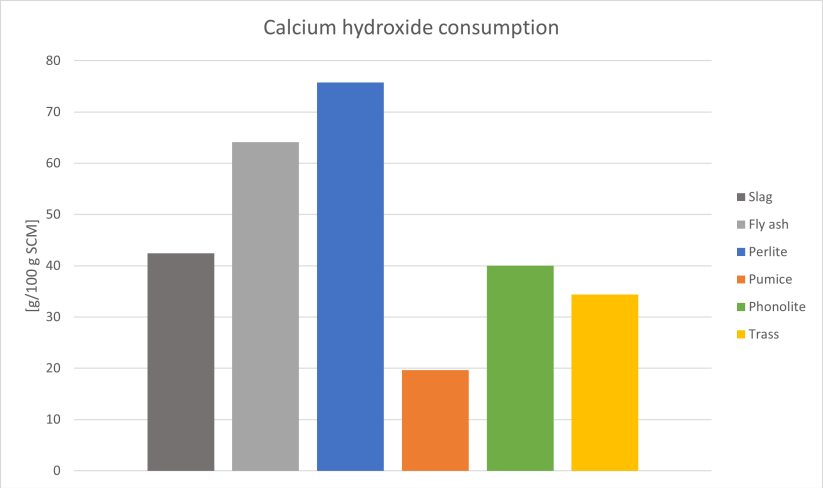

Figure 3.19: Overview calcium hydroxide consumption of the raw materials, determined from thermogravimetric analysis as is described in 3.2.4.

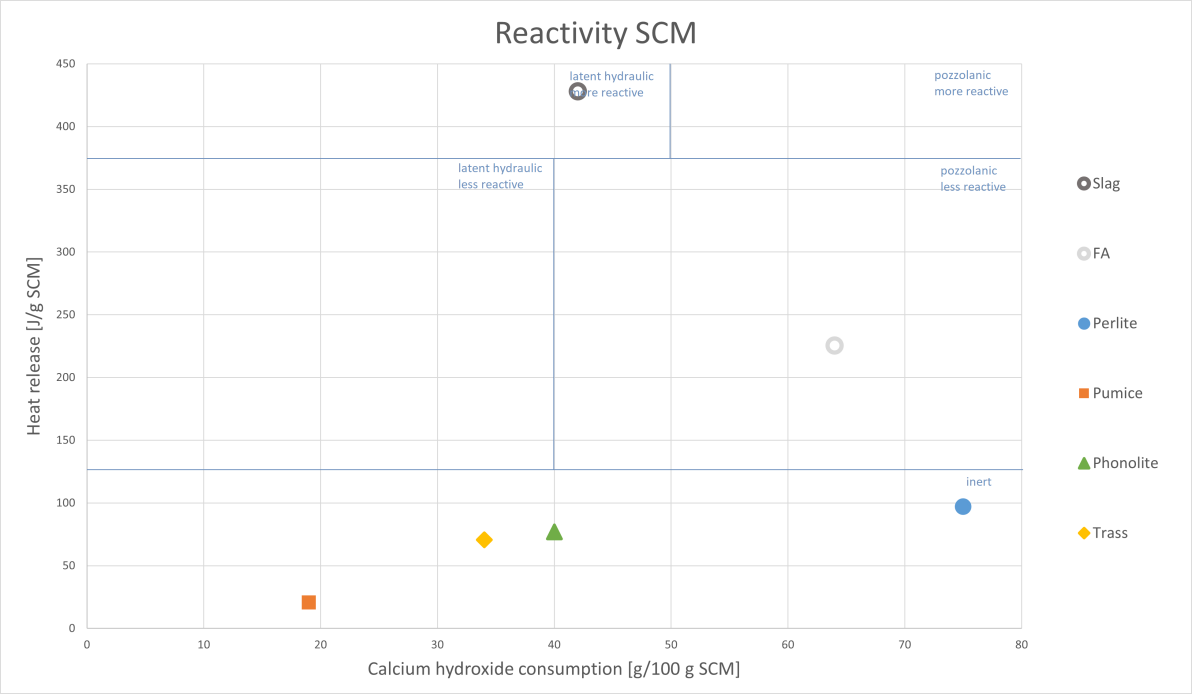

Figure 3.20: Classification of the volcanic materials and blast furnace slag and fly ash as references (inert, pozzolanic, latent hydraulic, less reactive, more reactive). Determined after modified R^3 method from Suraneni et al. [36].

3.7. Conclusion

The reactivity of four volcanic materials is assessed by analyzing particle size, chemical composition and microstructure. Finally, the materials are classified by determining the heat release and calcium hydroxide consumption.

In the raw state, all four materials are classified as inert. Meaning that, as they are, the reactivity of these materials is too low to contribute to the mechanical strength of alkali-activated binders. To further test the possible pozzolanic characteristics of these materials, they should be treated to increase their reactivity.

Considering the PSD, microstructure and chemical composition, there are several ways to activate these materials. Table 3.5 shows how each of the materials perform based on the three important properties with regard for reactive behaviour. For perlite and pumice, the main limiting factor seems to be the particle size

Table 3.5: Overview of the performance on reactive properties of volcanic materials.

	Particle size	Amorphous phase content	Chemical composition	Classification
Trass	Sufficient, specific surface area of $8000 m^2/kg$	Low, 30%	Sufficient silicates and aluminates, low ratio	inert
Phonolite	Sufficient, specific surface area of $3500 m^2/kg$	Low, 5%	Sufficient silicates and aluminates, low ratio	inert
Perlite	Insufficient, specific surface area of $1500 m^2/kg$	High, 80%	Sufficient silicates and aluminates, high ratio	inert
Pumice	Insufficient, specific surface area of $1000 m^2/kg$	High, 95%	Sufficient silicates and aluminates, high ratio	inert

of these materials. Grinding is an efficient way to lower the particle size of materials and consequently, increasing the specific surface area. Therefore, perlite and pumice could be activated by grinding. The limiting factor for phonolite and trass is likely to be the crystalline microstructure. Calcination, the thermal treatment of materials at temperatures above 700 °C [35], could enhance the microstructure of materials, making calcium and magnesium available to react. To activate phonolite and trass, they could be calcined.

II

Phase 2

4

Properties of pre-treated materials

4.1. Introduction

Phase 1 determines the initial reactivity of the raw materials. The outcome of the research shows that the volcanic materials all show insufficient reactivity when applied raw. However, based on the XRD and PSD measurements, one could enhance the reactivity of all four materials.

As discussed in chapter 4, perlite and pumice will be ground to improve their particle size, and phonolite and trass will be calcinated. After manipulating these materials, the reactivity will be again assessed in the same manner as is done in phase 1. This chapter will look into the properties of the pre-treated materials, which are:

- Particle size distribution and morphology
  - Grinding and sieving

    Perlite and pumice both have too coarse particles to show reactive behaviour. Grinding will reduce the particle size of these materials, sieving will remove agglomerates that may have formed during grinding.
  - Laser diffraction analysis

    The particle size distribution after grinding and sieving is measured by LDA to check the fineness of the ground material, more finely grained material leads to higher reactivity.
  - BET surface area analysis

    The surface area of the ground materials are measured since a higher surface area leads to an increase in space for the nucleation and growth of reaction products. Therefore, a larger surface area leads to higher reactivity.
  - X-ray fluorescence

    The chemical composition of the sieved fraction of a material is compared to the chemical composition of the raw material. This gives an indication on the homogeneous or heterogeneous nature of the material.
- Mineral phases
  - Calcination

    Because of their crystalline nature, trass and phonolite are activated by thermal treatment (calcination). By calcinating these materials, volatile components are removed and reactive components (CaO, MgO) could become available to react.
  - X-ray diffraction

    After calcination, the microstructure of trass and phonolite are examined to examine the effect of calcination.
- Classification of the pre-treated materials

- Isothermal calorimetry

  To determine the reactivity of the pre-treated materials the heat release of samples using these pre-treated materials is determined by performing isothermal calorimetry.

- Thermogravimetric analysis

  To determine whether the pre-treated material is hydraulic or pozzolanic the portlandite consumption is measured using thermogravimetric analysis.

4.2. Methods

4.2.1. Grinding

As discussed before, the particle size of perlite and pumice was not sufficiently small. Both materials are manipulated by grinding and sieving. Note that sieving will result in a relatively small fraction of the material being applied in practice and is therefore not a viable option for industrial applications. However, analyzing the sieved fraction of material can gain more insight into the properties of a material. For example, the smaller particles might have a different chemical composition than the larger particles, indicating a heterogeneous material. The XRF measurement are performed in the same way as is described in chapter 3.

Grinding is performed using a ball milling machine, which supposedly will lead to fine grained particles and therefore a large surface area. By performing the modified R^3 test on the ground samples, the influence of particle size can be investigated. Perlite and pumice are both ground for one and a half hours at 200 rpm.

Sieving is performed using sieves of $250\mu m$, $125\mu m$, $63\mu m$ and $52\mu m$. This research uses the material left in the bottom two sieves ($< 63\mu m$) for further tests.

After manipulating the materials, LDA measurements determine the PSD, and BET measurements determine the surface area of the ground materials. Also, SEM analysis is performed on the ground materials to analyse the particle shape after grinding. The LDA, BET and SEM measurements are performed in the same way as is described in chapter 3.

4.2.2. Calcinating

As discussed in phase 1, both trass and phonolite show little reactivity, probably because of their crystalline nature. Calcination might be an option to enhance the reactivity of crystalline materials. To calcinate the materials, they are placed in an oven at 900°C for three hours. By heating the material to such high temperatures, all internal volatile components are removed. The most well-known calcination reaction is carbonates into oxides [35].

After calcinating the materials, the material should contain more oxides. To check if this assumption is correct, XRD is performed on the calcinated materials. The XRD measurements are performed in the same manner as is described in chapter 3.

4.2.3. Classification of pre-treated materials

The reactivity of the manipulated materials is assessed in the same manner as is done in phase 1, by performing calorimetry for ten days and afterwards TGA measurements. Comparing the outcome of the results, one can determine whether or not the grinding/calcinating of the materials has a satisfactory effect on the reactivity of the volcanic materials.

4.3. Particle size distribution and morphology of ground perlite and pumice

Table 4.1: D10, D50 and D90 values (raw from sieving, ground from LDA) and BET surface area raw and ground materials (G = ground).

	D10 [μm]	D50 [μm]	D90 [μm]	[m^2/kg]
Perlite	65	360	780	1567,9
Perlite G	8	28	48	6753,6
Pumice	-	300	3000	982,8
Pumice G	4	16	33	3540,5

After assessment of the reactivity of the four raw volcanic materials, it is determined that two materials (perlite and pumice) should be ground to have sufficiently fine-grained particles to be reactive. Both perlite

and pumice are ground in the milling machine for 90 minutes. After grinding the PSD of the ground materials is determined. Both of the materials are also sieved and the fraction $< 63\mu m$ is used for further analysis. Figure 4.1 shows the obtained PSD of the ground materials. Table 4.1 shows the obtained percentages and specific surface area of both the ground and raw materials.

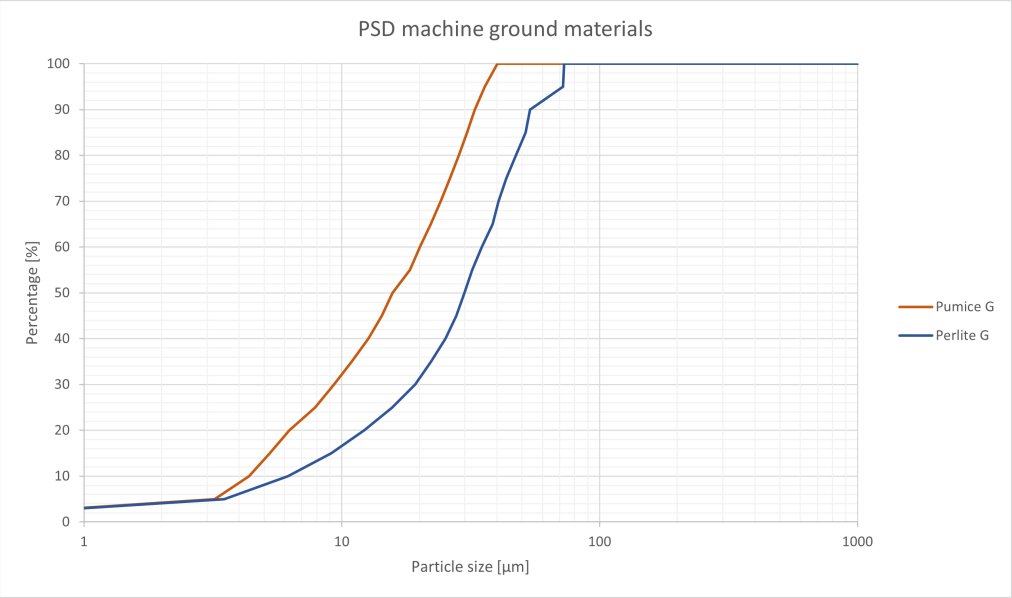

Figure 4.1: PSD of ground perlite and ground pumice, determined by wet LDA, ground using a milling machine (G = ground). Cumulative undersize volume [%].

A discrepancy is visible in the results. The PSD shows that pumice is more fine-grained than perlite. However, ground perlite has a significantly higher surface area than ground pumice. This difference can be explained by the SEM images (Fig.4.2). It can be seen that the ground perlite strongly agglomerates. Since the used LDA equipment does not sufficiently disperse the agglomerates they are measured as large particles, which is shown in the PSD.

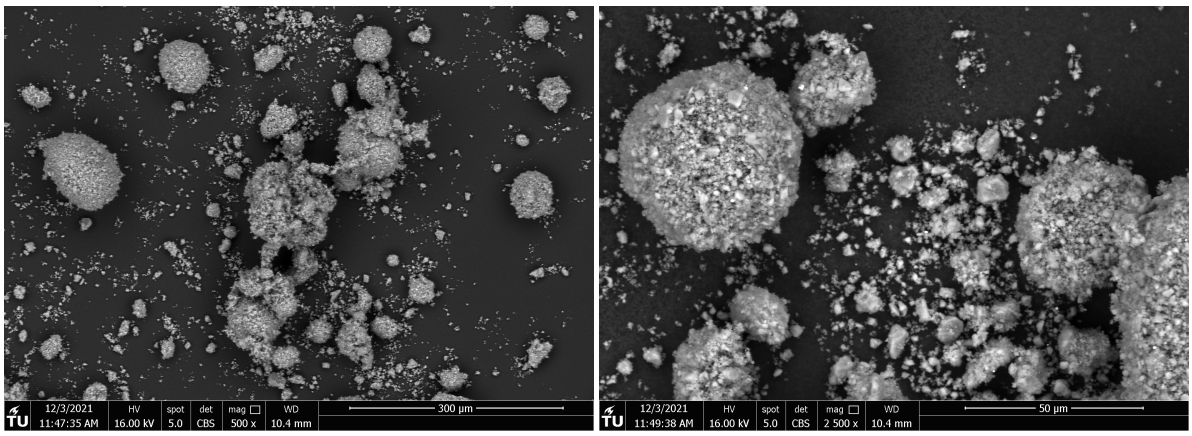

Figure 4.2: SEM images of ground perlite, left: overview, right: ground perlite tends to agglomerate.

The SEM images of ground pumice (Fig.4.3) show that, even though the amount of fine particles have significantly increased compared to raw pumice, there are still some more coarse particles visible. Looking more closely at the larger particles (Fig.4.4), it can be seen that they have pores which are filled with the finer particles. By comparing the surface area of the raw and the ground materials, it can be concluded that pumice and perlite are both ground sufficiently fine.

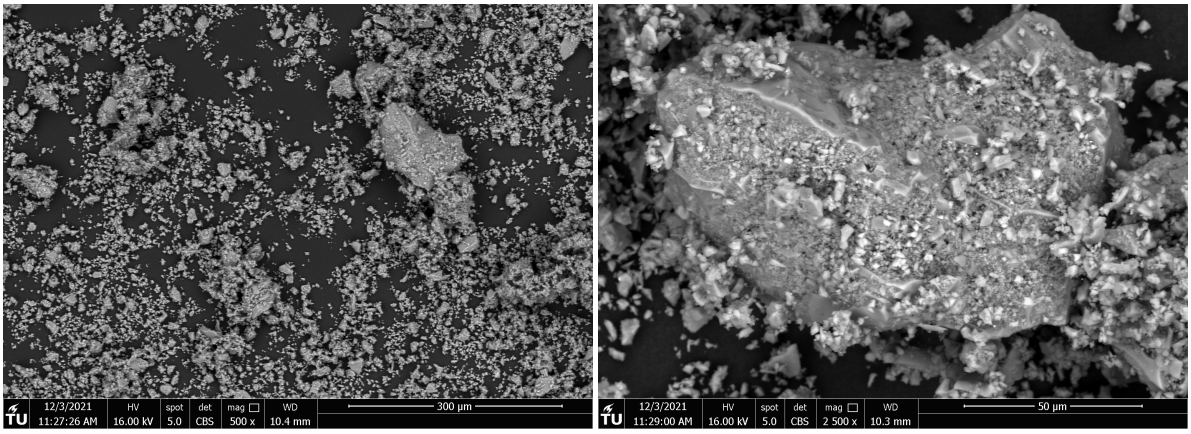

Figure 4.3: SEM images of ground pumice, left: overview, right: particle that has not been ground.

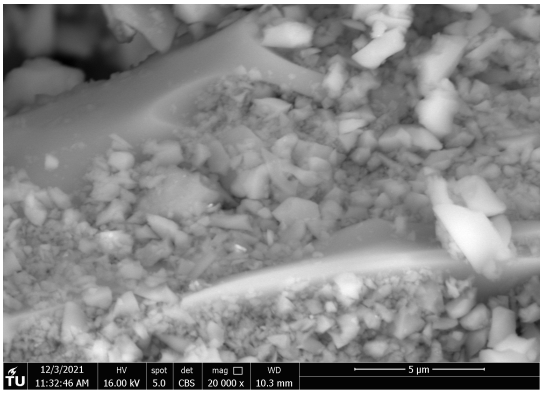

Figure 4.4: SEM image of ground pumice, close-up of a pore which is filled with smaller particles.

4.4. Chemical composition

The chemical composition of the sieved fractions of perlite and pumice are determined to assess if the material is homogeneous. Table 4.2 shows the results.

Table 4.2: Chemical composition of perlite and pumice, raw and sieved samples.

[wt.%]	Perlite raw	Perlite sieved	Pumice raw	Pumice sieved
SiO_2	76,315	73,992	74,946	75,582
Al_2O_3	13,426	13,978	13,091	13,129
Na_2O	5,170	5,358	3,987	4,754
K_2O	2,174	2,741	3,827	3,841
Fe_2O_3	0,770	1,556	1,461	1,556
CaO	1,647	0,978	1,640	1,426
MgO	0,139	0,217	0,434	0,527
TiO_2	0,097	0,092	0,127	0,209
Cl	-	-	0,306	0,309

The chemical composition of the sieved perlite sample is nearly identical to the chemical composition of raw perlite. These chemical compositions indicate that perlite is a homogeneous material. The sieved pumice sample also presents a similar chemical composition to the raw sample, indicating that pumice too is a chemically homogeneous material.

4.5. Mineral phases of calcined trass and phonolite

After calcination of phonolite and trass, the XRD patterns of the calcined materials are determined. Below are the XRD patterns of trass and phonolite visible from before calcination and after calcination.

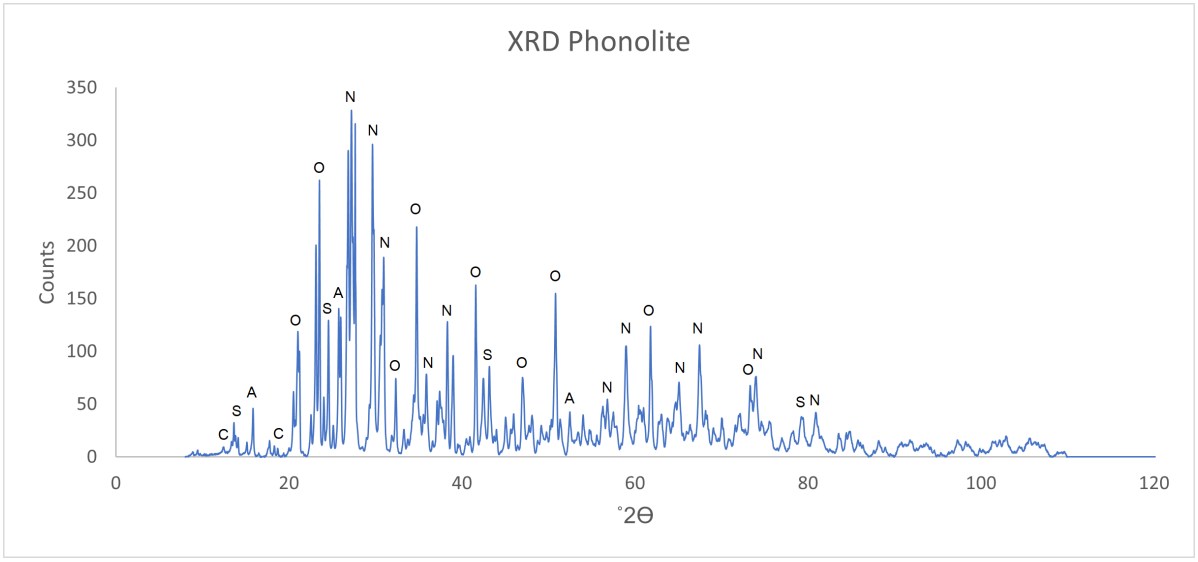

Figure 4.5: XRD pattern raw phonolite (A = Analcime, C = Clinochlore, N = Nepheline, O = Orthoclase, S = Sodalite).

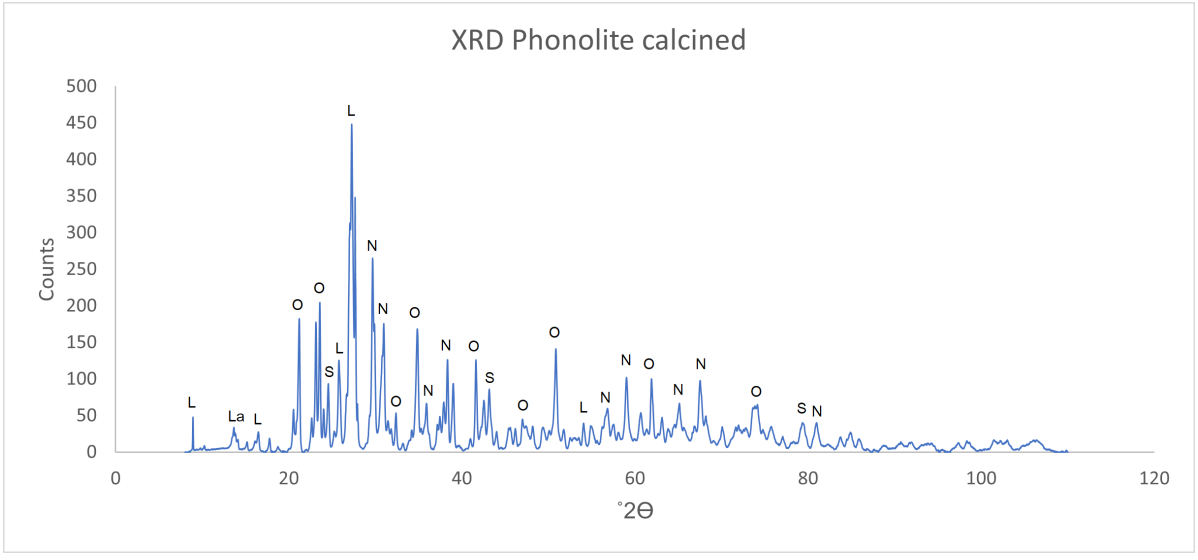

Figure 4.6: XRD pattern calcined phonolite (La = Lazurite, L = Leucite, N = Nepheline, O = Orthoclase, S = Sodalite).

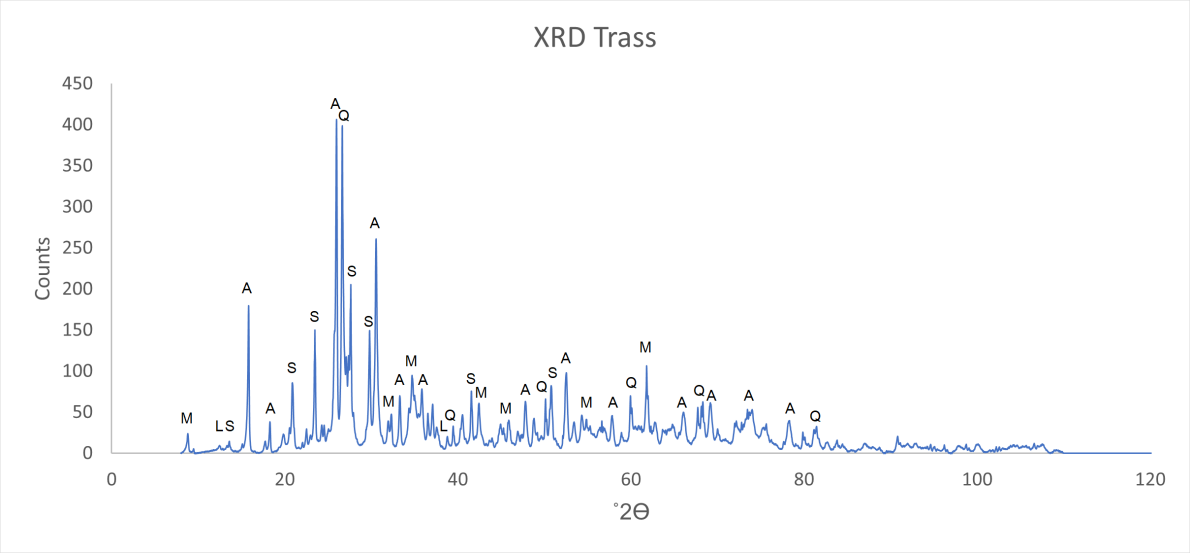

Figure 4.7: XRD pattern raw trass (A = Analcime, L = Lizardite, M = Muscovite, S = Sanidine, Q = Quartz).

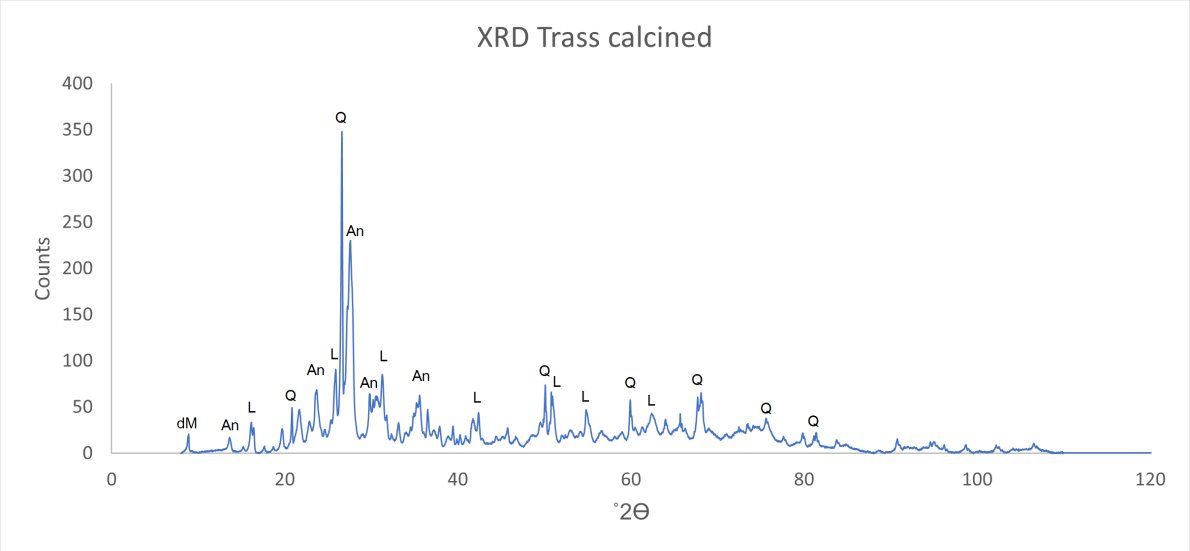

Figure 4.8: XRD pattern calcined trass (An = Anorthoclase, dM = dehydroxylated Muscovite, L = Leucite, Q = Quartz).

Phonolite			
Raw		Calcined	
Orthoclase	$KAlSi_3O8$	Orthoclase	$KAlSi_3O8$
Nepheline	$Na_{0.75}K_{0.25}Al(SiO_4)$	Nepheline	$Na_{0.75}K_{0.25}Al(SiO_4)$
Sodalite	$Na_8Al_6Si_6O_{24}Cl_2$	Sodalite	$Na_8Al_6Si_6O_{24}Cl_2$
Analcime	$NaAl(Si_2O_6).(H_2O)$	Lazurite	$Na_3CaAl_3Si_3O_{12}S$
Clinochlore	$Mg_{3.75}Fe^{2+}_{1.25}Si_3Al_2(OH)_8$	Leucite	$KAl(Si_2O_6)$

Table 4.3: Overview of the measured phases from XRD in raw and calcined phonolite.

Table 4.3 shows the measured phases of the raw and calcined phonolite samples. It clearly shows that the phases orthoclase and nepheline are present in the raw and the calcined sample. Also sodalite is detected in both materials, but because of the low intensity it is not shown in the XRD patterns. The patterns (Fig.4.6) show that the intensity of the peaks of these materials differs, however this difference is not sufficiently large to clearly state that one of the phases has decreased/increased after calcination. The phases analcime and clinochlore were detected in the raw sample, but were not measured in the calcined sample. These phases have changed into Lazurite and Leucite. This is plausible since the chemical composition of analcime and clinochlore combined barely differ from the chemical composition of lazurite and leucite.

Trass			
Raw		Calcined	
Quartz	SiO_2	Quartz	SiO_2
Muscovite	$KAl_3Si_3O_{10}(OH)_{1.8}F_{0.2}$	Dehydroxylated Muscovite	$KAl_3Si_3O_{10}(OH)_{1.8}F_{0.2}$
Sanidine	$K_{0.75}Na_{0.25}AlSi_3O_8$	Anorthoclase	$Na_{0.75}K_{0.25}AlSi_3O_8$
Analcime	$NaAl(Si_2O_6).(H_2O)$	Leucite	$KAl(Si_2O_6)$
Lizardite	$Mg_3Si_2O_5(OH)_4$		

Table 4.4: Overview of the measured phases from XRD in raw and calcined trass.

Table 4.4 shows the measured phases of the raw and calcined trass samples. The quartz phase is measured in the raw and the calcined trass samples. Muscovite seems to have dehydroxylated during calcination. There are less phases present after calcination. Looking at the chemical composition of the measured phases, a decrease in MgO is detected. This is because lizardite, which contains 42,62% Magnesium oxide, has disappeared after calcination. Both the dehydroxylation and the decrease in MgO could lead to an increase in reactivity. Analcime and sanidine have together a similar chemical composition as anorthoclase and leucite, which indicates that sanidine and analcime turned into anorthoclase and leucite after calcination.

Since there is little calcium and magnesium present in trass and phonolite, it is unlikely that calcination had much effect on the reactivity. However, magnesium that is present in the raw minerals (clinochlore and lizardite) is not present in the calcined minerals. The modified R^3 tests should show if calcinating has increased the reactivity of phonolite and trass.

4.6. Classification of pre-treated materials

The reactivity of the ground perlite and pumice, and the calcined trass and phonolite are determined as described in chapter 3. The results from the calorimetry measurements are shown below.
As can be seen in the Figure 4.9, ground pumice and ground perlite clearly show higher heat release than the raw pumice and perlite. This reactivity increase is expected, since the material simply has a larger specific surface area. The larger surface area causes more space for growth and nucleation of hydrates [13]. The difference in reactivity of ground pumice and ground perlite is most likely because of the specific surface area. Ground perlite has an almost twice as high specific surface area as ground pumice.

Figure 4.9 also shows that calcination of phonolite and trass did not have the expected results. Calcined trass shows a similar heat release average but a higher standard deviation. Calcined phonolite even shows a significant decrease in reactivity. The reactivity of trass would be expected to increase due to the released MgO. Whereas the reactivity of phonolite would be expected to stay somewhat the same, since the phases are for a large part similar to the raw phonolite. It might be possible that the calorimeter measured lower heat release overall and therefore the outcome of the reactivity tests becomes lower. It may also be the case that the phases that are formed during calcination are less reactive than the phases of the raw materials. To

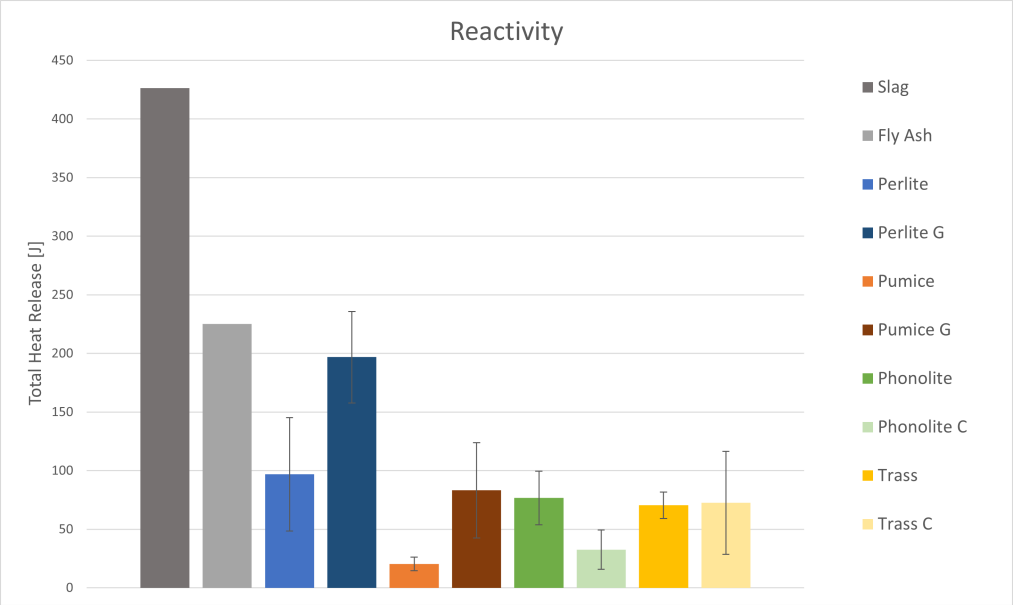

Figure 4.9: Total heat release volcanic materials with blast furnace slag and fly ash as references. Determined by the area under the heat flow curve from isothermal calorimetry (ten days) (G = ground, C = calcined).

investigate extensively why calcination lowered the reactivity of phonolite and not affect the reactivity of trass is outside the scope of this research.

A large increase in the reactivity of phonolite and trass was not specifically expected because both materials have very little CaO and MgO in their chemical composition, which are the main phases you wish to oxidize using calcination [35].

The measured total heat release of the pre-treated materials show that activation using grinding worked well. Activation using calcination was less successful. Ground perlite shows satisfactory reactivity, a little less than fly ash on average.

The calcium hydroxide consumption (TGA measurements) results are shown below (Fig.4.10 & Fig.4.11).

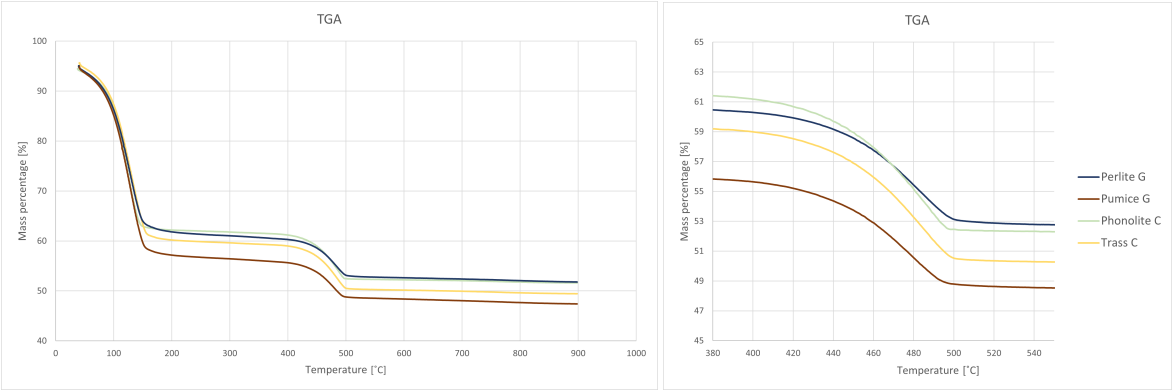

Figure 4.10: Mass loss [%] plotted to increasing temperature for the pre-treated volcanic materials, measured by thermogravimetric analysis. left: 0 - 1000 °C, right: 380 - 550 °C (G = ground, C = calcined).

Perlite shows the lowest peak for the $Ca(OH)_2$ consumption in Figure 4.11, this indicates that perlite has the highest portlandite consumption. This correlates with the pozzolanic nature of perlite and the high reactivity measured during calorimetry. From performing the same calculations as are performed in phase 1, the total $Ca(OH)_2$ consumption is determined. Figure 4.12 shows an overview of the total $Ca(OH)_2$ consumption of the raw and the pre-treated materials.

What stands out is the very large difference between the calcium hydroxide consumption of the raw and the ground pumice. The raw pumice shows least calcium hydroxide consumption and ground pumice shows

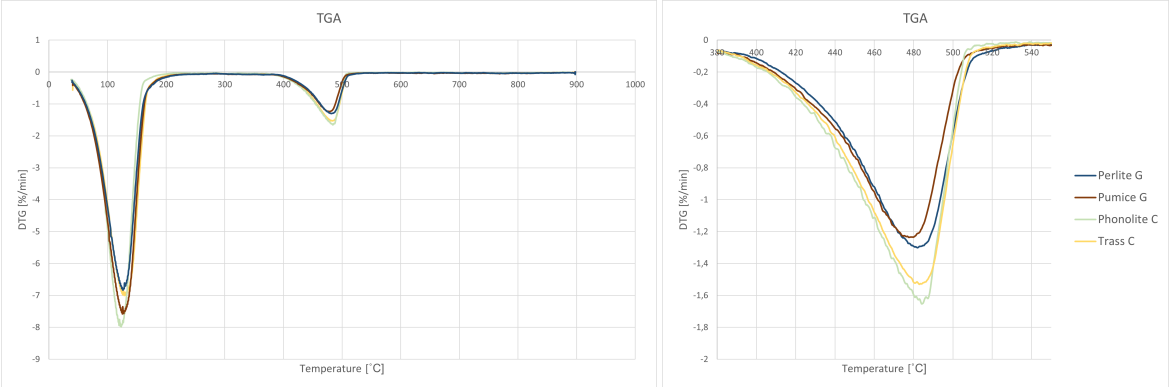

Figure 4.11: Rate of mass loss [%/min] plotted to increasing temperature for the pre-treated volcanic materials, measured by thermogravimetric analysis. left: 0 - 1000 °C, right: 380 - 550 °C (G = ground, C = calcined).

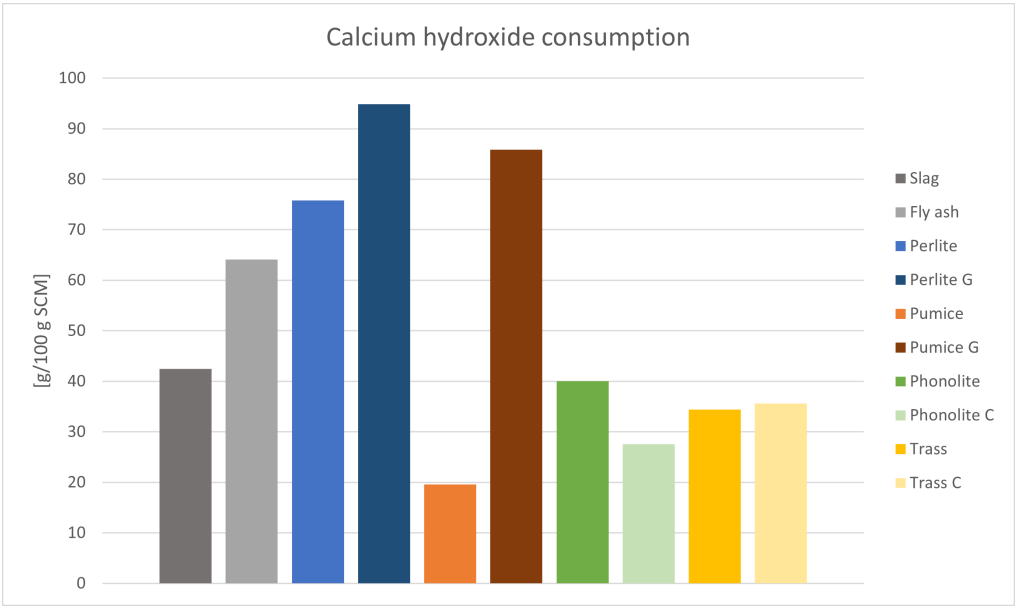

Figure 4.12: Overview calcium hydroxide consumption of the raw and pre-treated materials, determined from thermogravimetric analysis as is described in 3.2.4. (G = ground, C = calcined).

most calcium hydroxide consumption. This shows that grinding of pumice has a significant effect on the consumption of portlandite. This correlates with the increase in reactivity that has taken place. Perlite also shows a significant increase in portlandite consumption. Note that phonolite shows a decrease in the consumption of $Ca(OH)_2$ and trass has a similar consumption, which correlates with the reactivity results from the calorimetry measurements.

As mentioned in phase 1, plotting the calcium hydroxide consumption to the total heat release, the materials can be classified. Figure 4.13 shows the classification of the raw and the pre-treated materials. What is clearly observed is that ground perlite is the only volcanic material that is classified as reactive (pozzolanic less reactive). The grinding of pumice seems to have an effect mainly on the portlandite consumption, the reactivity increased as well, but insufficient to be classified as less reactive. Calcination of trass and phonolite seems to barely show effect on the reactivity of the material. Trass has a slight increase in consumption and reactivity, phonolite shows a decrease in portlandite consumption and reactivity. The newly developed phases in both these materials seem to have similar or even less reactive properties than the phases of raw trass and phonolite. To further investigate the difference between these raw and calcined materials is outside the scope of this research.

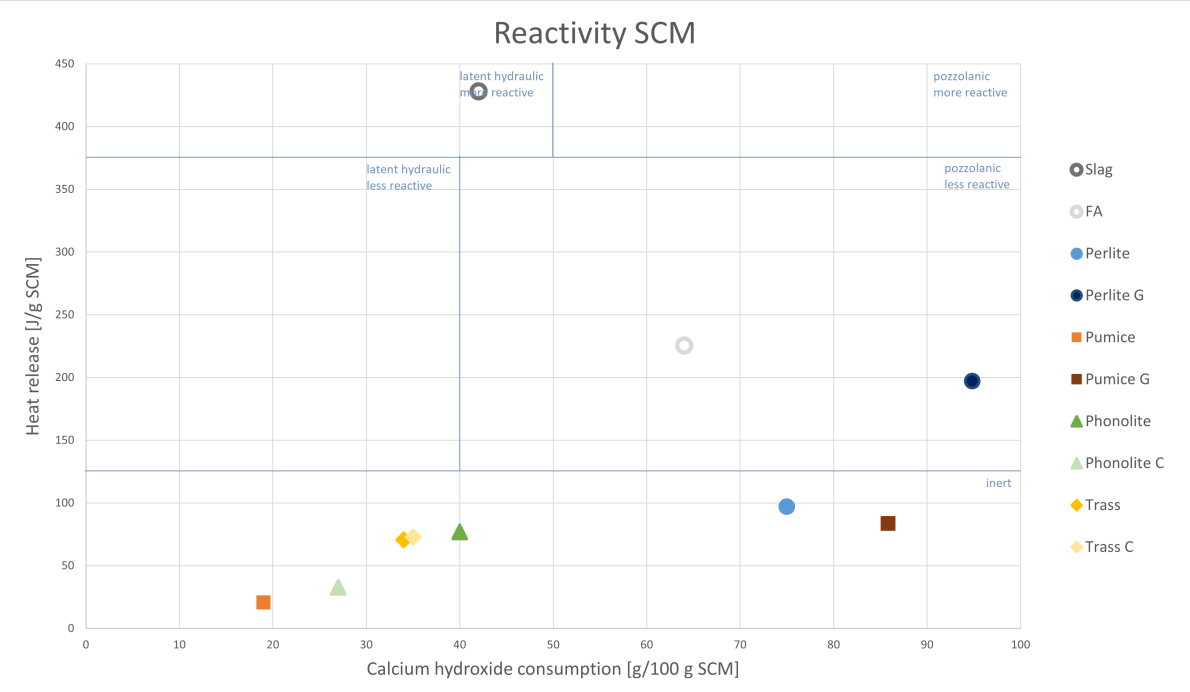

Figure 4.13: Classification of the volcanic materials and blast furnace slag and fly ash as references (inert, pozzolanic, latent hydraulic, less reactive, more reactive). Determined after modified R^3 method from Suraneni et al. [36] (G = ground, C = calcined).

4.7. Conclusion

Phase 1 showed that all four volcanic materials exhibit inert behaviour. Perlite and pumice are too coarse to be reactive and were therefore ground. Trass and phonolite are both crystalline materials and to improve their reactivity they were calcinated. After these activation treatments, the reactivity of the pre-treated materials was tested. Of all four pre-treated materials, ground perlite shows the highest reactivity. Ground pumice shows lower reactivity than ground perlite, even though it has a higher amorphous phase content. The lower measured reactivity is most likely because of the lower specific surface area of pumice. Perlite has an almost twice as high specific surface area after grinding it for the same time. Calcination of trass and phonolite did not have the desired effect, probably due to a lack of CaO and MgO in the chemical composition. The measured reactivity even decreased, this could be because the newly formed phases are less reactive than the old phases, but this must be confirmed by further research. Table 4.5 shows how each of the pre-treated materials behave on the important properties with regard for reactive behaviour.

Table 4.5: Overview performance on reactive properties of volcanic materials (G = ground, C = calcined).

	Particle size	Amorphous phase content	Chemical composition	Classification
Trass C	Sufficient, specific surface area of 8000 m^2/kg	Low, 30%	Sufficient silicates and aluminates, low ratio	inert
Phonolite C	Sufficient, specific surface area of 3500 m^2/kg	Low, 5%	Sufficient silicates and aluminates, low ratio	inert
Perlite G	Sufficient, specific surface area of 6500 m^2/kg	High, 80%	Sufficient silicates and aluminates, high ratio	pozzolanic, less reactive
Pumice G	Insufficient, specific surface area of 3500 m^2/kg	High, 95%	Sufficient silicates and aluminates, high ratio	inert

It is concluded that calcined trass and phonolite are both not sufficiently reactive to be applied as precursor in alkali-activated binders. This is in line with the findings from the literature review (sections 2.2.4 and 2.2.5). If pumice is ground to contain more fine particles, it might eventually be sufficiently reactive. How-

ever, because the reactivity of perlite is measured to have sufficient reactivity with the same level of grinding, it is determined that perlite is the best material to apply as precursor in alkali-activated binders. This is also expected in view of the literature review.

III

Phase 3

5

Application of perlite in mortar

5.1. Introduction

In phases 1 and 2, the reactivity and the critical properties (particle size, microstructure, and chemical composition) of four volcanic materials were determined. From the results, one could conclude that ground perlite shows sufficient reactive behaviour and, therefore, is promising to act successfully as a precursor in alkali-activated binders. Phase 3 investigates alkali-activated mortar made with ground perlite.

First of all, several mixtures are designed using ground perlite as a precursor. AAMs present a wide range of variables on their obtainment route, as it relies on the implementation of precursors with different chemical compositions. These different precursors, for instance, display differences in reactions according to the activator. Currently, there are no standards that dictate an optimum mix design, which makes the designing of a mixture complex. Factors that need to be taken into account are:

- Water-to-binder ratio (or solution-to-binder ratio).
- Type of precursor.
- Precursor content.
- Type of activator.
- Activator content.

Since this research focuses on the application of perlite, only elements relevant for the application of perlite are discussed. This chapter finally determines on several alkali-activated mix designs containing perlite as precursor which are investigated in this research.

5.1.1. Materials

The mortar mixtures contain perlite, BFS, $NaOH$ solution, waterglass and sand. Perlite and its' origin is already discussed in section 3.1.1. The perlite is ground to a specific surface area of approximately 6500 m^2/kg. The slag used in this research comes from Ecocem. The slag has a specific surface area of 410-443 m^2/kg and the chemical composition is shown below (Tab.5.1)[82].

Table 5.1: Chemical composition of BFS from Ecocem, from [82].

[wt.%]	CaO	SiO_2	MgO	Al_2O_3	Fe_2O_3	Mn_2O_3	Cl^-	S^{2-}	Na_2O	K_2O
BFS	39,32	35,32	9,13	12,24	0,31	0,27	0,01	0,64	0,35	0,56

For the activator, $NaOH$ solution and waterglass ($Na_2O.rSiO_2$) are used. The sodium hydroxide solution is a 50% $NaOH$ solution from Brenntag and the waterglass has a SiO_2/Na_2O ratio of 2,0 from PQ Corporation. The sand used is standard sand, as is described in NEN-EN 196-1.

5.2. Background information

Due to the high silica content, perlite is not expected to gain sufficient mechanical properties at room temperature [45, 63, 64]. To be applied in industry, hardening at room temperature is preferred. Therefore, it is chosen to use a blended precursor, combining of BFS and perlite. BFS contains amorphous CaO and is known to produce alkali-activated binders with excellent properties [4, 7, 83].

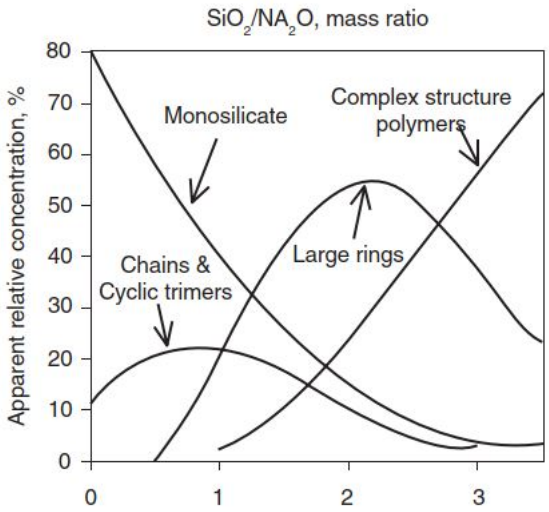

Figure 5.1: Relation between the SiO_2/Na_2O ratio and the hydration products, from [64]

Often, alkali-activated slag cement is made using waterglass, and a sodium hydroxide solution. The waterglass activator provides additional dissolved silica in the dissolution, which is beneficial for the reaction products. A higher SiO_2/Na_2O ratio in the dissolution leads to more complex hydrate structures, shown in Figure 5.1 [4, 46, 64]. An increase in the SiO_2/Na_2O ratio also leads to a reduction in the porosity and microcracks, which generally leads to higher strength. However, Qureshi and Ghosh [84] found that at ratios of 1,2 cracks would form at the interface between CSH and unreacted silica, which indicates that there is an optimum in the amount of silicates to be added to the mixture. Figure 5.1 shows the relation between the SiO_2/Na_2O ratio in the solution and the formed hydration products. It shows that the lower ratio favors the formation of monomer silicate species, and therefore slows the poly-condensation of the hydration products. The hydration products formed under the lower SiO_2/Na_2O ratio conditions, also perform less stable than hydration products from higher ratios [64].

Since ground perlite contains mainly amorphous silica, it could be a great addition to BFS and decrease the need for waterglass. Several studies have already shown similar use of silica fume or metakaolin [85, 86, 87, 88]. An estimation should be made on the SiO_2 addition from perlite to predict the SiO_2/Na_2O ratio in the perlite/BFS mixture. Dissolution tests were performed to determine the amount of dissolved silica ground perlite provided.

5.3. Dissolution tests

5.3.1. Methods

The amount of silica that dissolves from perlite must be determined to design a mixture which accounts for the reactive portion of perlite. Dissolution tests were performed to determine the dissolved silica content. One gram of ground perlite with a specific surface area of approximately $6500 m^2/kg$ is added to a 1 L $NaOH$ solution. Three repetitions of the test are performed for a 4M and a 6M solution. Three plastic bottles were cleaned with nitric acid prior to testing. Then, the bottles with $1L$ of the solution were prepared and left stirring for the test. After 1 hour, 1 g of ground perlite was added to the solution. After 24 hours, the solution was vacuum filtrated twice using a 1,6 μm pore size glass microfiber filter from Whatman. 25 mL of the filtrated solution was used for optically emission spectroscopy - inductively coupled plasma (OES-ICP) tests to determine the amount of dissolved silica in the solution.

After performing these dissolution tests, the amount of silica that ground perlite will provide to the dissolution of the binder can be estimated and used to design a mixture.

5.3.2. Results

The dissolution tests were performed to determine the amount of dissolved silica from perlite in 4M and 6M $NaOH$ solutions. The results of the ICP tests are shown below in Table 5.2, in dissolved Ca, Al & Si in mg/L.

Table 5.2: Results ICP tests: amount of dissolved Ca, Al and Si in mg/L from 1 gram of perlite.

	Sample	Ca	Al	Si
1	4M	5,7	31,0	111
	4M	4,0	29,2	105
	4M	3,8	31,4	114
Average	4M	4,5	30,5	110
2	6M	4,1	32,6	116
	6M	4,1	32,6	117
	6M	3,6	31,2	113
Average	6M	3,9	32,6	115,3

From the dissolved Si in mg/L, the percentage SiO_2 dissolved from 1 g of perlite in a 4M and a 6M $NaOH$ solution can be calculated. The results are shown in Table 5.3.

Table 5.3: The weight percentage of dissolved SiO_2 from 1 gram of perlite.

[wt. %]	Dissolved SiO_2 from perlite
4M $NaOH$	23,5 ± 1
6M $NaOH$	24,5 ± 0,5

As can be seen, the difference in dissolution for a 4M and 6M $NaOH$ solution is relatively small, suggesting that the dissolution of perlite doesn't significantly increase in higher alkaline environments, which corresponds with the findings of Tsaousi et al. [64]. Using the molar mass of the elements, the amount of silica that perlite adds to the solution can be calculated in percentages. For 4M $NaOH$, 23,5% of the total perlite mass. For 6M $NaOH$, 24,5% of the total perlite mass. Note that these differences are marginal, taking the standard deviation into account. These values are used for the mix designs (Table 5.4).

5.4. Mix design

From the percentage of dissolved SiO_2, found in figure 5.3, one can determine on mix designs. The amount of precursor and sand and the water/binder ratio are determined by the standard NEN-EN 196-1. For the amount of perlite added in the precursor and to determine the activator, the main factor that is considered is the SiO_2/Na_2O ratio.

The precursor is a blend of BFS and perlite. There are six mix designs, three for a 4M $NaOH$ solution and three for a 6M $NaOH$ solution. For both 4M and 6M $NaOH$ mixes, a reference sample with 100% BFS is made for comparison. It was found by Tsaousi et al., and Qureshi and Ghosh, that a higher SiO_2/Na_2O ratio results in more complex hydration structures and a reduction in porosity and micro-crakcs, which often leads to higher strength (Figure 5.1) [64, 84]. However, Qureshi and Ghosh stated that a too high SiO_2/Na_2O ratio leads to cracks between the formation products and the unreacted silicates, indicating that there is an optimum ratio. Literature states that this optimum is between 0,9 and 1,5 [89]. For this research, the SiO_2/Na_2O ratio is fixed at 1,5. By fixing the molarity of the sodium hydroxide solution and the SiO_2/Na_2O ratio, the amount of $NaOH$, the amount of waterglass ($Na_2O.2SiO_2$), and the extra water needed can be determined. Crucial to take into account is the extra SiO_2 provided by perlite, it is determined to take into account 100% of the reactive SiO_2 from perlite, determined from the dissolution tests (Table 5.3). Next to the 100% BFS reference (Ref 4M and Ref 6M), also two 70% BFS and 30% perlite samples are made where there is no compensation for the extra silica from perlite in the activator (B.2 and E.2). The mix designs are shown in table 5.4.

As shown in the table, perlite causes an increase in the amount of SiO_2, to keep the SiO_2/Na_2O ratio at 1,5, there is a decrease in the SiO_2 from waterglass (SS). The $NaOH$ solution increases to compensate for the

loss of Na_2O from fewer waterglass. The w/b ratio of 0,5 is ensured by embedded water from the activator in combination with tap water.

Table 5.4: Overview of the mix designs (BFS = blast furnace slag, P = perlite, SS = sodium silicates). Note that the SiO_2/Na_2O ratio is set at 1,5, where the total amount of SiO_2 comes from (a combination of) perlite (SiO_2 P) and sodium silicates (SiO_2 SS).

	BFS/P	BFS [g]	P [g]	SiO_2/Na_2O	w/b ratio	SiO_2	SiO_2 P	SiO_2 SS	sand [g]
Ref 4M	100/0	450	0	1,5	0,5	41,8	0	41,8	1350
A 4M	80/20	360	90	1,5	0,5	41,8	21,2	20,6	1350
B 4M	70/30	315	135	1,5	0,5	41,8	31,7	10,1	1350
B.2 4M	70/30	315	135	2,6	0,5	73,5	31,7	41,8	1350
C 4M	60/40	270	180	1,5	0,5	41,8	41,8	0	1350
Ref 6M	100/0	450	0	1,5	0,5	62,8	0	62,8	1350
D 6M	80/20	360	90	1,5	0,5	62,8	22,1	40,7	1350
E 6M	70/30	315	135	1,5	0,5	62,8	33,1	29,7	1350
E.2 6M	70/30	315	135	2,3	0,5	95,9	33,1	62,8	1350
F 6M	60/40	270	180	1,5	0,5	62,8	44,1	18,7	1350

6

Properties of alkali-activated perlite slag mortar

6.1. Introduction

Using the mix designs from section 5.4, mortar samples are produced. The compressive strength of the mortar samples is determined at curing ages of 1, 3 and 7 days. By comparing the strength of the samples, a conclusion can be made whether or not perlite contributes to the mechanical strength development of mortar. By investigation of the hydration products, the contribution of perlite can be further assessed. Therefore, the reacted phases of the pastes are investigated by XRD and TGA. The goal of using alkali-activated binders is to lower the environmental impact of concrete. Therefore, it is essential to know what the environmental impact of perlite is compared to the impact of cement and BFS.

6.2. Methods

6.2.1. Casting

Once the mix designs are determined, mortar tests are executed. Six mix designs and four reference mixes, which are discussed in section 5.4, are cast and used for further testing. The casting procedure is as follows:

1. 24 hours prior to casting, the activator of the mix design is prepared. The activator is made using the $NaOH$ solution and the waterglass solution as described in section 5.1.1, combined with tap water. The liquids are measured in a plastic bottle, then shaken and left for 24 hours. Before casting, first, one should stir the prepared activator again.
2. The right amount of sand, BFS and perlite are measured and put together in a mixing bowl from the Hobart mixing machine, as described in NEN-EN 196-1.
3. First, the sand, BFS and perlite are mixed for two minutes at slow speed.
4. After the sand and precursors are well mixed, the activator solution is slowly added while the mixer runs at a slow speed.
5. After all the components are added together, the mixer runs at slow speed for two more minutes.
6. Then the mixer is stopped, and the mortar adherent to the walls of the bowl is scraped and placed in the middle of the bowl.
7. Finally, the mixer runs for two more minutes at high speed.
8. After mixing, the mixture is scooped out of the bowl and added to 40 x 40 x 40 [mm] moulds. The moulds are filled halfway and then put on a vibrating plate to compact the mixture. After vibrating the first time, the moulds are filled, and the vibrating plate runs again.
9. Once the moulds are filled and the air is released from the mixtures, the top of the samples are equalized using a metal scraper.

10. A foil is put over the moulds of the samples to ensure no moisture loss can occur.

11. The samples are stored for 24 hours at room temperature before they are demoulded.

The casting procedure is a variation on NEN-EN 196-1, more commonly used to cast AAMs.

6.2.2. Mechanical properties

The mechanical properties of the mortar cubes are tested after one, three and seven days. The compressive strength is measured according to NEN-EN 196-1.

6.2.3. Phase formation

Simultaneously with mortar casting, pastes for all mixes from Table 5.4 were cast. The cast pastes were made by first mixing the BFS and perlite powder and preparing the activator. For making the pastes, the activator is added to a plastic container with the mixed powder and stirred for 3 minutes. After that, the containers were closed and left curing for seven days. After seven days, the pastes were removed from the container and crushed into powder using mortar and pestle. The powder of mixes Ref 4M, Ref 6M, A, B, C, D, E and F were assessed by XRD analysis. This way, the resulting phases were identified and compared. The powder from mixes Ref 4M, B, B.2 Ref 6M, E and E.2 were assessed by TGA measurements to quantitatively analyze the hydrated phases. The XRD and TGA measurements are performed as described in sections 3.2.3 and 3.2.4 respectively.

6.3. Results

6.3.1. Compressive strength

Ten mortar mixes were designed (Tab.5.4), and the compressive strength of these mixes has been determined after one, three and seven days. The results of the compressive strength tests of samples Ref 4M, Ref 6M, A, B, C, D, E and F are shown in Figure 6.1 and Figure 6.2.

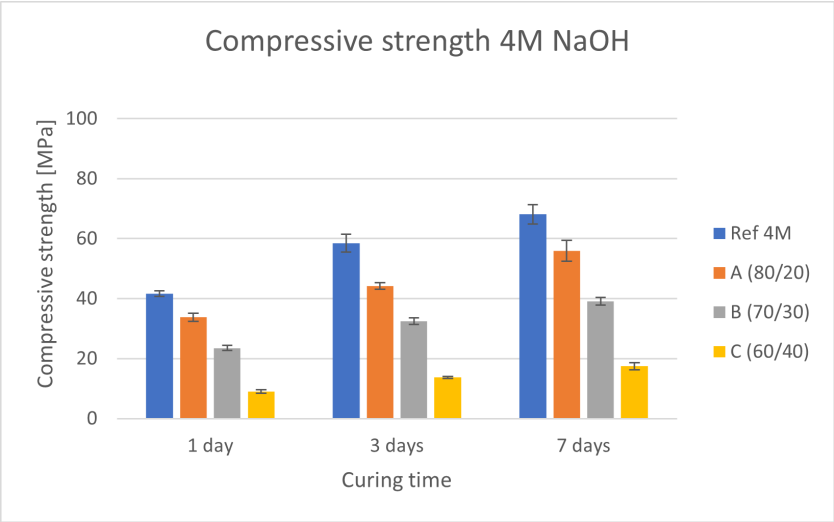

Figure 6.1: Compressive strength after one, three and seven days for the 4M $NaOH$ mixes.

What stands out are the inconsistent results from the 6M $NaOH$ mixes. Mix E ([70/30] 6M) shows meagre compressive strength, and mix D ([80/20] 6M) shows a substantial standard deviation. These inconsistent results are because of the short setting time of the 6M mixes. There was insufficient time to properly compact the concrete when casting, resulting in granular cubes presented in Figure 6.3. The short setting time of the 6M mixes is probably due to the combination of high molarity $NaOH$ and a low amount of silicates from waterglass in the activator. The high molarity causes a small number of silicates to hydrate immediately. Suppose there were more silicates present, which is the case for the Ref 6M mix. In that case, the alkalinity becomes available later on, and the hydration of the silicates is delayed, resulting in a slower setting time [90, 91, 92, 89]. Also, the fast dissolution of perlite in a higher molarity $NaOH$ might have caused the short setting time. Because of the quick setting time, the measured compressive strength depends more on the

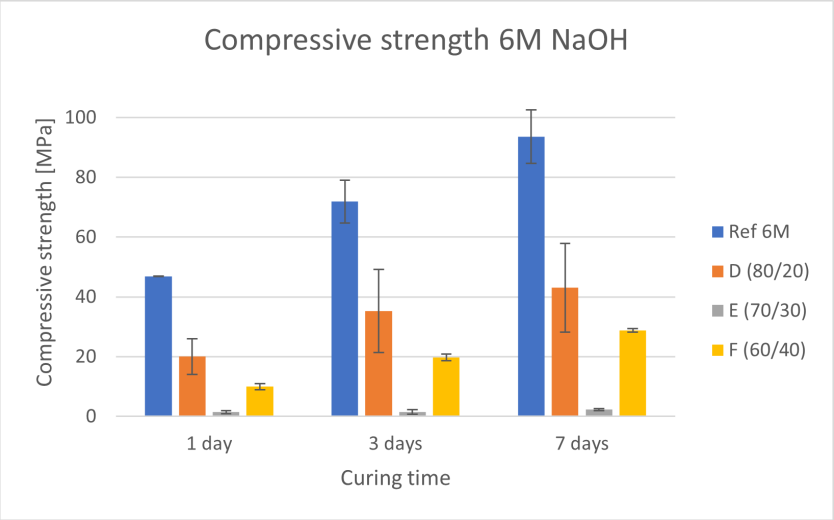

Figure 6.2: Compressive strength after one, three and seven days for the 6M $NaOH$ mixes.

activator composition than on the perlite addition. Therefore, the 6M mixes are not representative to assess the contribution of perlite to the compressive strength of mortar.

Figure 6.3: Poorly compacted mortar cubes from mix D (left) and E (right).

The 4M $NaOH$ mixes show a clear trend regarding the development of the compressive strength. An increase in perlite and a decrease in silicates from waterglass (shown in Table 5.4) results in lower strength. The hydration of perlite is a pozzolanic reaction which is a slow reaction. Therefore, it is expected to see the effect of perlite at a longer curing time. As a result, the contribution of perlite is predicted to cause a decrease in the compressive strength of several mixtures over time. However, the differences in the compressive strength of the mixtures only increase. The pozzolanic effect of perlite is therefore not visible in the results. It can be concluded that perlite in these mixes is not sufficiently reactive to compensate for the decrease in silicates from waterglass and the decrease in slag.

One possible explanation for why perlite does not seem to contribute to the strength of the samples may be due to the reaction mechanisms. The perlite grains immediately react because there is a lack of dissolved silicates in the initial dissolution resulting in a highly alkaline environment. The hydration products from perlite form a passivating layer around the perlite particles, preventing the particle from further reacting [93]. The slag continues to react without sufficient silica present in the dissolution, which leads to a C-S-H-gel with lower cross-linking than if silica was present in the dissolution. A lower degree of cross-linking leads generally to a lower density of the hydration products [4, 30]. Once the hydroxyl ions can penetrate through the passivation layer of the reacted perlite, the slag has already formed its' reaction products, and there is not

enough space for the perlite to react [93]. This complies with the findings of Ramezanianpour et al. [61]. The authors found that in more porous concrete, the effect of perlite on the compressive strength was higher than for more dense concrete, simply because there was more space for the formation of new gel in the pores.

Two extra mixes were cast (B.2 and E.2) in which there was no compensation in the activator for the sili-

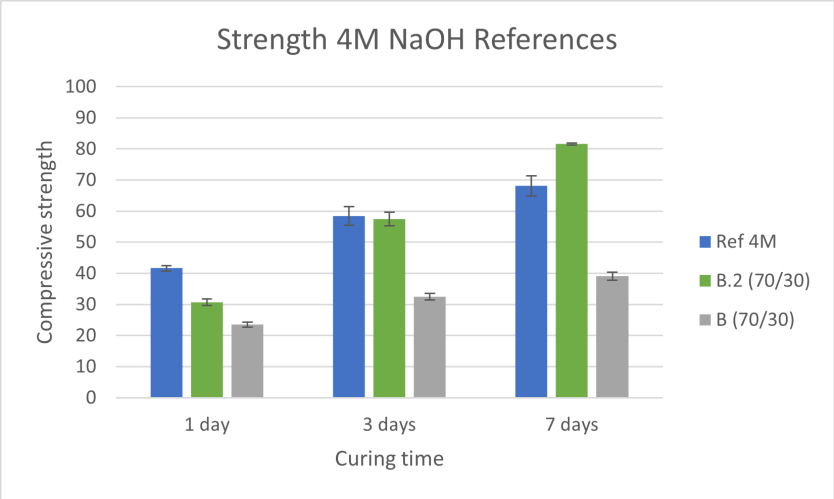

Figure 6.4: Compressive strength after one, three and seven days for the 4M *NaOH* Ref, B and B.2 mixes.

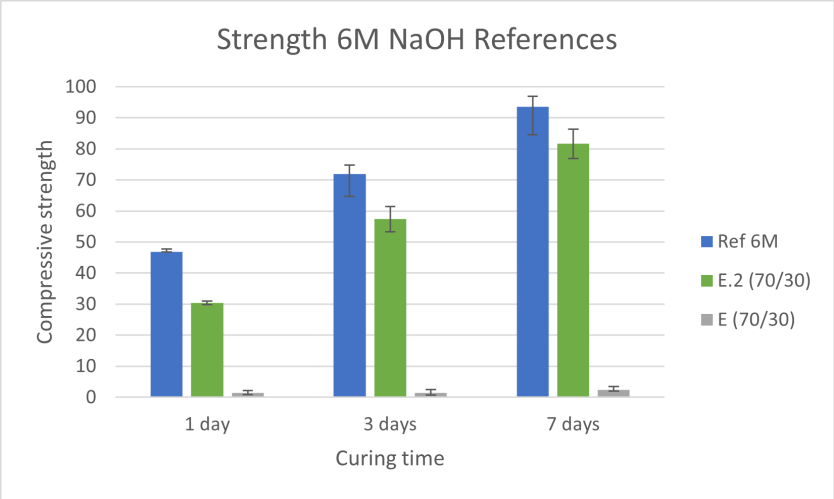

Figure 6.5: Compressive strength after one, three and seven days for the 6M *NaOH* Ref, E and E.2 mixes.

cates from perlite. These mixes consist of 70% slag and 30% perlite and are activated with the Ref 4M and the Ref 6M activators. Using these activator compositions means there is no compensation for the added amount of silicates from perlite in the activator. The compressive strength results from these mixes are presented in Figures 6.4 and 6.5, together with the Ref 4M, Ref 6M, B and E mixes.

Noticeable in the 4M *NaOH* reference mixes is that the Ref 4M mix initially has a higher compressive strength than sample B.2. These mixes have the same activator, but mix B.2 has a precursor containing 70% BFS and 30% perlite. However, after seven days, B.2 has a higher compressive strength than the Ref 4M mix. This strength increase means that, even though the initial strength is lower, perlite contributes to the compressive strength later. This complies with the pozzolanic nature of perlite, which is slower than the latent hydraulic reaction of BFS. Because of the silicates from waterglass, the initial alkalinity is not as high. The perlite grains do not react as fast and are available for reaction later [4, 30, 89, 94]. Mix E.2 does not exceed the compressive strength of the Ref 6M mix. Comparing the seven days of compressive strength, the following order is noted:

$$\text{Ref 6M} > \text{E.2} = \text{B.2} > \text{Ref 4M}.$$

The following hypothesis could explain this behaviour: an optimum amount of silicate species per BFS. This theory is similar to what Qureshi and Ghosh found in their research [84]. If this optimum amount of silicates is already achieved by the dissolved silicates from waterglass, adding perlite to the mixture will only result in less slag and thus fewer reaction products, along with the cracks that occur at the interface between CSH-gel and unreacted silicates species. Luukkonen et al. [89] also found an optimum in SiO_2/Na_2O ratio, they mentioned this ratio to be between 0,9 and 1,5. Reaching this optimum probably happened for the 6M mixes. The Ref 6M mix has the optimum amount of silicate per BFS from the activator, therefore, exchanging BFS for perlite only disrupts this optimum and results in lower strength (mix E.2). For Ref 4M, this optimum is not yet reached. By exchanging BFS for perlite (mix B.2), the SiO_2/Na_2O ratio is improved, resulting eventually in higher compressive strength. This hypothesis would also explain the similar compressive strength from B.2 and E.2 mixes. The optimum amount of silicates per BFS is reached in the B.2 sample, so the extra silicates introduced by the activator in the E.2 sample do not contribute to the compressive strength.

From the compressive strength tests of several mixes, it can be concluded that perlite can contribute to the compressive strength of mortars. However, it is not sufficiently reactive to completely compensate for the already dissolved silicates from waterglass. This low reactivity might be improved by further grinding of the perlite.

However, if a sufficient amount of dissolved silicates from waterglass is present in the mixture, perlite can contribute to the compressive strength. To fully optimize the contribution of perlite in a mixture, there should be sufficiently dissolved silicates present in the initial dissolution from waterglass and silicates from perlite, which come available later.

Note that the compressive strength in this research has been measured up to seven days of curing time. Since this research investigates a pozzolanic reaction, compressive strength up to 28 or even 56 days would give better insight into perlite reactivity. However, because of feasibility reasons, this is not investigated.

6.3.2. Phase formation

To better understand the contribution of perlite to the compressive strength, simultaneously with the mortars, a paste of the same composition as the mortars have been produced and characterized. After seven (± one) days, the pastes were ground to a powder, and this powder was analyzed using XRD characterization and TGA measurements. The Ref 4M, Ref 6M, A, B, C, D, E and F mixtures are analyzed by XRD characterization. All eight results can be found in appendix E. The results from mix Ref 4M and mix B are highlighted in this section.

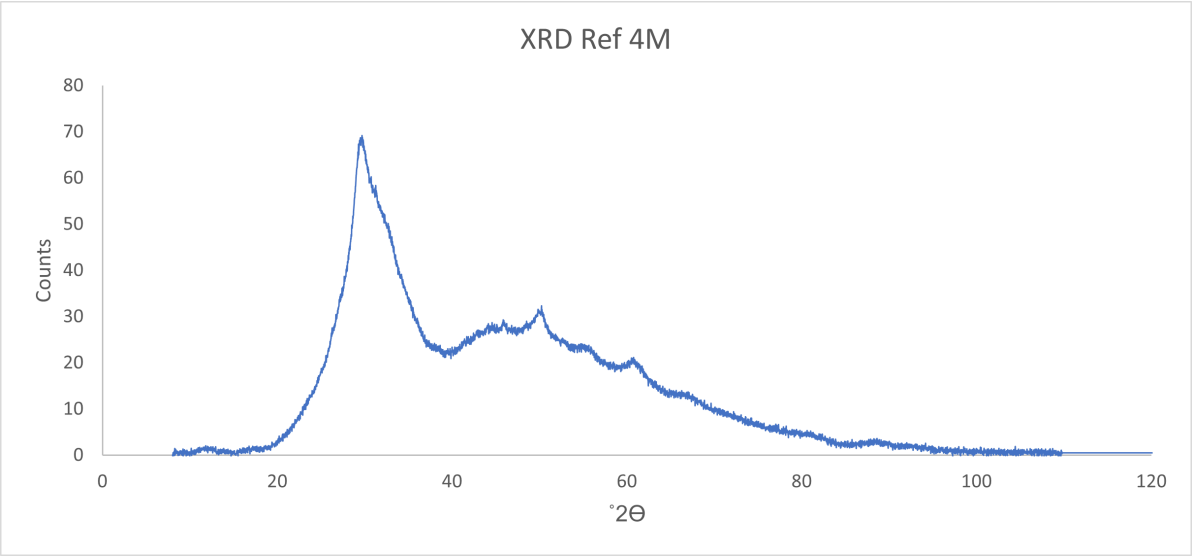

Figure 6.6: XRD pattern paste mix Ref 4M (no crystalline phases were identified).

Figure 6.6 shows the XRD pattern of mix Ref 4M and Figure 6.7 the pattern of mix B. The main visible difference is that more crystalline phases are present in mix B than in mix Ref 4M. The obtained crystalline phases are quartz and anorthite, which are the crystalline phases present in perlite. Since mix B contains a

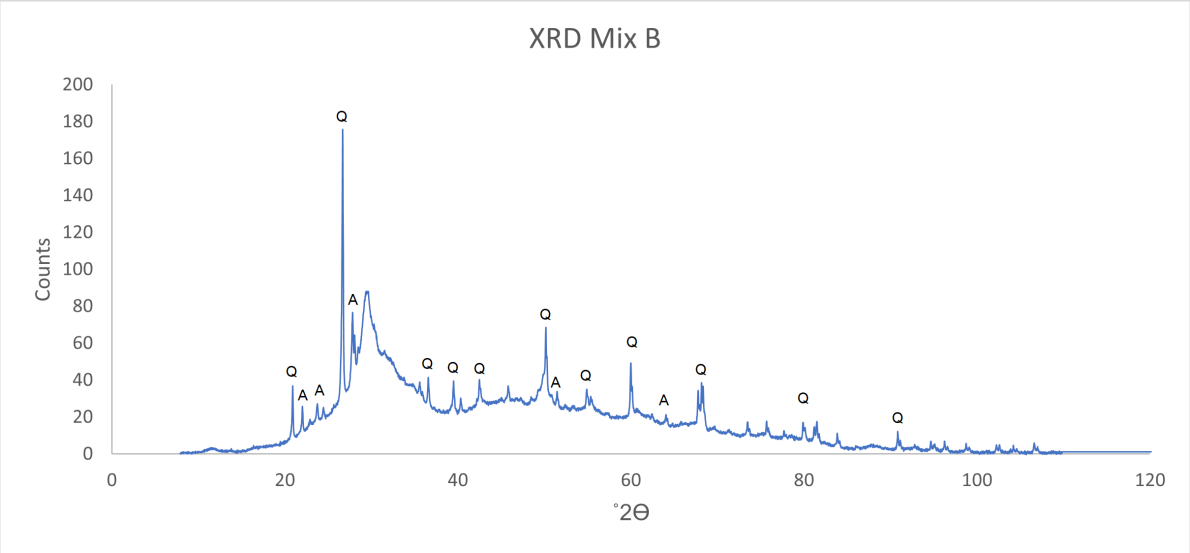

Figure 6.7: XRD pattern paste mix B (A =Anorthite, Q = Quartz.

precursor with 30% perlite, these phases are expected. This trend is found in the XRD patterns of all eight mixes.

In all eight patterns, a clear hump can be identified around 30 °2θ. This peak represents the C-A-S-H-gel and the N-A-S-H-gel, the expected hydration products from an alkali-activated BFS paste [95]. Apart from the increase in crystalline phases, a clear difference in the reaction products is not identified.

The mixtures Ref 4M, Ref 6M, B, B.2, E and E.2 (from Figures 6.4 and 6.5) are assessed by performing TGA measurements. The results are shown in Figure 6.8 and 6.9.

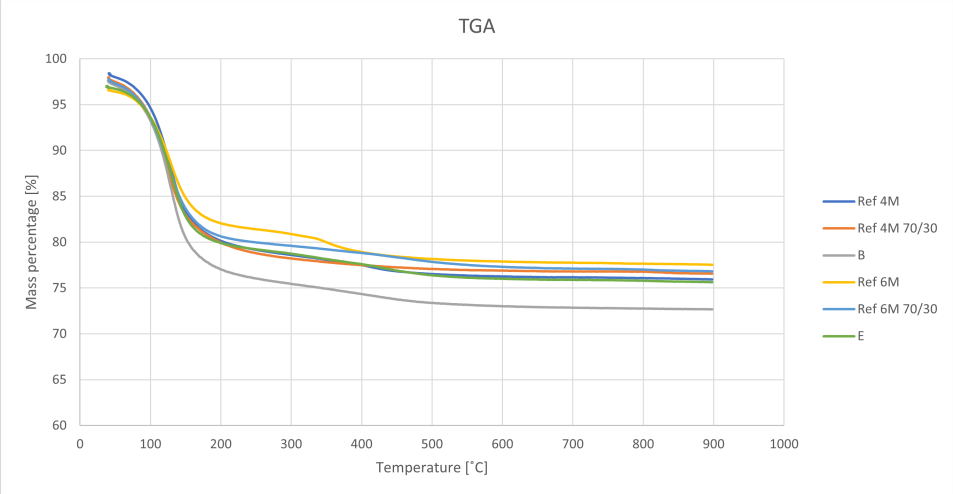

Figure 6.8: Mass loss [%] plotted to increasing temperature for the pastes from mix Ref 4M, B, B.2, Ref 6M, E, E.2, measured by thermogravimetric analysis, at 0-1000 °C.

The sizeable initial drop in Figure 6.8, visible at approximately 50 - 200°C is caused by the decomposition of the primary hydration phases (C-A-S-H and N-A-S-H gel). The decomposition of secondary hydration phases is visible at higher temperatures (300-500°C) [73]. Figure 6.9 shows the rate of mass loss at 300-500°C. The peak from the Ref 6M at 300-400°C is hydrogarnet (C_2ASH_4), and the decomposition of calcium hydroxide causes the small shoulder that is visible at 400-500°C [73]. The mixtures containing perlite show a lower mass-loss rate, indicating fewer secondary reaction products present in these samples. This is expected because of the pozzolanic nature of perlite, which consumes calcium hydroxide [3].

The primary hydration phases are mainly responsible for the compressive strength of the mortars. Figure

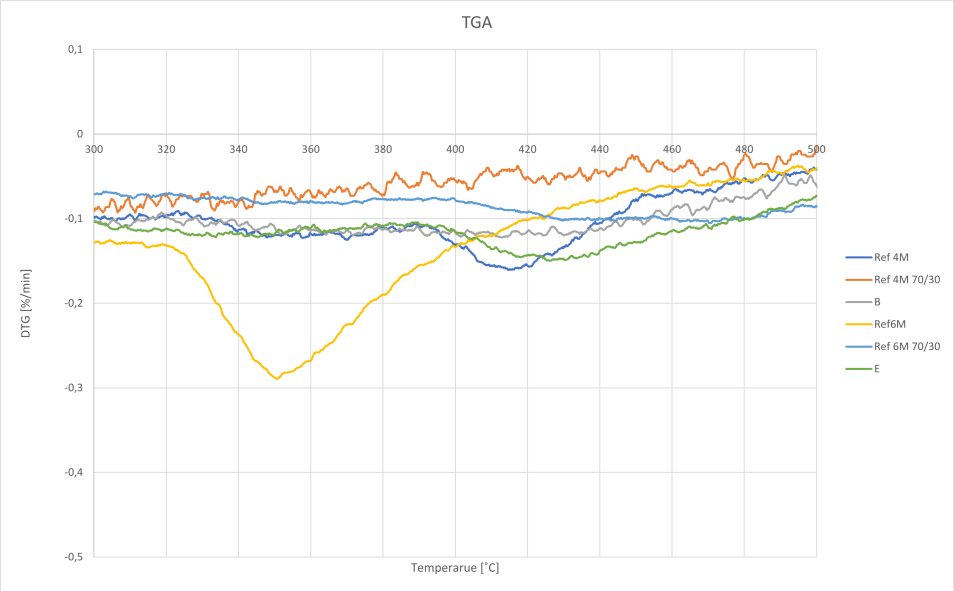

Figure 6.9: Rate of mass loss [%/min] plotted to increasing temperature for the pastes from mix Ref 4M, B, B.2, Ref 6M, E, E.2, measured by thermogravimetric analysis, at 300-500 °C.

6.10 shows the relation between the mass loss between 50 and 200 °C (caused by the loss of physically bound water in the gel pores) and the compressive strength of the mixes. Note that Figure 6.10 does not show mix E because the compressive strength of mix E depends on the setting time and not on the influence of perlite and is therefore not representative.

Figure 6.10: The relationship between the strength and the mass loss between 50 and 200 °C of mix Ref 4M, B, B.2, Ref 6M, E.2.

Figure 6.10 shows that a higher compressive strength correlates with a lower percentage of mass loss. Higher compressive strength can be due to an increase in gel phases or due to a more dense gel. Since the mass loss between 50 and 200 °C is due to the loss of physically bound water from the gel pores, the decrease in the mass loss at higher strength indicates that, for these samples, a higher compressive strength comes from a more dense gel. This makes sense since both reference mixtures (B.2 and E.2) show higher compressive strength, whereas they contain less slag. So it is unlikely they have reacted into more phases than a 100% slag mixture (Ref 4M). Multiple researchers found that an increase in silicates leads to a more dense gel. Tänzer et al. performed mercury intrusion porosimetry (MIP) analyses and found more dense hydrates and a reduction

in pore size, as also mentioned by Brough and Atkinson, Qureshi and Ghosh, and Fernández-Jiménez et al. [30, 84, 94, 96]. Zivica found similar effects from a silica fume activator. The author found that an SF activator instead of an $NaOH$ activator resulted in an increased content of hydration products, lower porosity and a lower pore median [88]. Gel with a lower porosity contains less water and shows less mass loss at 50-200°C.

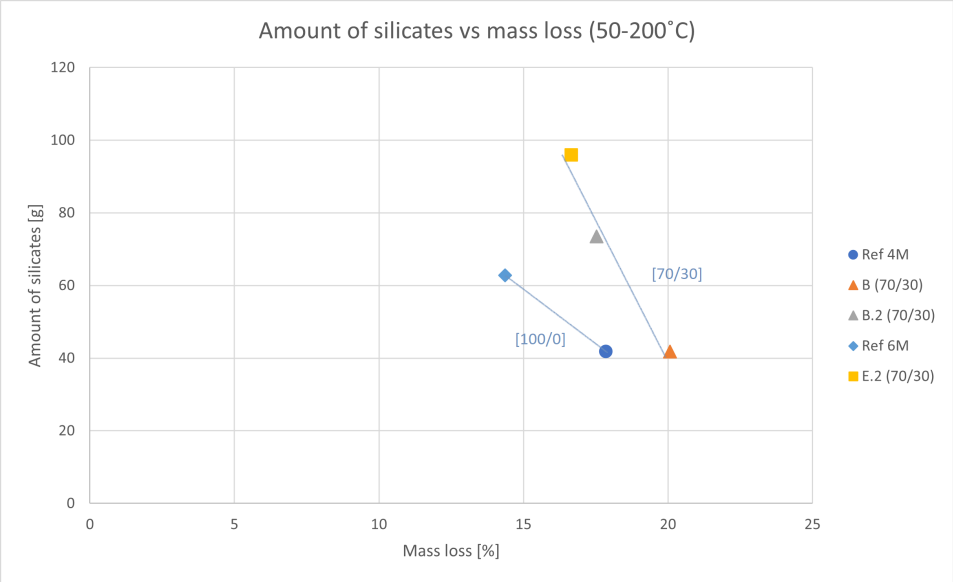

Figure 6.11: The relationship between the number of silicates and the mass loss between 50 and 200 °C of mix Ref 4M, B, B.2, Ref 6M, E.2.

Figure 6.11 shows the relation between the total amount of silicates (from perlite and waterglass) and mass loss at 50-200°C. Two trends are found, one for the [70/30] precursors and one for the [100/0] precursors. The lower the mass loss, the denser the gel. If a distinction between the uniform precursors and the blended precursors is made, it shows that an increase in silicates leads to a decrease in mass loss and thus a more dense gel, as expected [4, 64, 84]. Figure 6.11 indicates that the silicates from perlite contribute less to the density of the gel than silicates from waterglass (present in the [100/0] mixes). However, mix B.2 has slightly less mass loss than mix Ref 4M, which illustrates that perlite does contribute silicates to the gel, just not as much as waterglass does. It is essential to note that, to verify this hypothesis further investigation on this subject is necessary. These results comply with the earlier mentioned theory on the reaction products' density, and the optimum amount of silicates in the gel.

6.4. Environmental impact

Since the main goal of AAMs is to lower the environmental impact of building materials, it is crucial to assess the impact of perlite. In this section, the environmental impact of perlite will be compared to the impact of OPC and BFS. Finally, an AAM mixture with BFS as a precursor will be compared to an AAM mixture with a BFS/perlite blend.

Erdogan [63] also analyzed the environmental impact of alkali-activated perlite binders. He states that perlite has a relatively low non-CO_2 related impact (such as human toxicity or freshwater toxicity). On the other hand, the use of waste materials, such as BFS and FA, is preferred over the mining of natural materials, such as perlite. Overall, Erdogan states that perlite could be a good material to use if it is available near the construction site and leaching of hazardous materials (such as FA) is not acceptable [63].

Table 6.1: CO_2 emissions during production from OPC, BFS and expanded perlite, after [2, 82, 56].

	OPC	BFS	Expanded perlite
CO_2 emissions from production $[kg/tonne]$	1000	34	438

For this research, the CO_2 emissions from the production of OPC, BFS and expanded perlite are compared since this research examined perlite in expanded form. Table 6.1 shows the results. As can be seen in the table, perlite has a considerably lower footprint than OPC, but a significantly higher footprint than BFS. Two

reasons can be found for this. First of all, BFS is classified as a waste product, so the emissions from the production of BFS are almost all appointed to steel production instead of BFS production. Second of all, this is the CO_2 footprint from expanded perlite, which means it has been treated at temperatures of 850-900 °C. This thermal treatment causes high CO_2 emissions [2]. If one would use raw perlite (not thermally treated), the CO_2 emissions will be considerably lower. The exact amount depends on the burning process, whether coal, gas or oil is used. Another option is to use recycled perlite. The CO_2 emissions from recycled perlite (from insulation for example) will come from grinding and transportation, which are always present.

The CO_2 footprint from expanded perlite is significantly higher than that from BFS, so when used in expanded form the environmental footprint from the alkali-activated binder will increase, all though it will still be less than the footprint from OPC. However, if one can apply perlite in its raw form or recycled, the CO_2 footprint will reduce significantly.

6.4.1. Life cycle analysis

A life cycle assessment (LCA) was performed to compare AAM mix designs with a perlite/BFS precursor blend and a 100% BFS precursor mix, as well as an OPC mix design. An LCA takes into account the costs of mitigating the environmental impact of products and is, therefore, a method to quantify the environmental impact. The values used in this analysis are derived from [97, 98, 99] and are presented in Table 6.2. The values for perlite refer to raw perlite. The mixtures used are (derived) from the standard mortar mixture from NEN-EN 196-1. It is essential to mention that these standard mixtures are used to compare the impact of perlite on the environmental impact of the mixture, the impact of possible transport is not taken into account.

Table 6.2: Overview of the environmental impact of the raw material input per impact category, values derived from [97, 98, 99]

	global warming (kg CO_2)	ozone layer depletion (kg CFK-11)	acidification (kg SO_2)	human toxicity (kg 1,4-DB)	Ecotoxicity, fresh water (kg 1,4-DB)	Ecotoxcity, marine water (kg 1,4-DB)	Ecotoxcity, terrestic (kg 1,4-DB)
Waterglass	8,50E-01	3,81E-07	4,19E-03	4,42E-01	6,86E-03	3,21E+01	2,34E-03
NaOH	6,77E-02	2,44E-05	2,67E-02	4,82E-02	2,88E-04	4,83E-03	2,36E-04
BFS	3,39E+01	4,18E-06	1,49E-01	8,46E+00	2,13E-01	3,60E+02	2,18E-01
Perlite	2,19E-01	1,15E-07	8,65E-04	2,39E-01	7,57E-03	1,02E-02	2,03E-01
CEMI	4,44E+02	3,80E-06	5,42E-01	1,52E+01	4,34E-01	3,62E+03	4,15E-01
Sand	9,00E-03	5,70E-10	2,90E-05	4,30E-03	5,40E-05	5,50E-01	3,20E-05
Water	3,40E-04	1,60E-11	8,00E-07	8,30E-05	1,30E-06	2,20E-02	1,50E-06

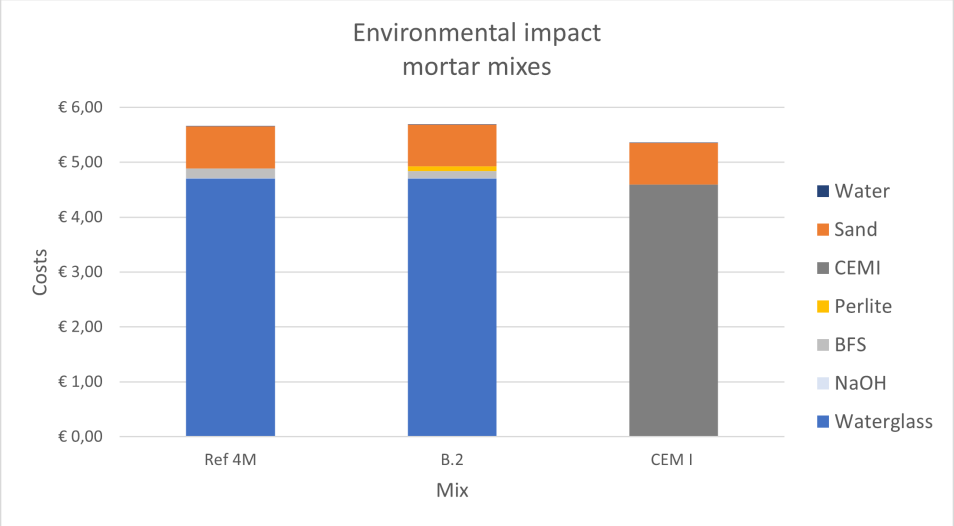

Figure 6.12: LCA values for mix Ref 4M, mix B.2 and a CEMI mix. Each mix component is visualized individually.

The AAM mixes considered are mix Ref 4M (7-day compressive strength of 68.11 MPa) and mix B.2 (7-day compressive strength of 81.59). The CEMI mix contains CEMI, sand and water according to EN-NEN 196-1. Note that each mix contains the same amount of sand and water and that the AAM mixes contain the same amount of water glass and NaOH. Figure 6.12 shows the total environmental impact of each of these 3 mortar mixes, also showing the impact of each component of the mix. Note that weighting factors are often used for LCA to address the importance of each impact category. For this study, all impact categories are considered equally important.

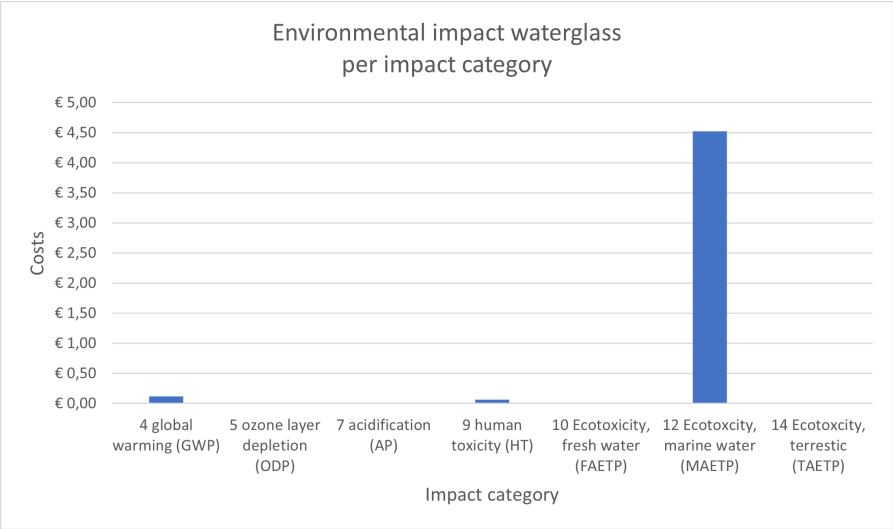

Figure 6.13: The environmental impact of 1 kg waterglass per impact category.

Figure 6.12 shows that the AAM mixtures have a higher environmental impact than the CEMI mixture, which is unexpected. As can be seen in the figure, this is mainly due to the waterglass component. This is an interesting aspect as it has been shown that the addition of perlite to a mixture can result in comparable compressive strength with a reduction of water glass in that mixture. The reason that waterglass has a high environmental impact is shown in Figure 6.13. As shown, the high environmental impact of waterglass is mainly due to the impact it has on *Ecotoxicity, seawater*. Usually this impact category has a low weighting factor (about 0,0001) compared to the *global warming potential* (0,5) or the *ozone layer depletion* (30) [99]. As a result, waterglass makes a much larger contribution to the total environmental impact than would be expected. Since this research mainly focuses on the CO_2 emissions, Figure 6.14 shows the environmental impact of the global warming potential.

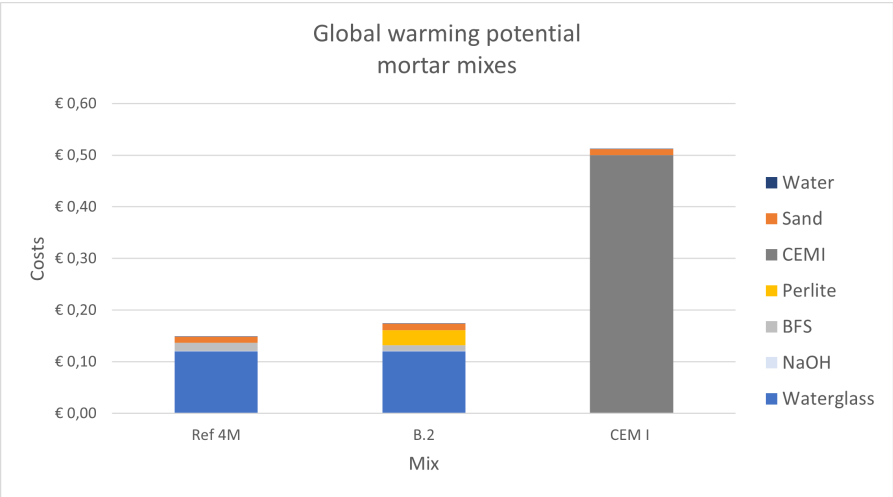

Figure 6.14: Global warming potential mix Ref 4M, mix B.2 and a CEMI mix. Each mix component is visualized individually.

As can be seen in Figure 6.14, with respect to global warming potential alone, the AAM mixes show a reduction of more than 60% compared to a standard CEMI mix. Water glass is still the most harmful component in the AAM mixtures but has a much less significant impact than CEMI. The contribution of perlite to the total impact in mix B.2 is greater than that of BFS. However, the contribution of perlite is less than that of waterglass, if the application of perlite can cause a reduction in waterglass without compromising the mechanical properties of the mixture, the overall impact will decrease. It can be concluded that the addition of perlite has no negative influence on the CO2 emissions of an AAM mixture.

6.5. Conclusion

In phase 3, alkali-activated mortars using a BFS/perlite precursor have been assessed by their compressive strength. This way, it can be determined if perlite contributes to the strength of the mortars and, consequently, can be successfully applied as a precursor in alkali-activated binders. Simultaneously with the casting of the mortars, pastes were made to assess the reaction products of the mixes. Finally, the CO_2 footprint of perlite was compared to OPC and BFS.

From comparing the compressive strength of the mortar mixes, it can be concluded that perlite can be successfully applied as a precursor in alkali-activated binders. However, with a specific surface area of 6500 m^2/kg, perlite is not sufficiently reactive to be used for the SiO_2 content instead of waterglass. Rather, it can be a great supplement next to waterglass, providing extra silicate species in later stages of the hydration process and increasing the density of the hydrates. To positively contribute to the compressive strength, there should be soluble silicates present to suppress the alkalinity and consequently suppress the fast hydration of the outer layer of perlite. However, the number of silicate species from waterglass should not be too high to prevent the saturation of the reaction products. Further grinding of perlite might increase the reactivity and give better results. However, extra grinding will also result in a higher environmental impact, which is a consideration that must be made.

The main goal of applying alkali-activated binders is to reduce the environmental footprint of concrete. Therefore, this research also assessed the CO_2 emissions from perlite production and compared them to the emissions from OPC and BFS. It was found that the CO_2 footprint from expanded perlite was twice as low as the emissions from OPC but also 15x higher than the emissions from BFS. This is because expanded perlite is thermally treated at 850-900 °C. If perlite is applied in its' raw form, then the CO_2 footprint from perlite would be considerably lower, similar to the footprint of BFS. LCA shows that the addition of perlite has a similar GWP value. It can be concluded that the addition of raw perlite does not negatively influence the environmental impact of AAM mixtures.

7

Conclusion, discussion and recommendations

This research aimed to assess the potential of volcanic materials as an alternative precursor in alkali-activated binders. The hypothesis is:

Volcanic materials can be sufficiently reactive to be used as precursors in alkali-activated binders, preserving adequate mechanical properties without compromising the reduction of CO_2 emissions.

This research has been divided into the following three phases to test this hypothesis:

1. Assessing the reactivity of raw volcanic materials.
2. Assessing the reactivity of pre-treated volcanic materials.
3. Assessing the mechanical properties of alkali-activated mortar produced with volcanic materials.

Four volcanic materials were investigated in this research: Trass, Phonolite, Perlite and Pumice. First, the research questions will be answered, after which the hypothesis can be either accepted or rejected.

7.1. Answers to the research questions

1: What properties are relevant in determining the reactivity of materials to be applied in alkali-activated binders?
From literature studies, three properties primarily influence hydraulic or pozzolanic reactivity: particle size, amorphous phase content, and chemical composition. The particle size must be sufficiently small to have enough surface area for a higher dissolution rate and an increase in nucleation sites. The material must contain sufficient amorphous phase content, so the alkaline activator can break down the microstructure and dissolve the material. Finally, the chemical composition must have amorphous alumina or silica species to exhibit pozzolanic behaviour or anhydrous calcium to display hydraulic behaviour.

2: Is the reactivity of volcanic materials originating from Europe sufficient to apply as a precursor in alkali-activated binders?
To assess the reactivity of the raw volcanic materials, properties influencing the reactivity of volcanic materials were tested, and, finally, by using modified R^3 tests, the materials were classified. In their raw state, all four materials were classified as inert, meaning that, as they are, none of these materials is sufficiently reactive. The identified limiting property of pumice and perlite was found to be the particle size, and the limiting property of trass and phonolite was found to be the lack of amorphous phase content.

3: Can the reactivity of materials be improved, to be able to be successfully applied as a precursor in alkali-activated binders?
For perlite and pumice, the limiting property was the particle size. Both were ground to lower the particle size and increase the surface area of these materials. Phonolite and trass showed to have too low an amorphous

phase content. They were calcinated to increase their reactivity. After calcination and grinding, the modified R^3 tests were performed again to classify the materials. It was found that pumice, trass and phonolite were still not sufficiently reactive. Trass and phonolite were not successfully activated, and calcination had no effect or even a negative effect. The reactivity of pumice was improved but not sufficiently to exhibit reactive properties; further grinding will most likely further increase the reactivity. Ground perlite did show reactivity and was classified as: pozzolanic, less reactive.

4: How does the application of volcanic materials influence the mix design of alkali-activated binders?
The chemical nature of the volcanic materials examined in this research were all aluminosilicates, containing almost no calcium. Considering the pozzolanic nature of perlite and the high SiO_2/Al_2O_3 ratio, it will only harden at elevated temperatures. It is best to apply perlite in combination with BFS so that the mixture will harden at room temperature, to be used in the industry. Since perlite mostly brings silicates to the mixture, adding perlite might lower the need for a sodium silicate activator. However, sodium silicates are essential to add to the activator, ensuring sufficient setting time for compacting, and delaying the high alkalinity so perlite can react. The addition of perlite will bring silicate species to the dissolution at a later stage in the reaction process and contributes to cross-linked C-S-H-gel at later stages.

5: What is the contribution of volcanic materials to the mechanical strength development of alkali-activated mortars?
The compressive strength of mortars containing perlite as precursor were tested after 1, 3 and 7 days. Exchanging sodium silicate activator and BFS for perlite leads to a constant decrease in compressive strength. The difference in compressive strength only increases over time, meaning perlite is not sufficiently reactive to compensate for sodium silicates and BFS. However, the addition of perlite to the precursor can increase strength at later stages. The mixture containing 30% perlite had a lower 1-day strength than the mixture containing 0% perlite using the same activator. However, at seven days, the 30% perlite mixture has exceeded the strength of the 0% mixture. This strength increase was not the case for similar mixtures but with an activator containing higher molarity sodium hydroxide and sodium silicates. The mechanical strength development of mixes containing perlite goes slower than mixes of 100% BFS, but the eventual strength can exceed the BFS mixes, depending on the mix design. Perlite can contribute to the mechanical strength of alkali-activated mortars up to seven days if sufficient soluble silicates are present to delay the alkalinity of the mixture.

Perlite contributes to mechanical strength development by bringing mainly silicates to the dissolution. These silicates can react with secondary reaction products such as portlandite into C-S-H-gel. The silicates can also cause a higher degree of cross-linking in the existing C-S-H-gel, resulting in lower porosity and stronger reaction products. It is crucial to note that perlite only contributes to the mechanical strength under certain conditions. As is seen in the Ref 6M mix compared to the other reference mixtures, adding waterglass instead of perlite will have a higher effect on the mechanical strength. Soluble silicates (from waterglass) are also essential to obtain satisfactory mechanical strength. There seems to be an optimum way to apply perlite, with sufficient, but not too much, waterglass.

6: What is the CO_2 footprint from alkali-activated binders with volcanic materials as precursor?
The CO_2 footprint from expanded perlite was, compared to BFS, relatively high (438 $kgCO_2/tonne$). This high value comes from the thermal treatment that leads to the expanded form of perlite. The thermal treatment occurs at temperatures of 850-900 °C. If this thermal treatment does not happen and perlite is applied in its' raw form, the CO_2 footprint reduces significantly, depending on the burning type. Raw and recycled perlite have a beneficial effect on the CO_2 footprint of mixtures if the origin of the material is nearby. An LCA of AAM mixtures with and without perlite and of a CEMI mixture, shows that the AAM mixtures have more than 60% reduction in CO_2 emissions compared to CEMI. Waterglass and CEMI are the components with the highest environmental impact. Perlite does have a higher environmental impact than BFS, however, since the present of perlite can result in a reduction of waterglass, the overall environmental impact can still decrease.

Considering the answers to the research questions, the hypothesis can be accepted. It can be concluded that volcanic materials can be sufficiently reactive to be used as precursors in alkali-activated binders, preserving adequate mechanical properties without compromising the reduction of CO_2 emissions.

7.2. Discussion

The hypothesis can be adopted; however, some remarks need to be made.

First of all, not all possible volcanic materials are investigated. Only four materials with a limiting range in chemical composition were assessed. Volcanic materials with different chemical compositions, such as anhydrous calcium, will show different results. This large variety in volcanic materials leads to the most critical remark on the results from this research: Yes, volcanic materials can be sufficiently reactive, but it strongly depends on the chemical composition of the amorphous phase content. Since volcanic materials have a large variety in chemical composition (as shown in figure 2.6), volcanic materials cannot be generalized, and each type of material needs to be assessed individually.

Perlite is able to contribute to the compressive strength of alkali-activated slag binders, but only in one specific case. Often, using waterglass is the option leading to better mechanical properties. However, using raw or recycled perlite as an additional silicate source instead of waterglass might have better environmental benefits. Therefore, using perlite as extra silicate addition next to waterglass can be a good option if the mechanical properties can be guaranteed and the environmental impact is considered.

Also important to note is that in order for perlite to harden, it needs to cure at elevated temperatures (>80°C), or it needs to be applied in combination with (for example) BFS. Therefore, BFS cannot be completely replaced with perlite.

To ensure that the reduction in CO_2 emissions is not compromised by using perlite, it is essential to use raw or recycled perlite. Expanded perlite, as is currently primarily available, has a significant CO_2 footprint, which is half of the footprint of OPC but almost 15 times higher than the footprint of BFS.

Finally, this research has shown that perlite can contribute to the compressive strength of alkali-activated mortars and, therefore, might be considered an interesting precursor. However, perlite is already used for multiple applications, such as potting soil and insulation. Whether or not a precursor is the best application for perlite has to be considered. Insulation or potting soil might be more beneficial applications for perlite.

This research has solely focused on the production of AAMs as replacement for concrete. However, alkali-activated perlite could have beneficial properties for other applications as well. It is likely that at higher activation temperatures (>80°C) a mixture with a 100% perlite precursor will harden. Therefore, perlite could be an interesting material for the ceramics industry or for the production of building bricks.

7.3. Recommendations

Some recommendations are stated for further research on using volcanic materials in alkali-activated binders.

As mentioned earlier, only four volcanic materials are analyzed in this research. Volcanic materials present a wide range in chemical composition and microstructure. Therefore, several volcanic material resources should be validated. Preferably, volcanic materials from volcanoes that were recently, or still are, active because these materials are more likely to have their amorphous microstructure since there was limited time for the atoms to form a crystal grid.

Considering the materials assessed in this research, it would be interesting to further analyze the effect of the particle size. For perlite, determining the optimum specific surface area is interesting, taking also the level of agglomeration into account. More finely grained particles are likely to increase the reactivity and make it easier for perlite to be applied in mixtures. For pumice, it is interesting to assess further grinding to a specific surface area, similar to that of perlite, and compare the reactivity. Likely the reactivity of pumice becomes equal to, or might even exceed, the reactivity of perlite at similar surface areas.

In this research, for the production of mortar containing perlite, perlite has been applied as a powder in a blended precursor. Bernal et al. [100] advise applying similar materials, such as silica fume and metakaolin, by adding it to a $NaOH$ solution 24 hours before casting. This way, the reactive silicate and alumina will dissolve before casting, making them immediately available to form hydrates. Considering industrial application, this method was not tested. However, it is still interesting to analyze the application of perlite in this way and compare the results to get a better insight into the dissolution ability of perlite.

Since this research only studied the application of perlite on mortar level, further research should assess the application of perlite on concrete level. Analyzing on concrete level is necessary for the promotion of the industrial application.

It is also recommended further to analyze the durability aspects of alkali-activated perlite binders. The increased density of the hydrates implicates that durability aspects such as carbonation and chloride ingress are not an issue. However, this should still be investigated, as well as shrinkage, freeze-thaw behaviour and

creep.

IV

Appendix

A

Cement types

hoofdtypen	aanduiding van de 27 producten (gewone cementsoorten)		samenstelling (gehalten in massaprocent [1])														
			hoofdbestanddelen														nevenbestanddelen
			klinker	hoogovenslak	microsilica	puzzolanen		vliegas		gebrande leisteen	kalksteen						
						natuurlijke	gebrande natuurlijke	siliciumhoudend	calciumhoudend								
			K	S	D [2]	P	Q	V	W	T	L	LL					
CEM I	portlandcement	CEM I	95-100	-	-	-	-	-	-	-	-	-					0-5
CEM II	portlandslakcement	CEM II/A-S	80-94	6-20	-	-	-	-	-	-	-	-					0-5
		CEM II/B-S	65-79	21-35	-	-	-	-	-	-	-	-					0-5
	portlandmicrosilicacement	CEM II/A-D	90-94	-	6-10	-	-	-	-	-	-	-					0-5
	portlandpuzzolaancement	CEM II/A-P	80-94	-	-	6-20	-	-	-	-	-	-					0-5
		CEM II/B-P	65-79	-	-	21-35	-	-	-	-	-	-					0-5
		CEM II/A-Q	80-94	-	-	-	6-20	-	-	-	-	-					0-5
		CEM II/B-Q	65-79	-	-	-	21-35	-	-	-	-	-					0-5
	portlandvliegascement	CEM II/A-V	80-94	-	-	-	-	6-20	-	-	-	-					0-5
		CEM II/B-V	65-79	-	-	-	-	21-35	-	-	-	-					0-5
		CEM II/A-W	80-94	-	-	-	-	-	6-20	-	-	-					0-5
		CEM II/B-W	65-79	-	-	-	-	-	21-35	-	-	-					0-5
	portlandleisteencement	CEM II/A-T	80-94	-	-	-	-	-	-	6-20	-	-					0-5
		CEM II/B-T	65-79	-	-	-	-	-	-	21-35	-	-					0-5
	portlandkalksteencement	CEM II/A-L	80-94	-	-	-	-	-	-	-	6-20	-					0-5
		CEM II/B-L	65-79	-	-	-	-	-	-	-	21-35	-					0-5
		CEM II/A-LL	80-94	-	-	-	-	-	-	-	-	6-20					0-5
		CEM II/B-LL	65-79	-	-	-	-	-	-	-	-	21-35					0-5
	portlandcomposietcement [3]	CEM II/A-M	80-94	←			6-20						→				0-5
		CEM II/B-M	65-79	←			21-35						→				0-5
CEM III	hoogovencement	CEM III/A	35-64	36-65	-	-	-	-	-	-	-	-					0-5
		CEM III/B	20-34	66-80	-	-	-	-	-	-	-	-					0-5
		CEM III/C	5-19	81-95	-	-	-	-	-	-	-	-					0-5
CEM IV	puzzolaancement [3]	CEM IV/A	65-89	-	←		11-35		→	-	-	-					0-5
		CEM IV/B	45-64	-	←		36-55		→	-	-	-					0-5
CEM V	composietcement [3]	CEM V/A	40-64	18-30	-	←		18-30	→	-	-	-					0-5
		CEM V/B	20-38	31-50	-	←		31-50	→	-	-	-					0-5

[1] De waarden in de tabel zijn uitgedrukt ten opzichte van de som van hoofd- en nevenbestanddelen.
[2] Het gehalte microsilica mag niet meer dan 10% bedragen.
[3] In het geval van portlandcomposietcement CEM II/A-M en CEM II/B-M, puzzolaancement CEM IV/A en CEM IV/B en composietcement CEM V/A en CEM V/B moeten de hoofdbestanddelen, anders dan klinker, in de aanduiding van het cement vermeld zijn.

Figure A.1: Overview cement types.

B

Tests

B.1. X-ray fluorescence

X-ray fluorescence (XRF) is used to determine the chemical composition of the raw materials. XRF spectrometry is based on the wavelength-dispersive principle, which states that an element emits a characteristic X-ray wavelength that can be estimated [101, 102]. An X-ray beam that passes through a material is susceptible to three processes: absorption, scattering and fluorescence. Fluorescence occurs when the primary beam of X-rays contains a high enough amount of energy to generate secondary radiation from the specimen. The secondary radiation is specific for each element. XRF isolates and measures each individual characteristic wavelength in order to determine the elements present in the measured sample. The measured characteristic intensities of the secondary radiation can be converted to elemental concentrations of the unknown material [103].

The main advantage of XRF is the relatively simple, systematic technique, which is independent of the chemical state of the elements. High accuracy is easily obtained by correcting interference in the X-ray radiation line. Also the sample preparation, grinding into a fine powder, is simple and fast [102]. The XRF analysis shall be performed according to NEN-EN 196-2 (REF EN196-2)

Some drawbacks of XRF should be considered as well. Firstly, not every XRF instrument has the ability to measure all the elements and are therefore restricted (generally to fewer than eleven elements). Secondly, the elements are generally calculated as counts instead of percentages, conversion to percentages requires quantitative analysis. Other drawbacks are stated, however, these do not apply to a powder that is analysed in a laboratory [102].

Important for XRF analyses is that samples must be larger than ten times the largest particle. This is necessary because the sample often must be ground into a fine powder, to equally expose each element to the radiation. Finally, it is important to ensure the purity of the sample, so accurate results can be obtained [104].

B.2. X-ray diffraction

X-ray diffraction (XRD) is a plot of the intensity of X-rays, scattered at different angles by a sample. In XRD, an X-ray tube sends a beam of X-rays to a sample, this sample scatters the X-ray beam, resulting in an output beam which is detected by a detector. The detector and the sample move around in a circle, the detector therefore only records the number of X-rays observed at angle 2θ. By rotating the sample as well, it is ensured that the X-ray beam is focused [73, 105]. A schematic representation of XRD is shown in figure B.1.
XRD technique depends on the crystalline planes of the material and is able to identify phases. Each phase has specific chemistry and atomic arrangement, for example, SiO_2 has the phases quartz, cristobalite and glass. In these phases, the chemical composition is identical, but the atomic arrangement differs, therefore the X-ray output is recorded at different angles [105]. From the XRD pattern, crystalline phases and the presence of amorphous material can be determined through qualitative phase analysis. The amount of each crystalline phase can be determined through quantitative phase analysis.

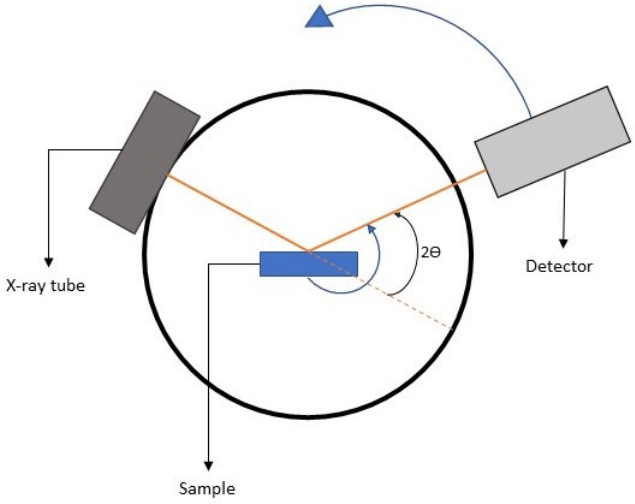

Figure B.1: schematization of XRD after [105]

B.2.1. Qualitative phase analysis

Qualitative phase analysis in XRD entails the comparison of peaks from an unknown material to peak patterns of known phases. Another option for identification is to compare the d-values (the spacing between the crystal planes) of the most intense XRD reflections of common cement phases to the peak positions in the recorded XRD pattern. Note that this way of identification is used for analysing cementitious materials. Using Rietveld analysis, the XRD scan can be decomposed into calculated contributions of phases that build up the material. Phase identification through XRD often only supplies a list of suggestions for the minor phases, in that case, the analyst should decide, preferably based on additional information, which phases are most likely to be present [73].

B.2.2. Quantitative phase analysis

The observed peak positions (2θ) can be converted into the interatomic distances (d_{hkl}) using Bragg's law:

$$d_h kl = \frac{\lambda}{2sin\theta} \tag{B.1}$$

Where λ refers to the wavelength of the incident X-ray radiation, often copper ($CuK\alpha$). It is important to note that the diffraction pattern is instrument depended. Therefore, relative intensities should be used, comparing the intensities of the peaks to the most intense '100% peak'. To determine the intensity, peak areas are more representative than peak heights [105]. In diffraction patterns, a high degree of peak overlap can occur. Other problems include the variability in composition and crystal structure that can result in significant variations in peak positions and relative intensity [73].

Whole-powder-pattern-fitting methods are enabled to overcome peak overlap problems. In whole-powder-pattern-fitting, all reflections of all phases are considered and an algorithm is used to create a diffraction pattern of the phases that matches the measured pattern. The calculated pattern can be a combination of measured standard patterns or can be calculated from structure data, as in the Rietveld method [73, 105].

B.2.3. Rietveld Analysis

In the Rietveld refinement method, a theoretical pattern is refined so that it matches the measured pattern. This is done according to the least-squares approach:

$$S_y = \sum_i w_i (y_i(obs) - y_i(calc))^2 \tag{B.2}$$

Where w_i presents the weighted average, $y_i(calc)$ presents the calculated intensity at a certain point and $y_i(obs)$ presents the observed intensity at a certain data point [73, 106].

Fundamental crystal structure models are used to obtain the calculated Rietveld pattern. Crystallite size, microstrain and preferred orientation can all be extracted from these models [105].The Rietveld refinement method requires appropriate software to be performed (GSAS and FULLPROF are the most widely used packages) [106].

B.3. Laser diffraction Analysis

The particle size distribution (PSD), as well as the specific surface area (SSA) are parameters that give information about the fineness of the powder. The particle size of a powder influences the handling, storage and domain use of a powder. For example, agglomerated particles need more liquid to become a flowable paste. Note that, since most of the particles are not spherical, when stating a diameter the measuring method has to be mentioned because the required diameter is method-dependent [73].

For the PSD, certain percentiles can be calculated such as D10, D50 and D90, where respectively 10%, 50% and 90% of the particles are below these diameters in the distribution graph. The sample must be representative of the material, therefore:

- The sample should be taken from a powder in motion, using rotary samplers of spinning rifflers.
- Several small samples should be taken at different time intervals.

When the two conditions mentioned above are applied, only 3 small samples are needed. The minimum weight of the sample can be calculated according to the following equation [73]:

$$W_m = 0,5\left(\frac{\rho_p}{\sigma_i^2}\right)\left(\frac{1}{w_1}-2\right)\left(\frac{D_1^3 - D_2^3}{2}\right) * 10^3 \tag{B.3}$$

In LDA a powder is dispersed in a liquid (wet LD) or a gas (dry LD), the LD measures the light that is scattered, diffracted and adsorbed by this powder. The laser light passes through a suspension (wet LD) or an aerosol (dry LD) and the variation of the light intensity is given by Azzopardi's formula:

$$I(\theta) = I_0 \int_0^\infty f(R)\left(\frac{RJ1\alpha\theta}{\theta}\right)^2 dR \tag{B.4}$$

A schematization of a laser diffractometer is given in fig B.2. When the dispersion of the particles is optimised, the results for wet LD and dry LD are very similar. One advantage of dry LD over wet LD is that for wet more grams of the sample can be used, which reduces the error [73].

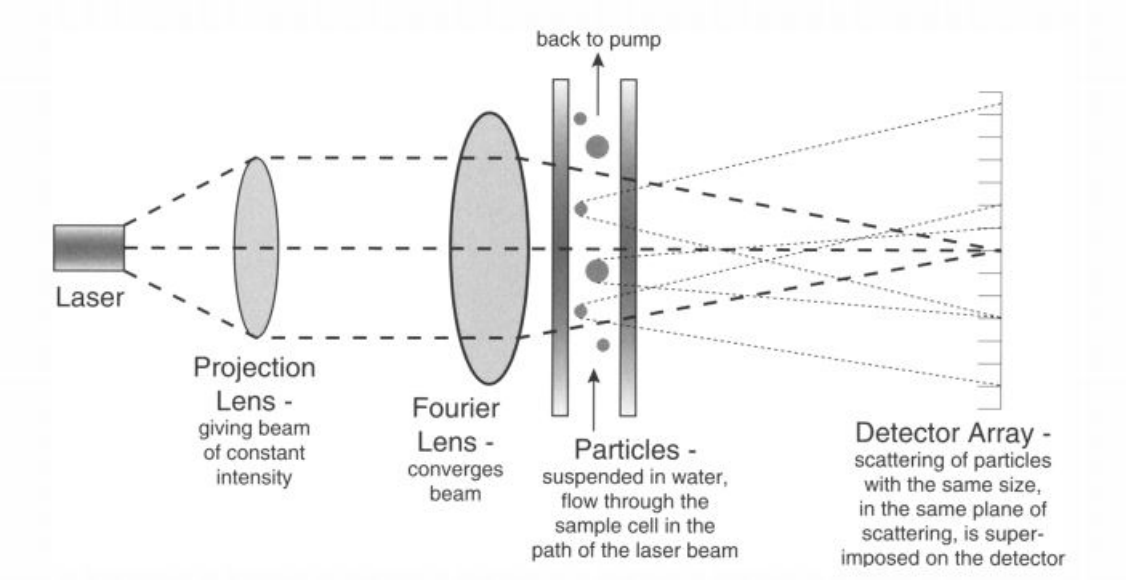

Figure B.2: Schematization of laser diffractometer Coulter^{TM} LS230 laser granulometry optical system [107]

To calculate the PSD from the LDA two optical models are used: the Fraunhofer diffraction model and the Mie theory. The Mie theory takes phenomena other than diffraction (such as transmission) into account and is, therefore, able to offer an exact solution to the scattering of light from a homogeneous sphere [108]. When a particle has a significant anisotropic shape, LD overestimates the width and gives bimodal distributions. Because the diffraction pattern of the particle depends on the orientation of the particle with respect to the laser beam. The image analyses are based on spherical particles, to that end determining the shape of the particles might be necessary [73, 109].

B.4. Isothermal calorimetry

Cement hydration is an exothermic reaction, meaning that heat is released during the reaction. Calorimetry is the measurement of heat and heat production rate [73]. Since a reactive material produces heat when it hydrates, calorimetry has been a useful tool to determine the reactivity of a material [36, 76]. There are several types of calorimetry, this section will focus on isothermal calorimetry.

An isothermal calorimeter consists of a thermostatic heat sink upon which two heat flow sensors are placed. The sample and the reference sample are both placed in an ampoule which is placed in an ampoule holder that is in contact with a heat flow sensor. The two samples are thermally connected by the heat flow sensors to a thermostatic heat sink. The difference between the output from the sample and the reference sample is the calorimeter output (NPR-CEN/TR). A schematization of an isothermal calorimeter is shown in figure B.3. The thermostatic heat sink ensures that the surrounding temperature remains constant, in order to establish correct heat measurements [73].

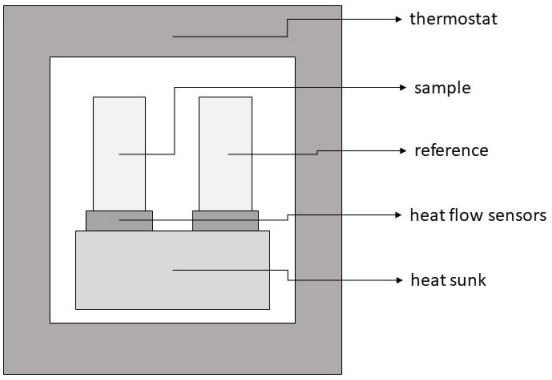

Figure B.3: Schematization of isothermal calorimeter after (NPR-CEN/TR)

A calorimeter uses a heat flow sensor that measures the heat in volts. The calibration coefficient (ϵ) is the parameter that transforms this voltage into thermal power. The signal that is measured when no heat is produced in the sample, is called the baseline (U_0). When the heat produced by a sample has been measured (U), thermal power (P) is calculated as follows:

$$P = \epsilon(U - U_0) \tag{B.5}$$

Where P is in watts, U in volts and ϵ in watts/volt.

When performing an isothermal calorimetry analysis, the following points should be taken into consideration when performing an isothermal calorimetry analysis [73](NPR-CEN/TR):

- Make a sample from a larger mix, in order to secure a representative sample.
- The baseline of the instrument should be repeatable and stable.
- The instrument should be calibrated.

- The ampoule should be vapour tight enough to ensure that endothermic thermal powers of evaporation do not influence the measurements.
- Weigh constituents in the calorimeter vial and mix inside the vial using a plastic spatula or on a test tube shaker. Since the reaction, and therefore the heat release, can occur relatively fast, mixing inside the vial ensures that the initial reaction is measured as well.
- Mixing can be performed inside the vial when it is in the calorimeter, however, in this case, it should be taken into account that the intensity of the mixing is relatively low. This will lead to a lower hydration rate than if standard mixing procedures are used.

B.5. Thermogravimetric analysis

Thermogravimetric analysis measures the change in weight of a sample as a function of time or temperature. The weight is recorded while the sample is subjected to a controlled heating or cooling environment [110]. Therefore, TGA can be used to examine thermal events as absorption, adsorption, desorption, vaporization, sublimation, decomposition, oxidation, and reduction. In addition to this, TGA can be utilized for the evaluation of products lost during chemical reactions, such as evaporation. Considering these data, TGA can be used to evaluate the thermal stability of the material [110].

The main part of the TGA apparatus is the thermobalance. A schematization of the thermobalance is shown in figure B.4. The thermobalance consists of a clamp that holds the arm of a microbalance. This is the part which is responsible for the heating of the sample and determining the difference in weight. Supplementary to the thermobalance is purge gas, this should contain less than 0,001% water content by mass [110].

The ouput of TGA is a mass-temperature curve as shown in figure B.5. From the curve the mass loss can be determined as follows:

$$m_l = \frac{m_s - m_f}{m_s} x100 \tag{B.6}$$

where m_s is the mass in milligrams at point A, and m_f is the mass in milligrams at point B [110].

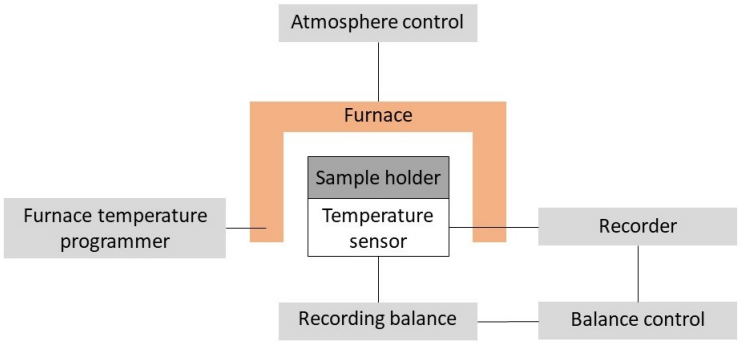

Figure B.4: Thermobalance schematization after [111]

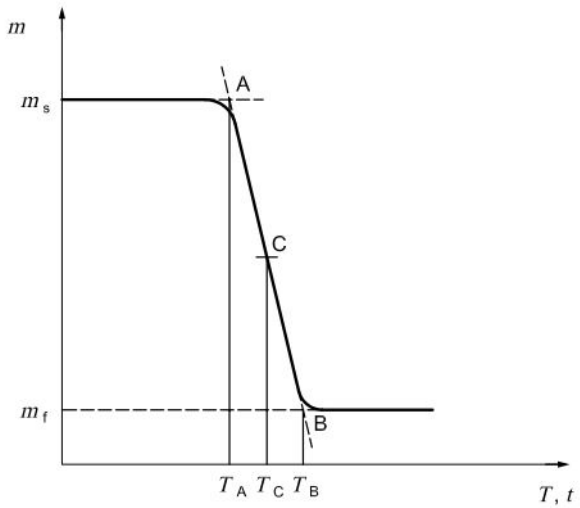

Figure B.5: TGA curve from [110]

C

Materials

Figure C.1: Pumice

Figure C.2: Trass

Figure C.3: Perlite

Figure C.4: Phonolite

D

SEM images

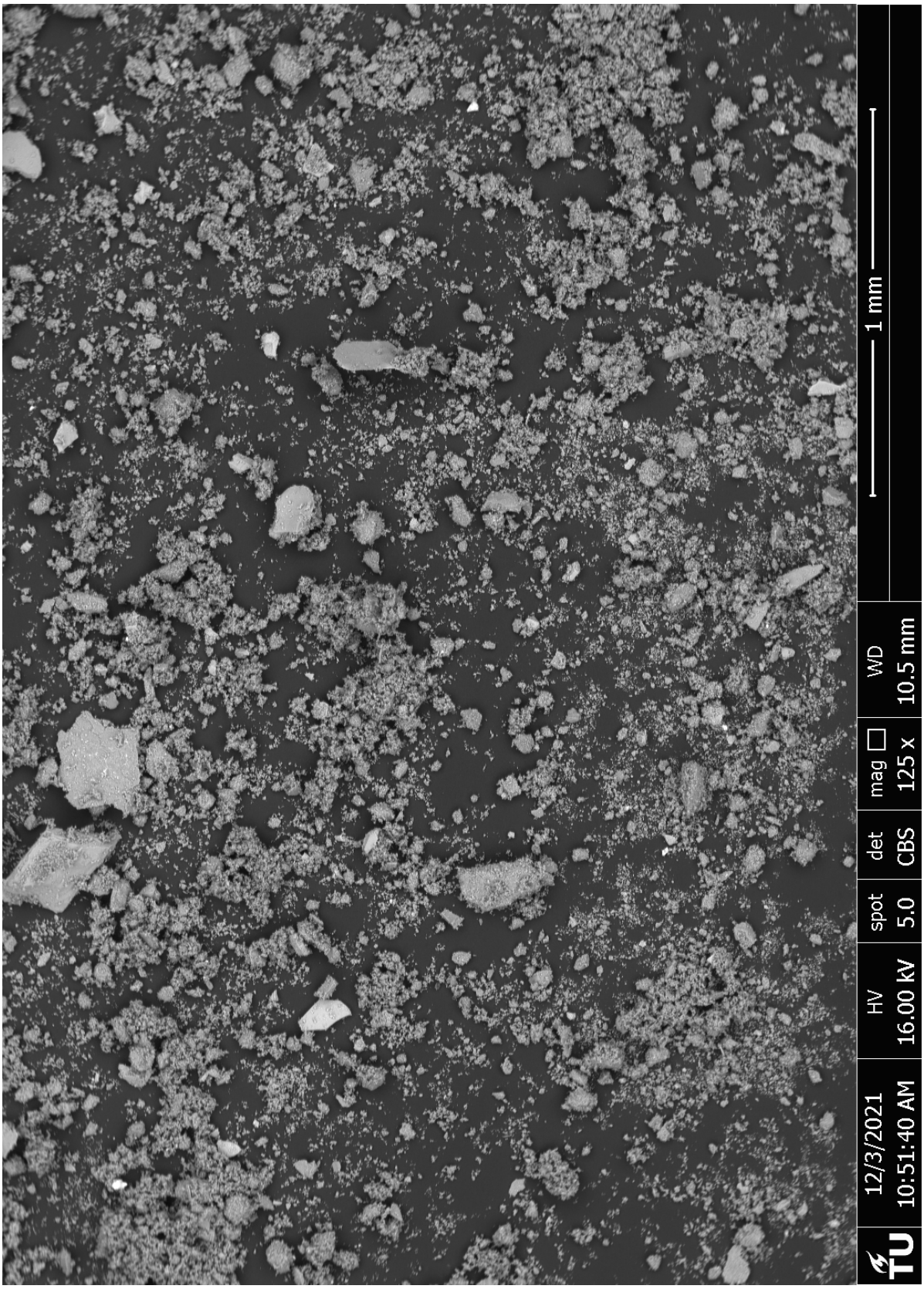

Figure D.1: Trass SEM 125x magnitude

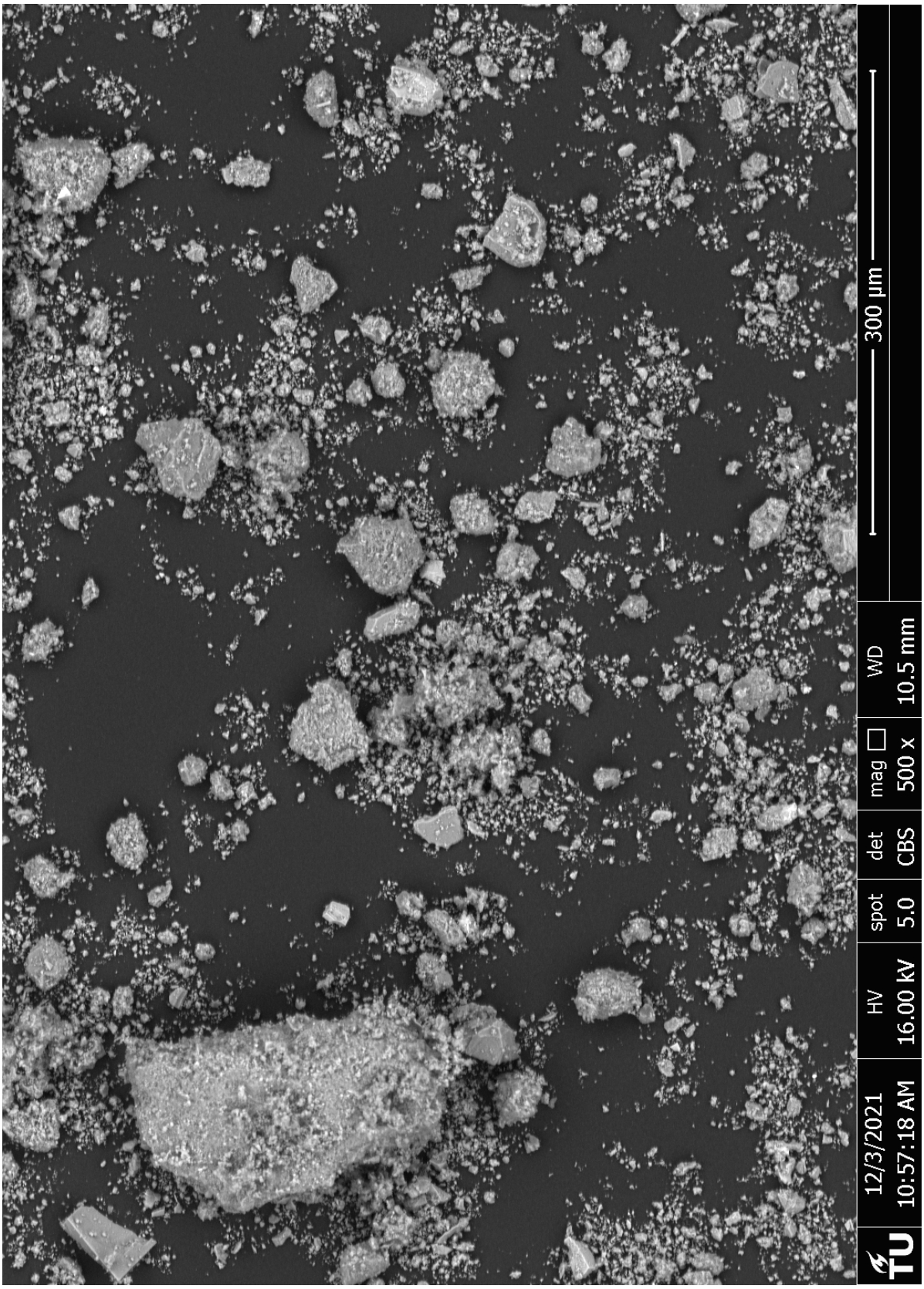

Figure D.2: Trass SEM 500x magnitude

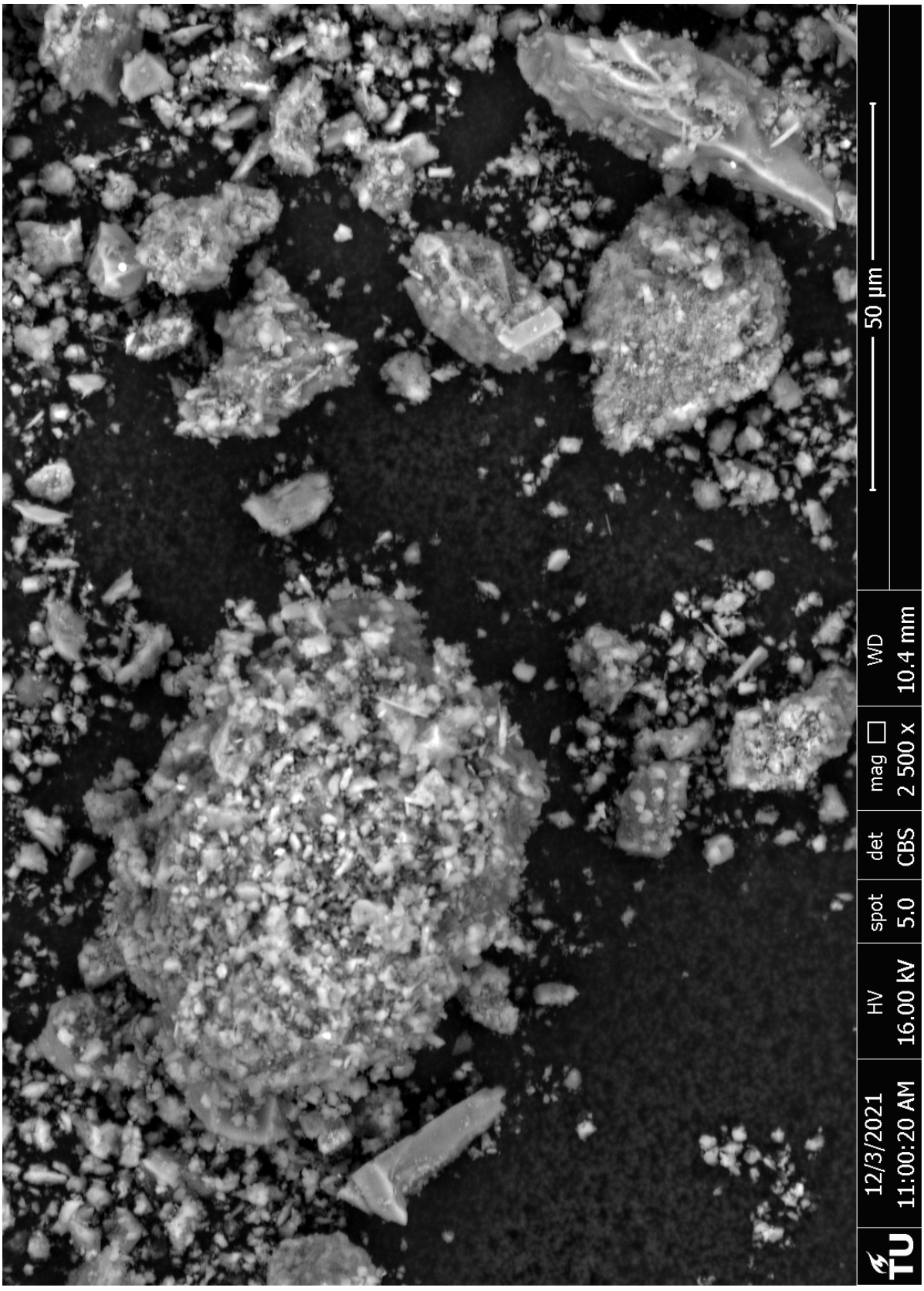

Figure D.3: Trass SEM 2500x magnitude

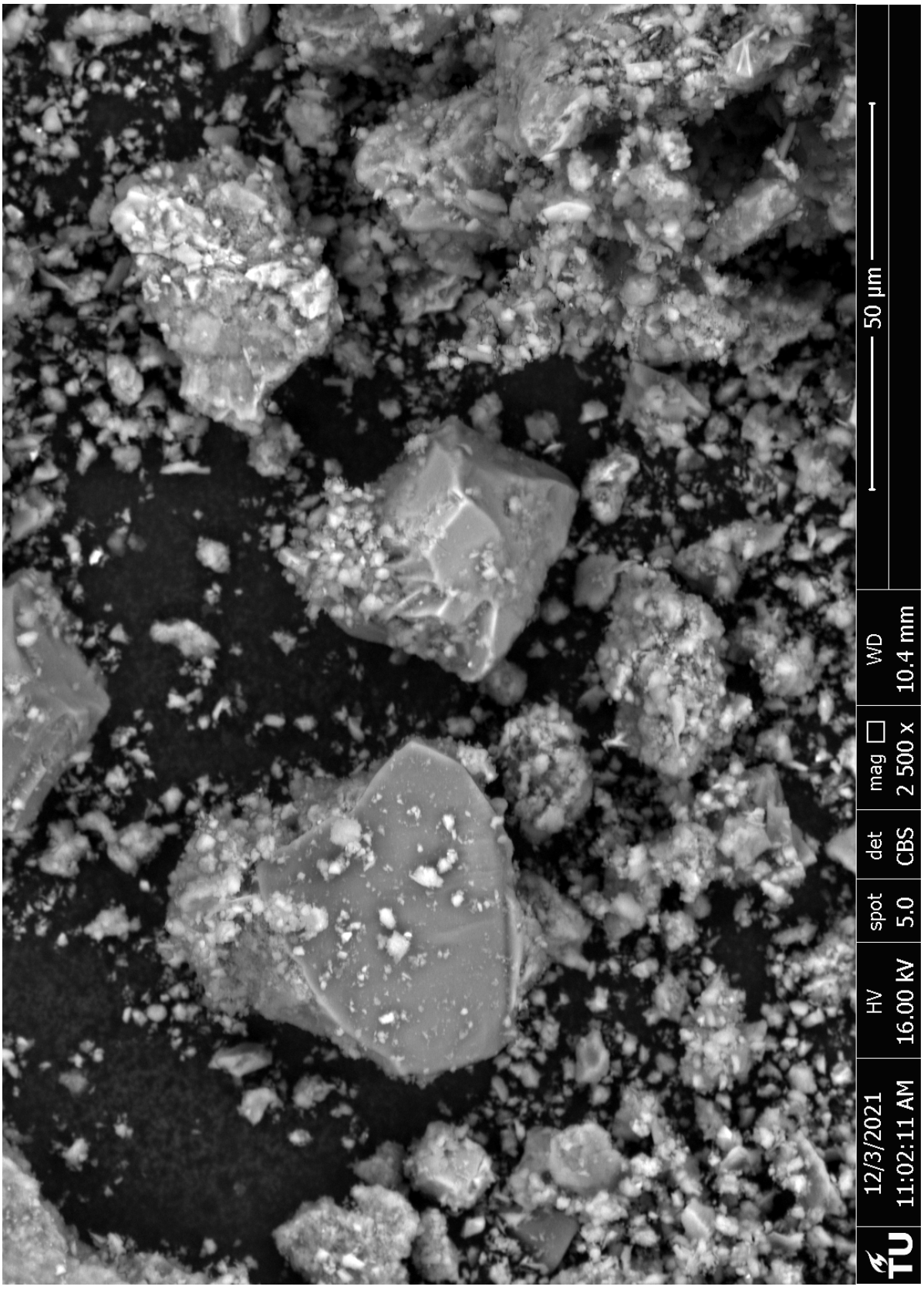

Figure D.4: Trass SEM 2500x magnitude

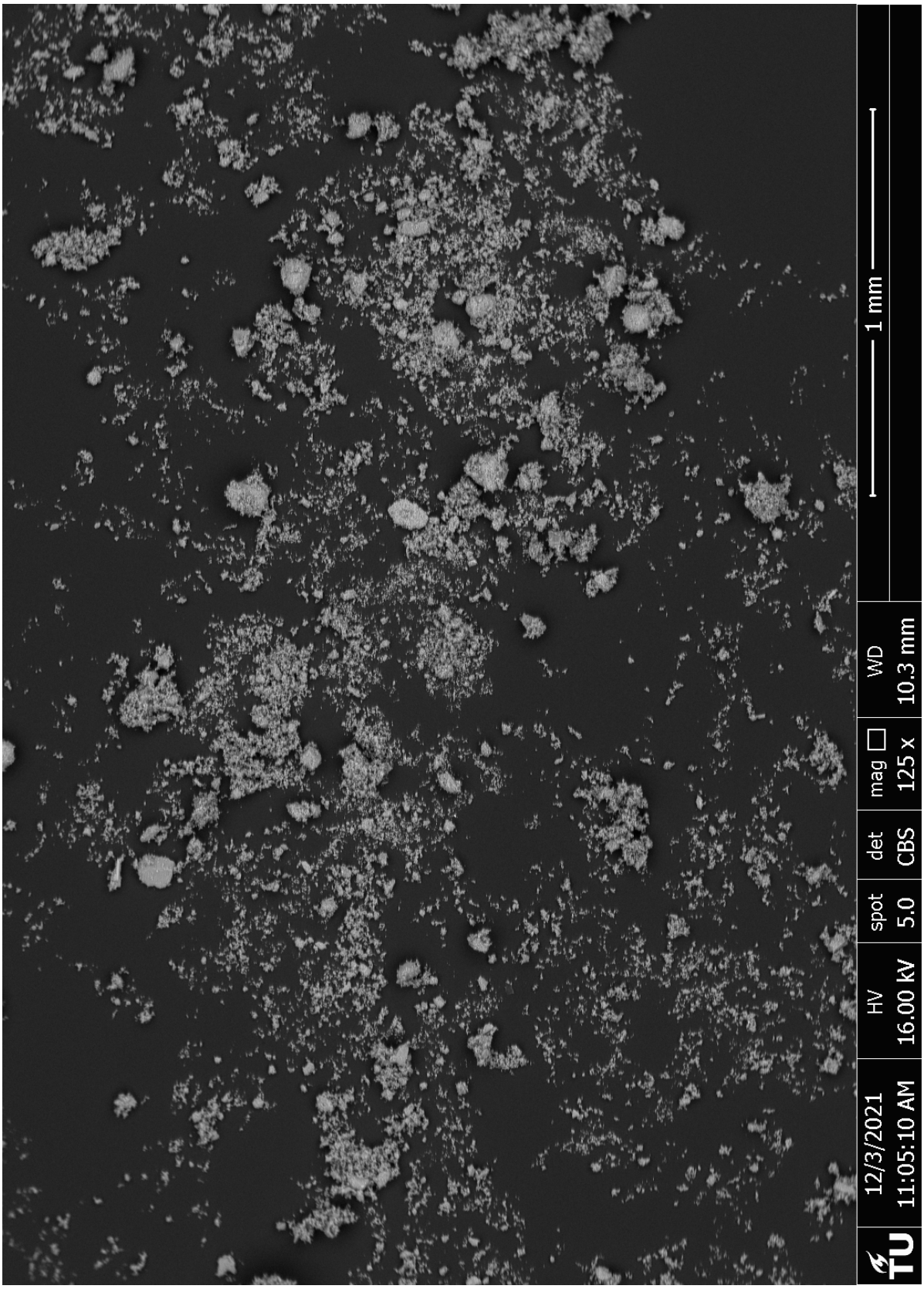

Figure D.5: Phonolite SEM 125x magnitude

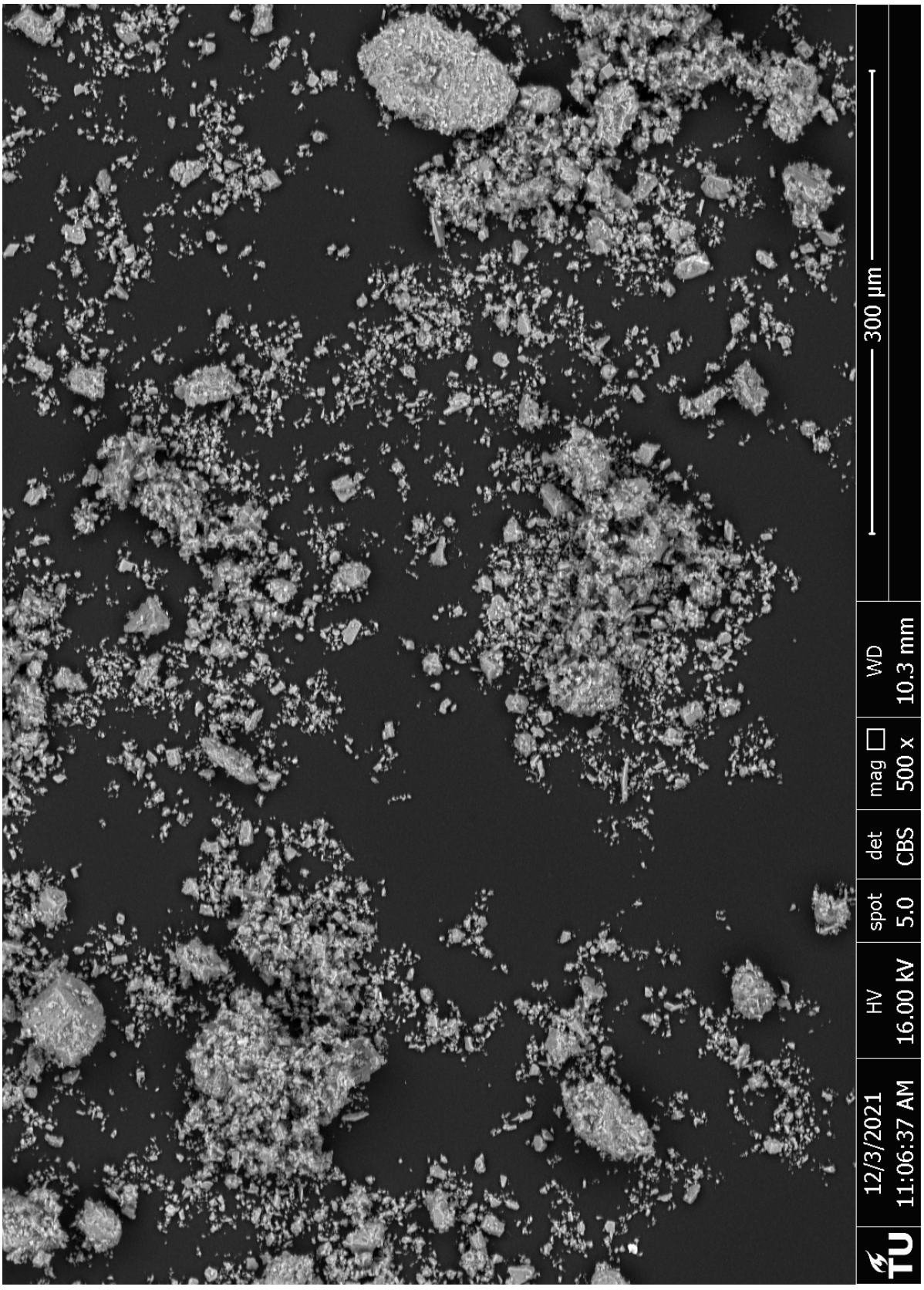

Figure D.6: Phonolite SEM 500x magnitude

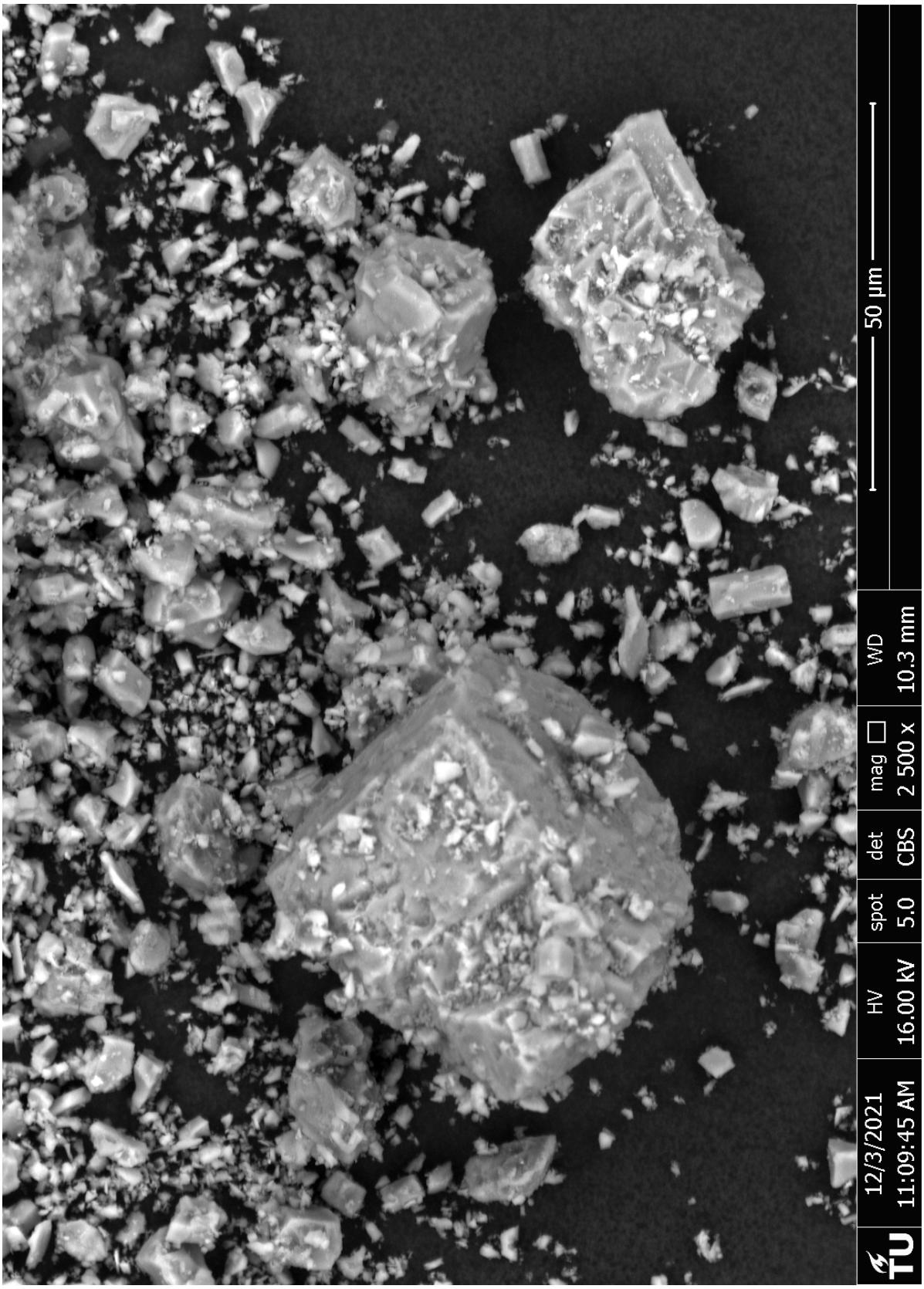

Figure D.7: Phonolite SEM 2500x magnitude

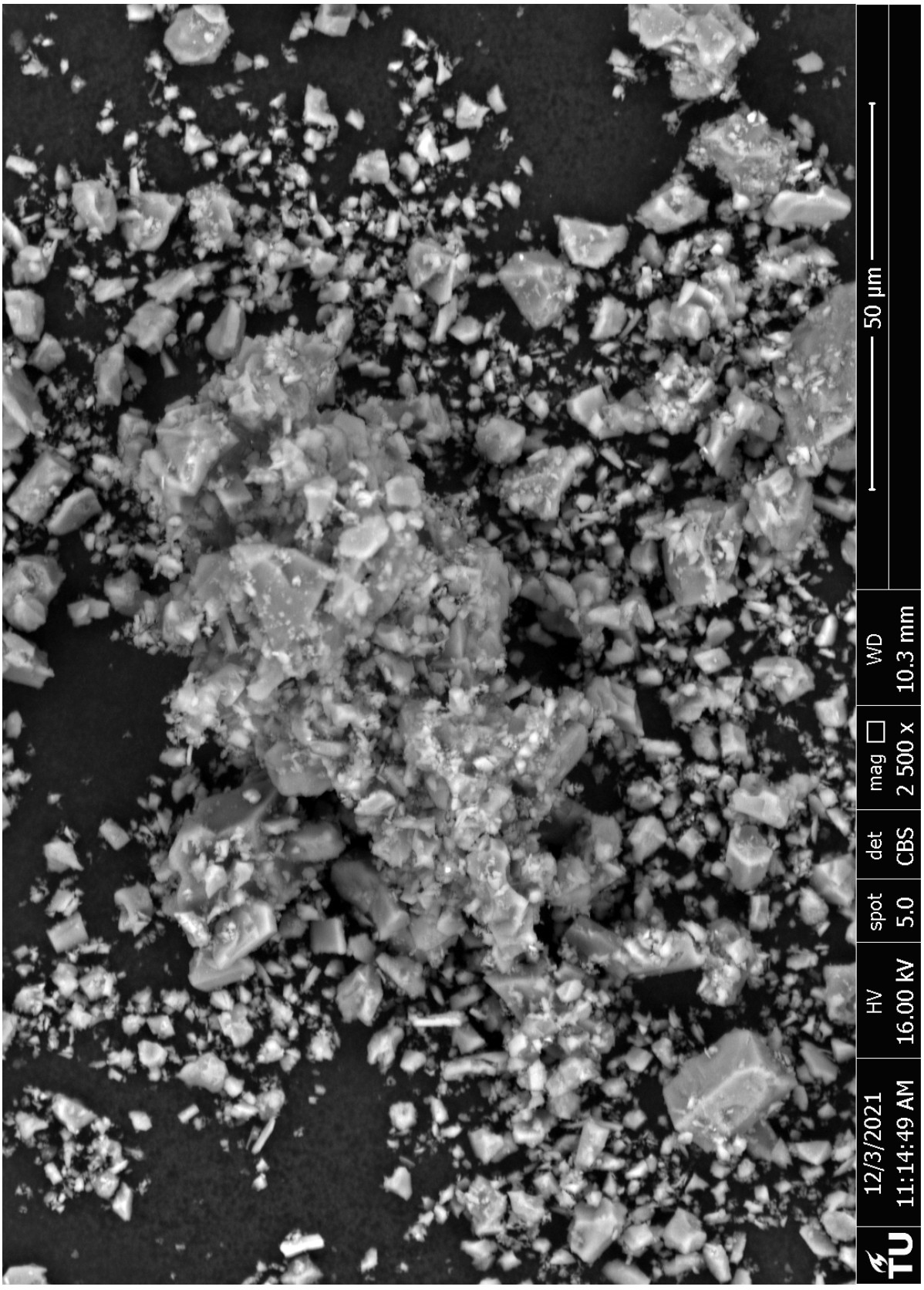

Figure D.8: Phonolite SEM 2500x magnitude

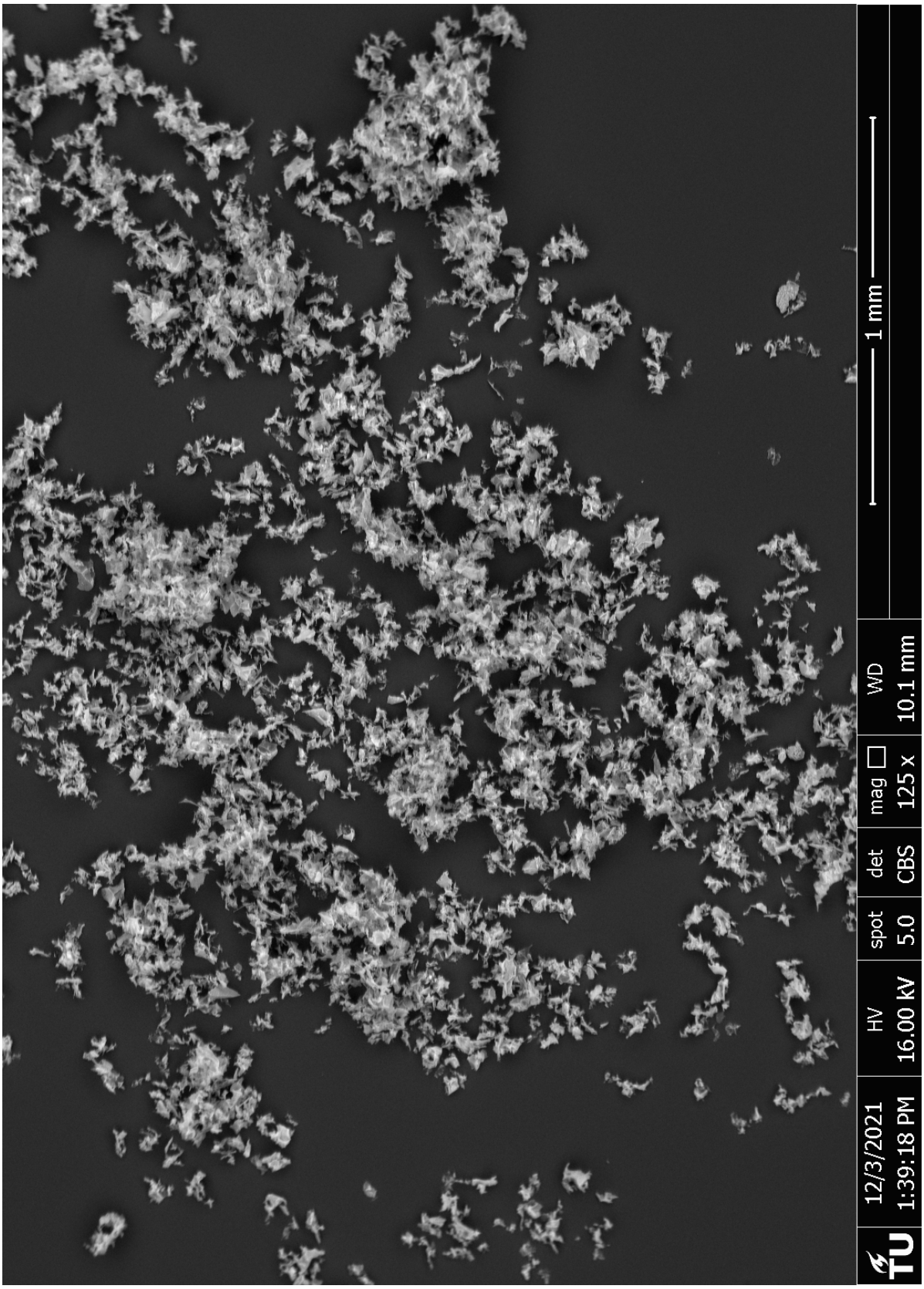

Figure D.9: Perlite SEM 125x magnitude

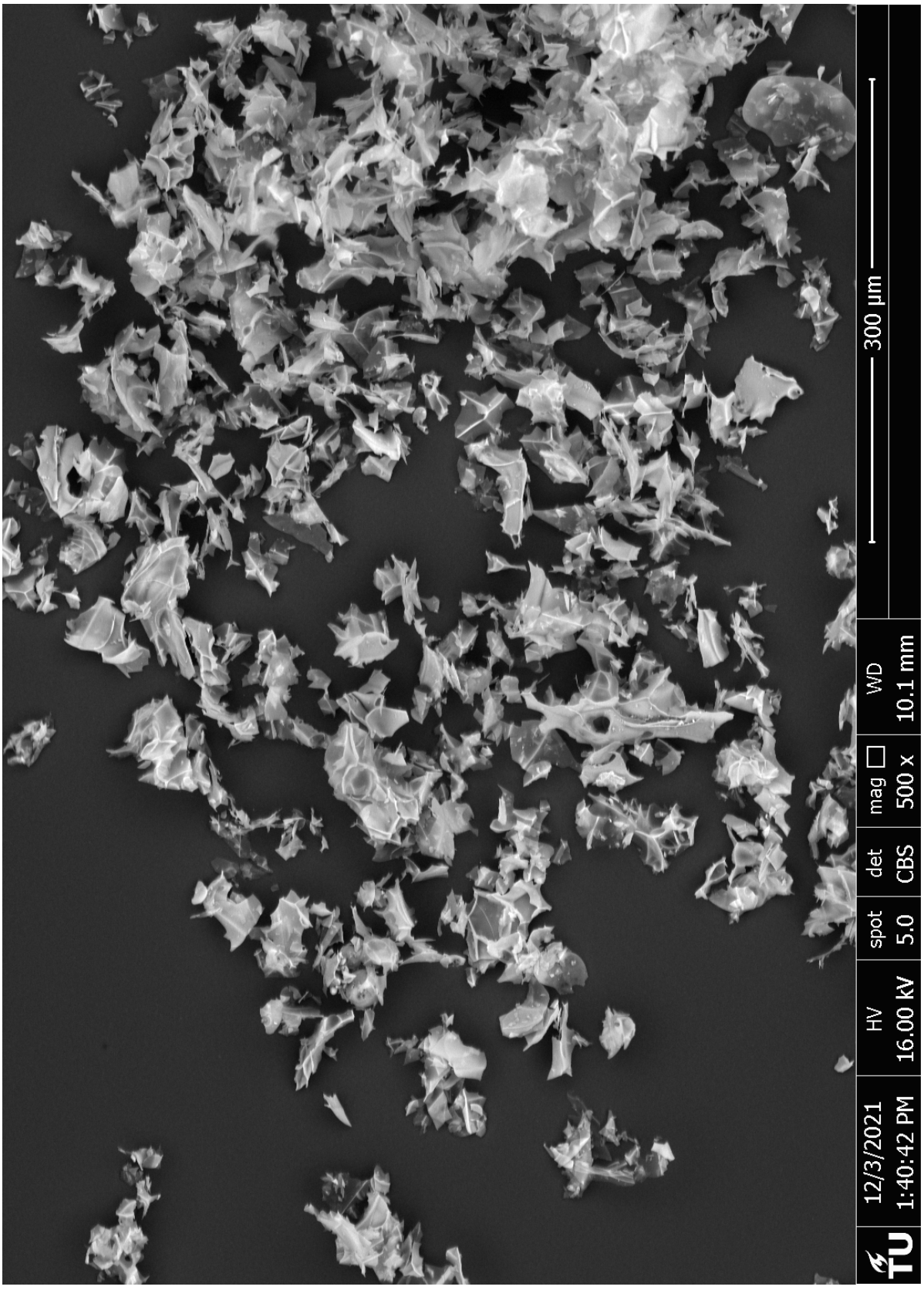

Figure D.10: Perlite SEM 500x magnitude

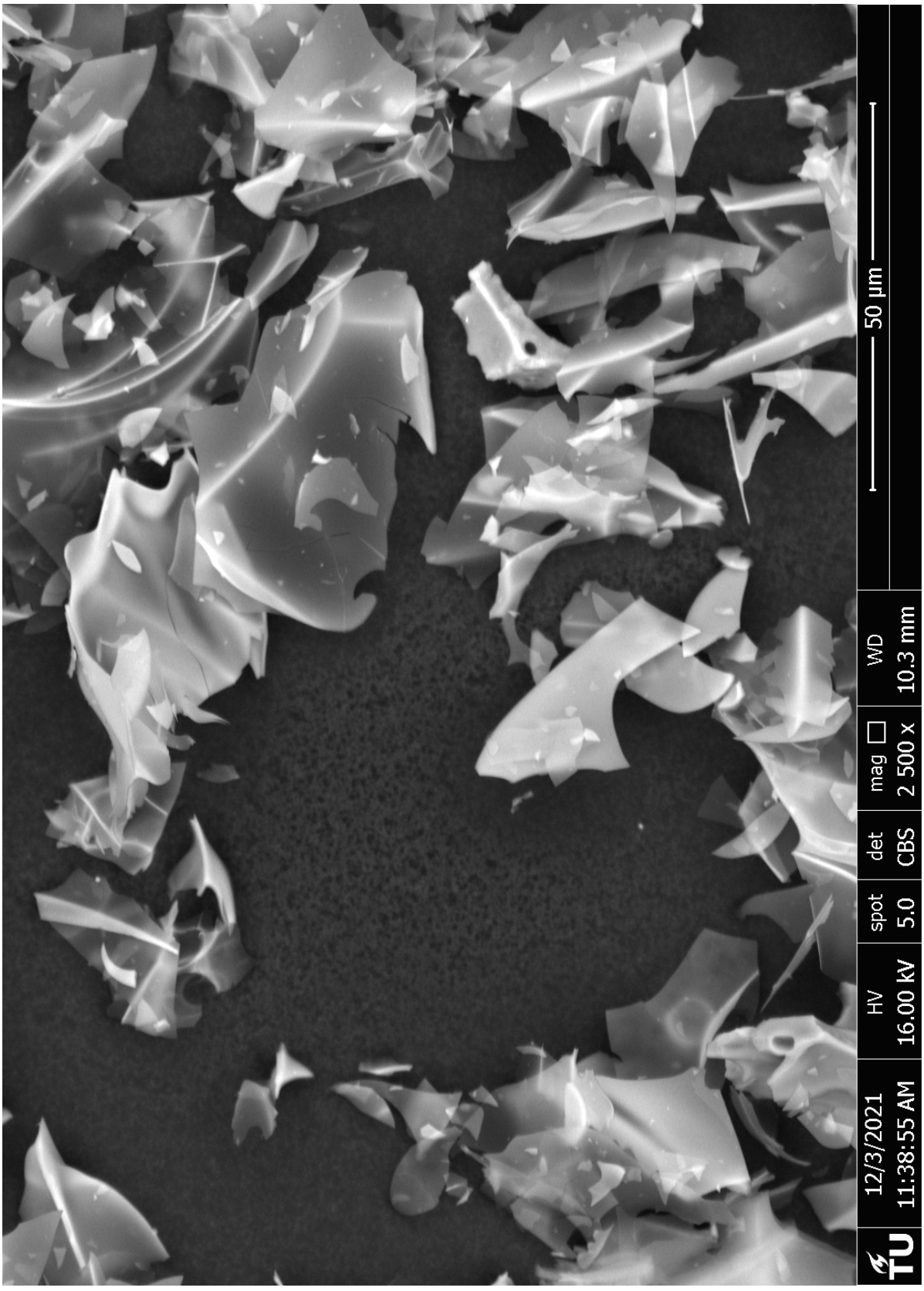

Figure D.11: Perlite SEM 2500x magnitude

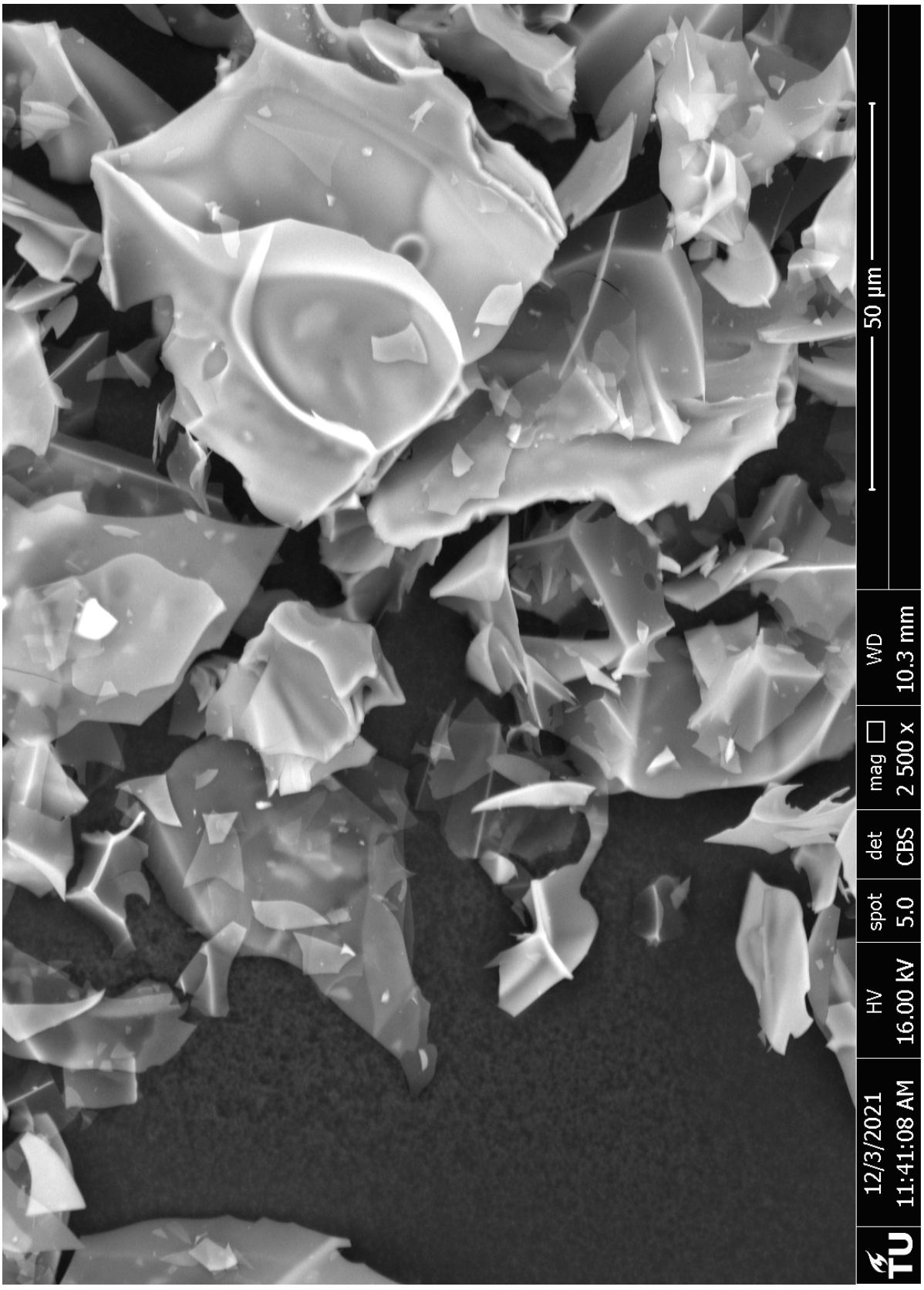

Figure D.12: Perlite SEM 2500x magnitude

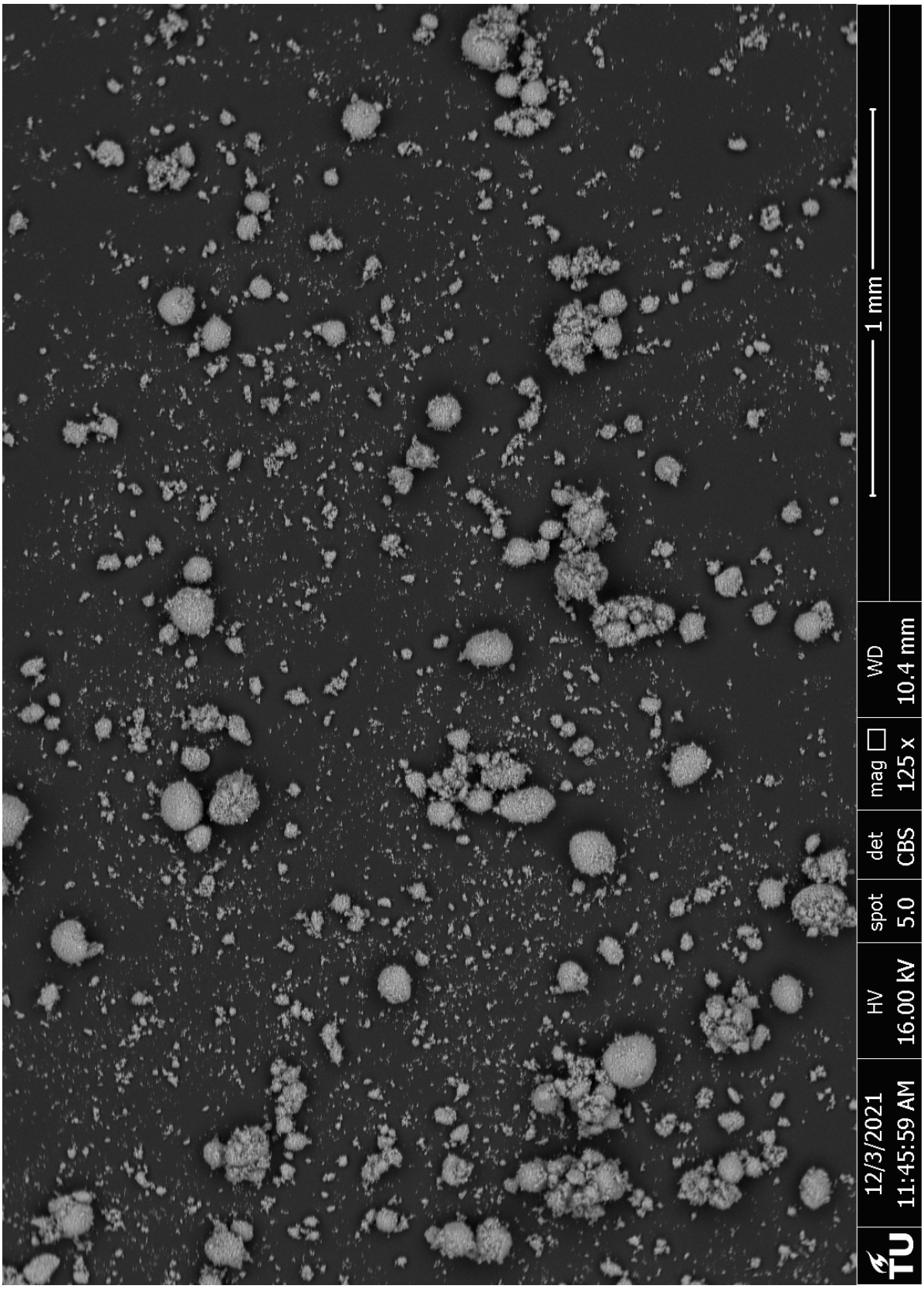

Figure D.13: Perlite ground SEM 125x magnitude

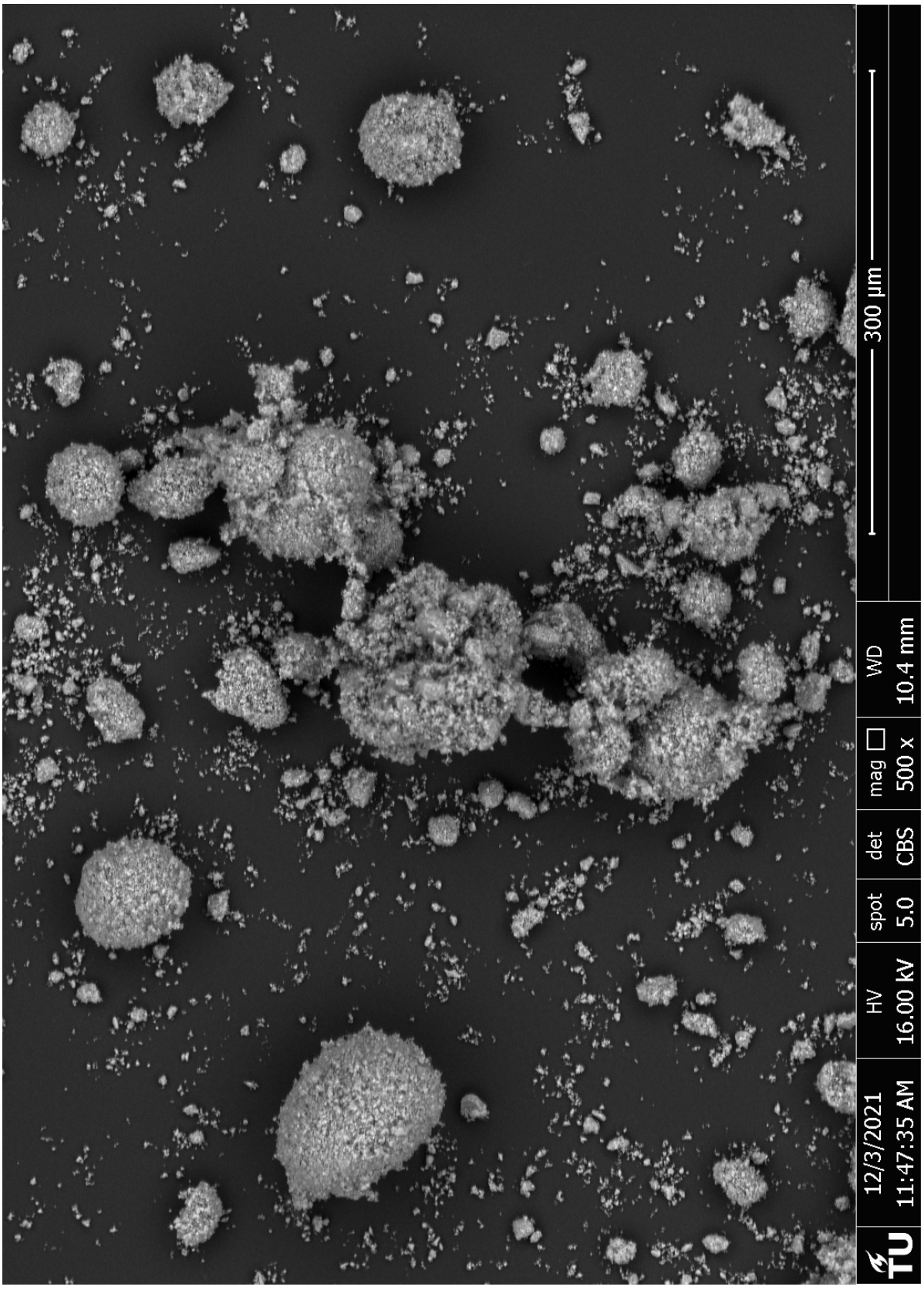

Figure D.14: Perlite ground SEM 500x magnitude

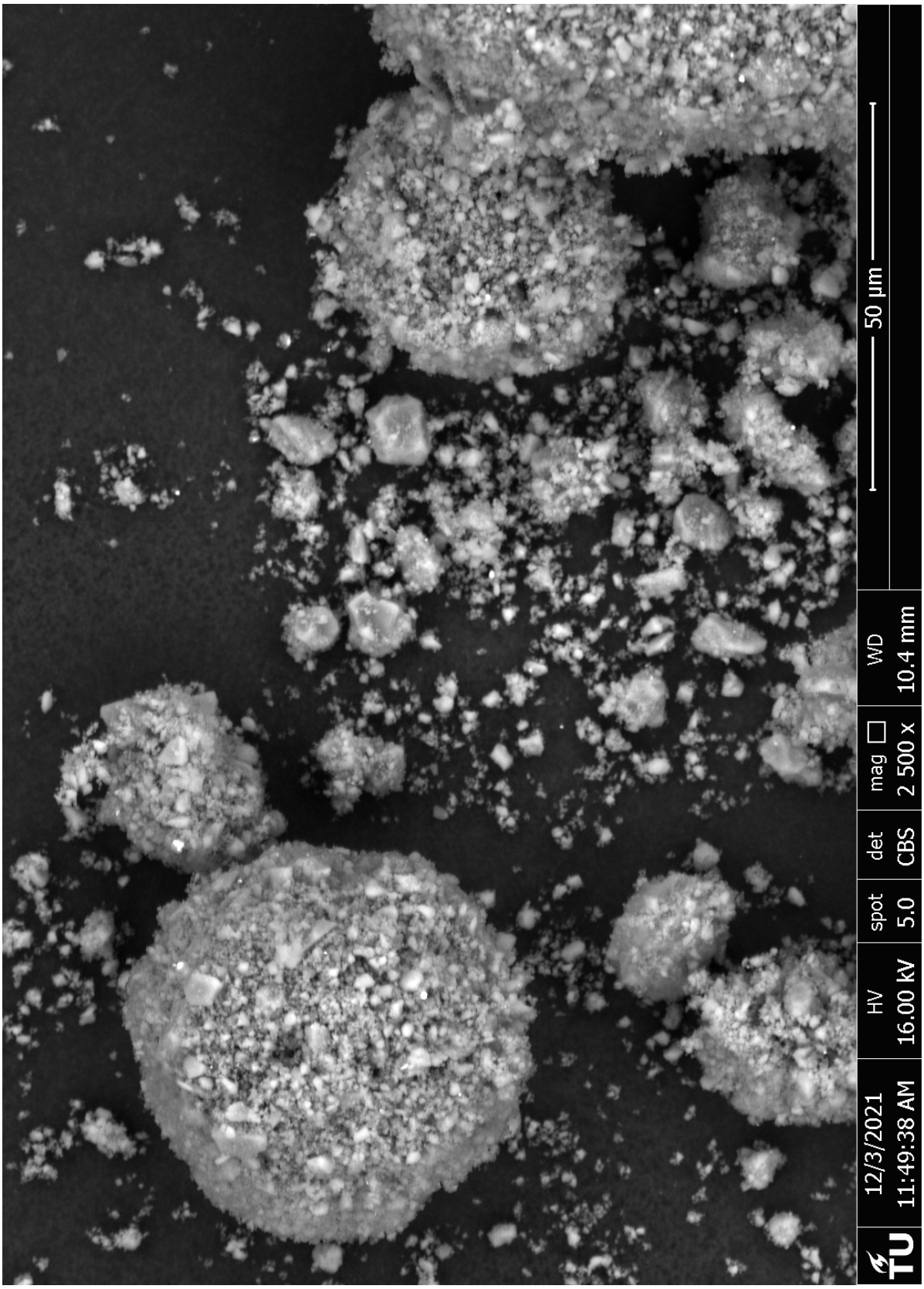

Figure D.15: Perlite ground SEM 2500x magnitude

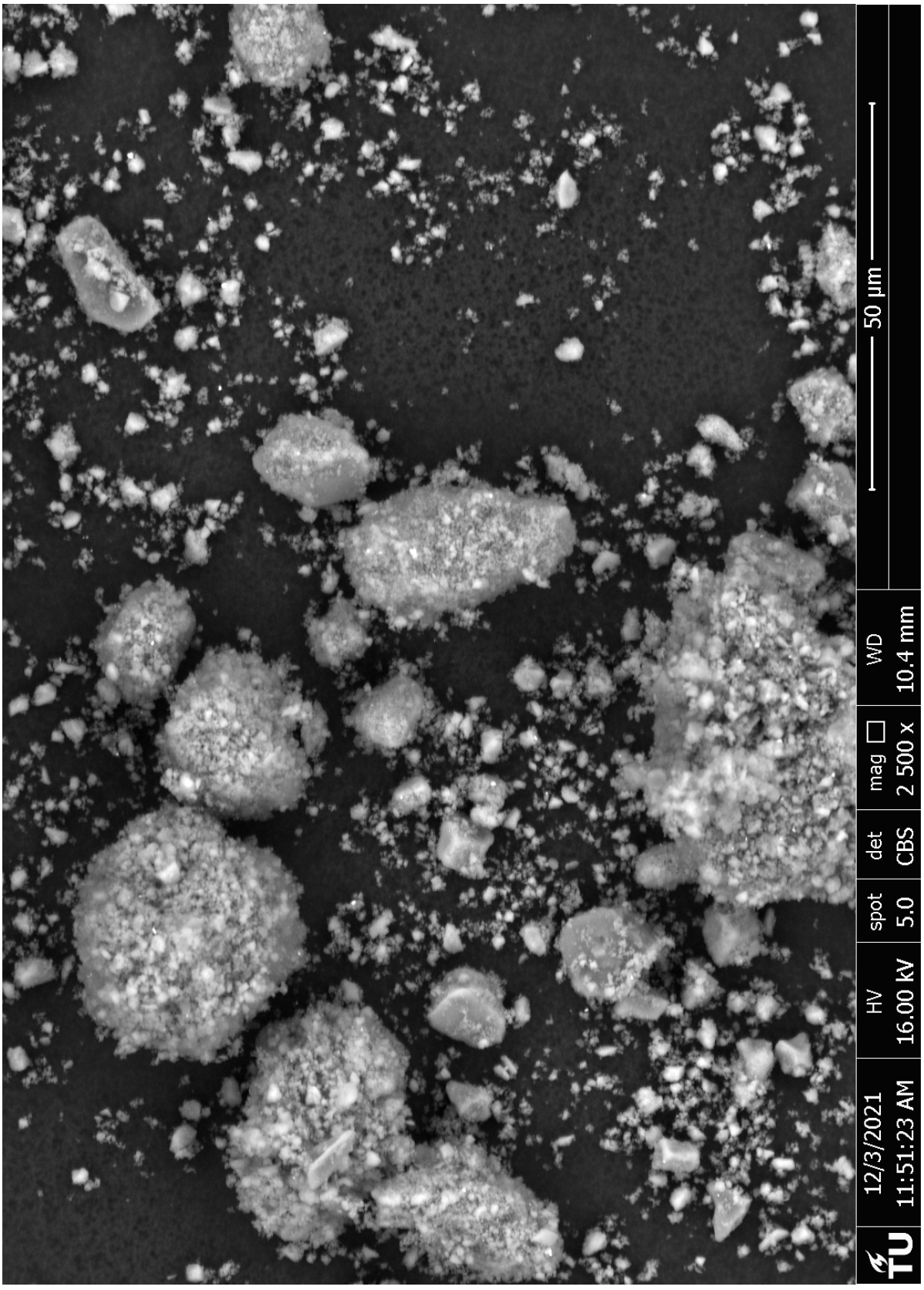

Figure D.16: Perlite ground SEM 2500x magnitude

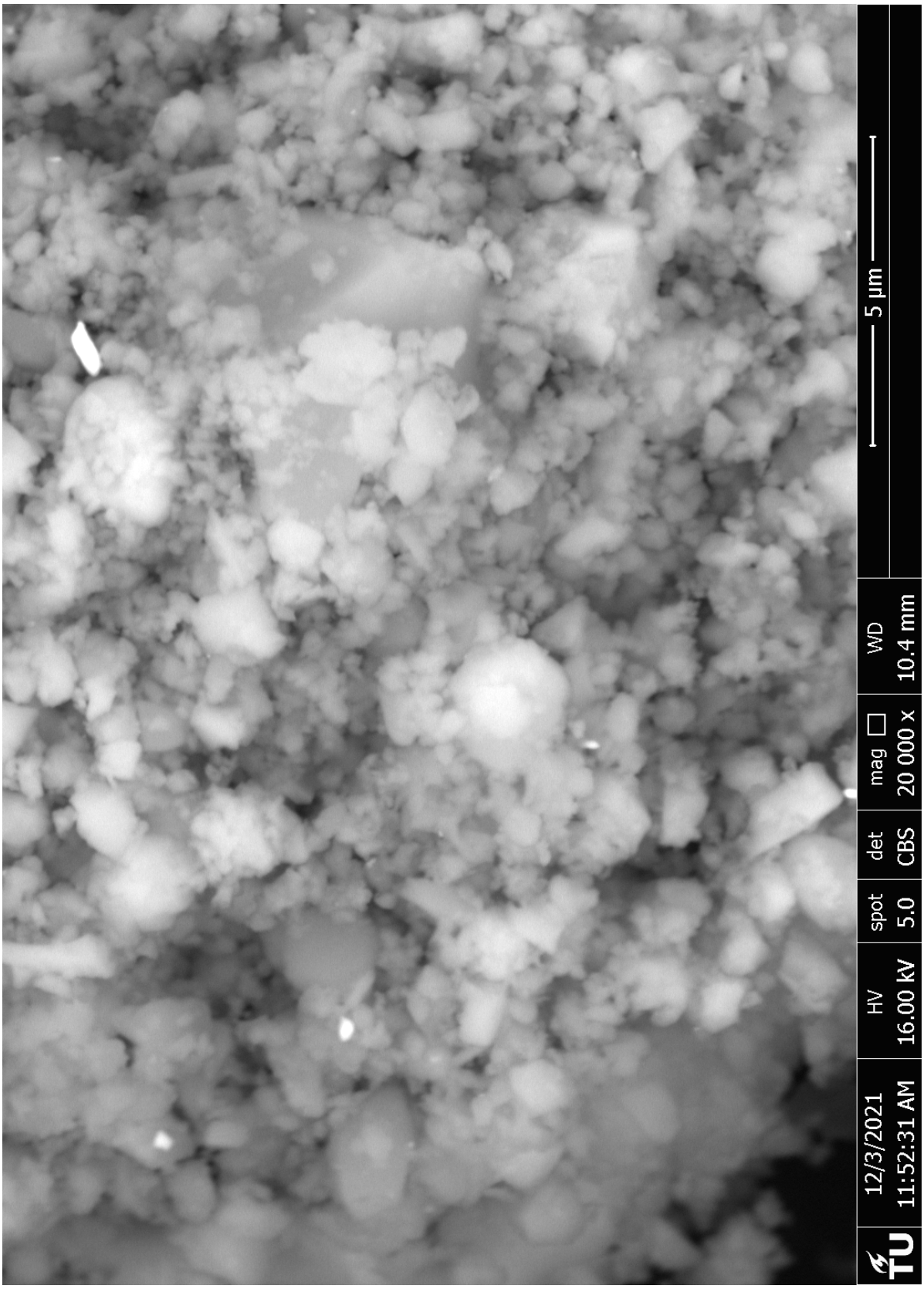

Figure D.17: Perlite ground SEM 20000x magnitude

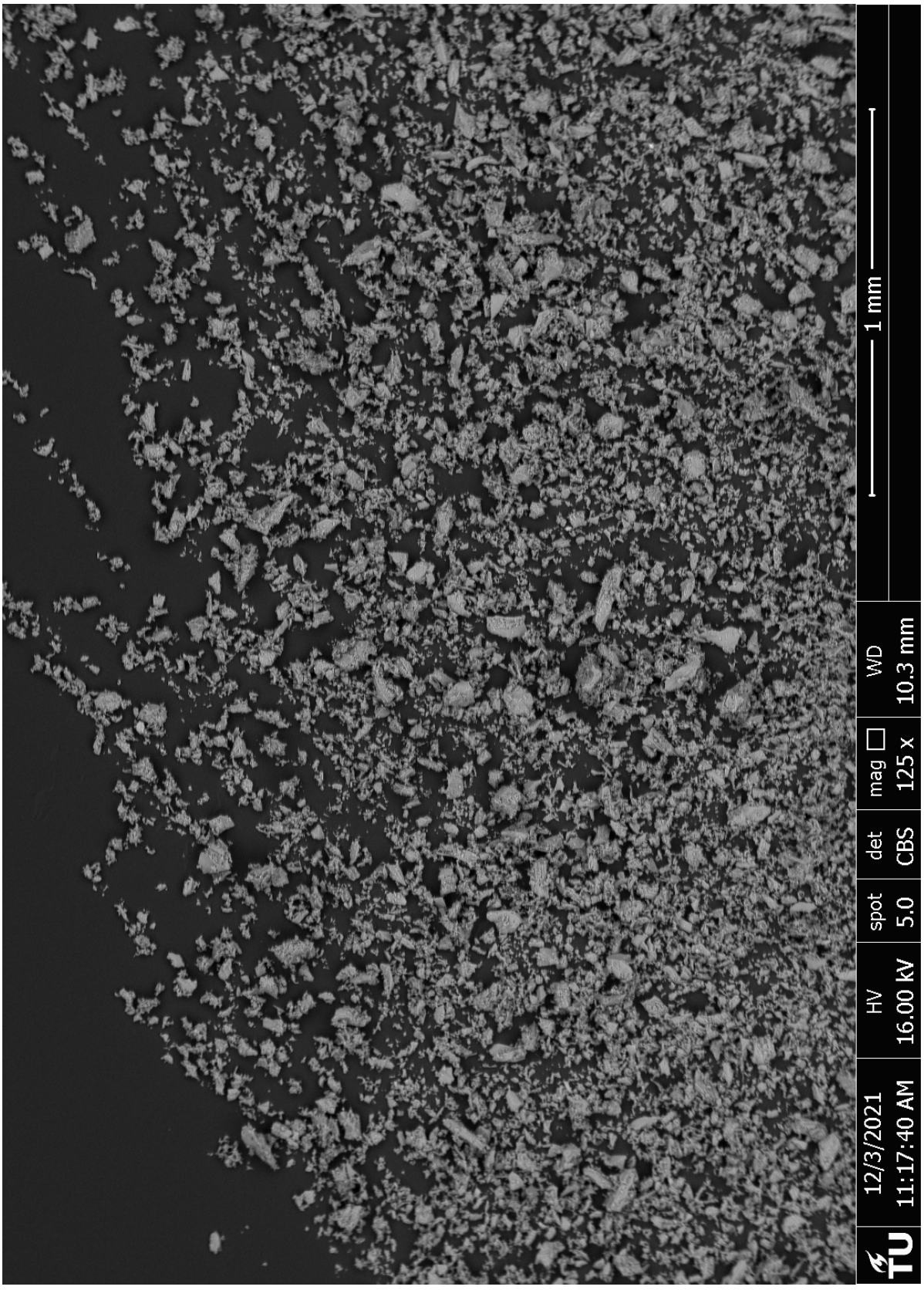

Figure D.18: Pumice SEM 125x magnitude

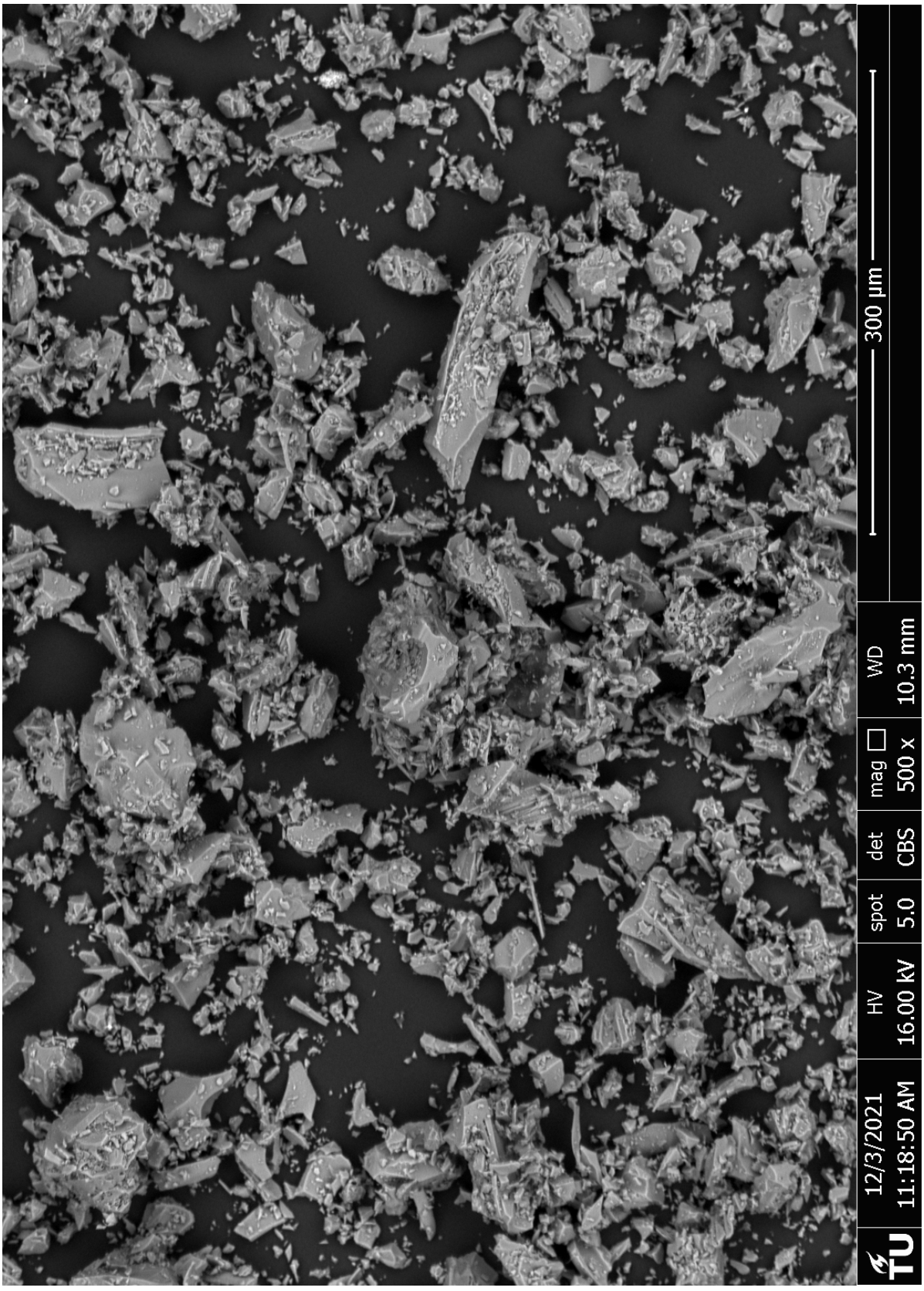

Figure D.19: Pumice SEM 500x magnitude

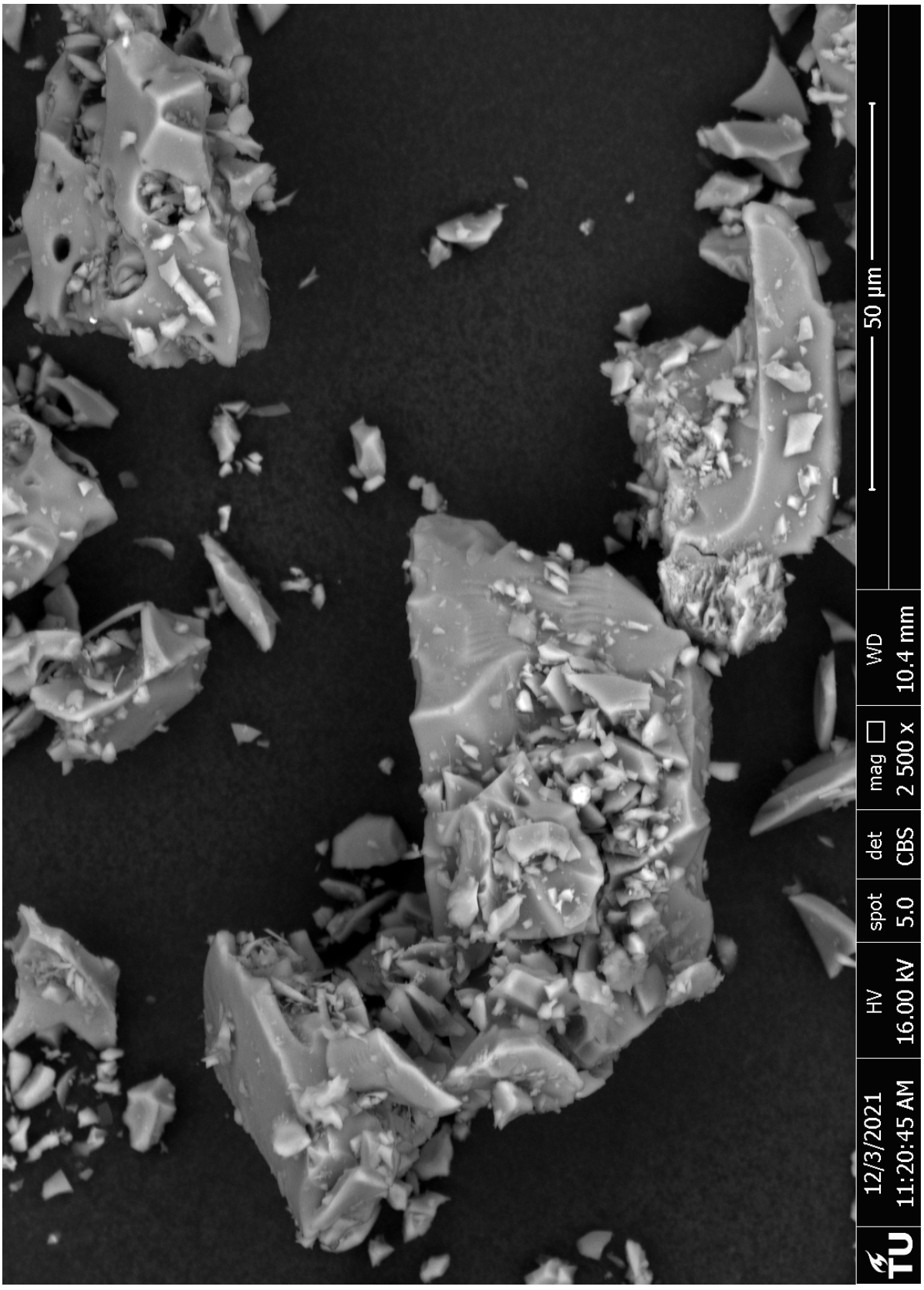

Figure D.20: Pumice SEM 2500x magnitude

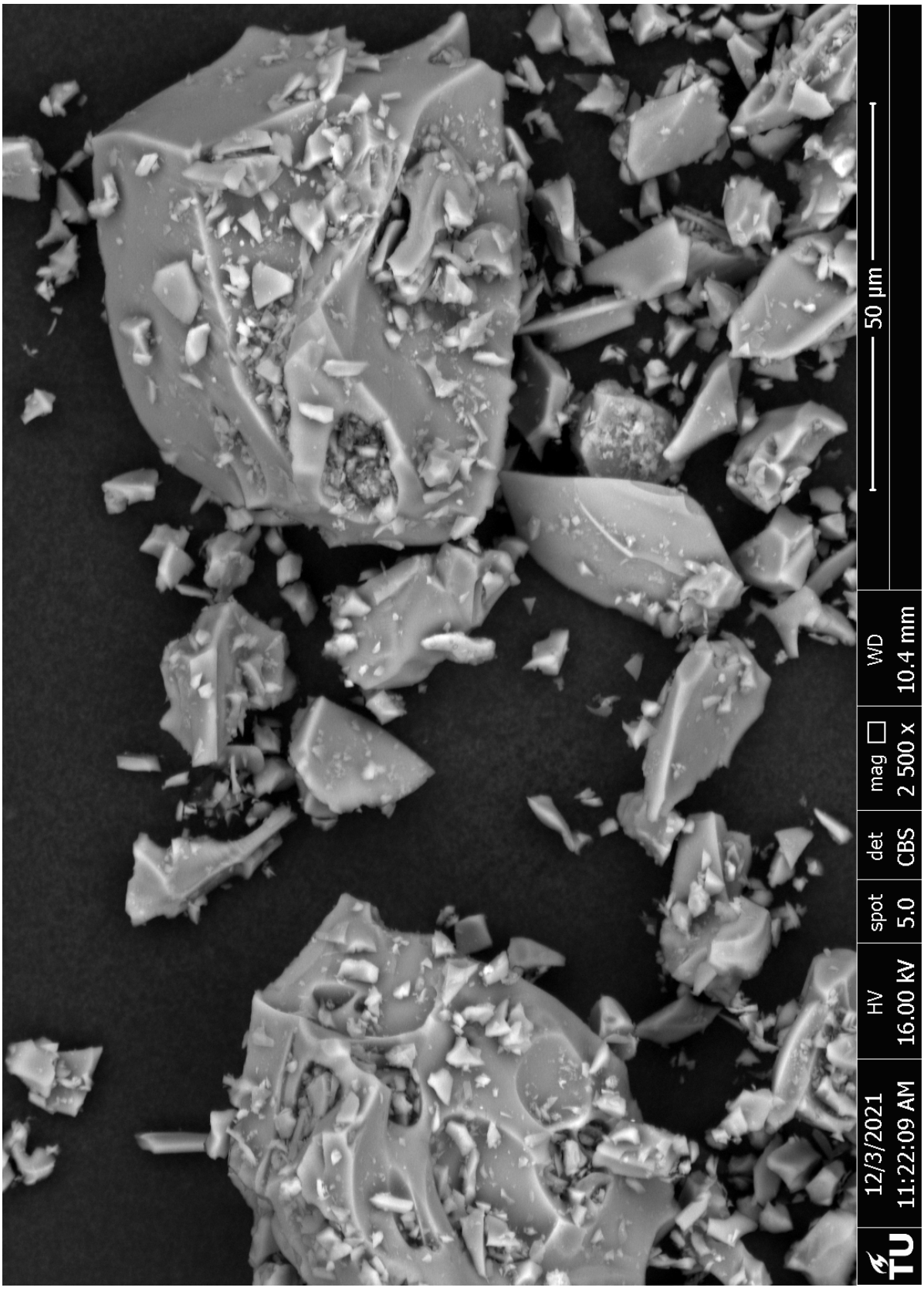

Figure D.21: Pumice SEM 2500x magnitude

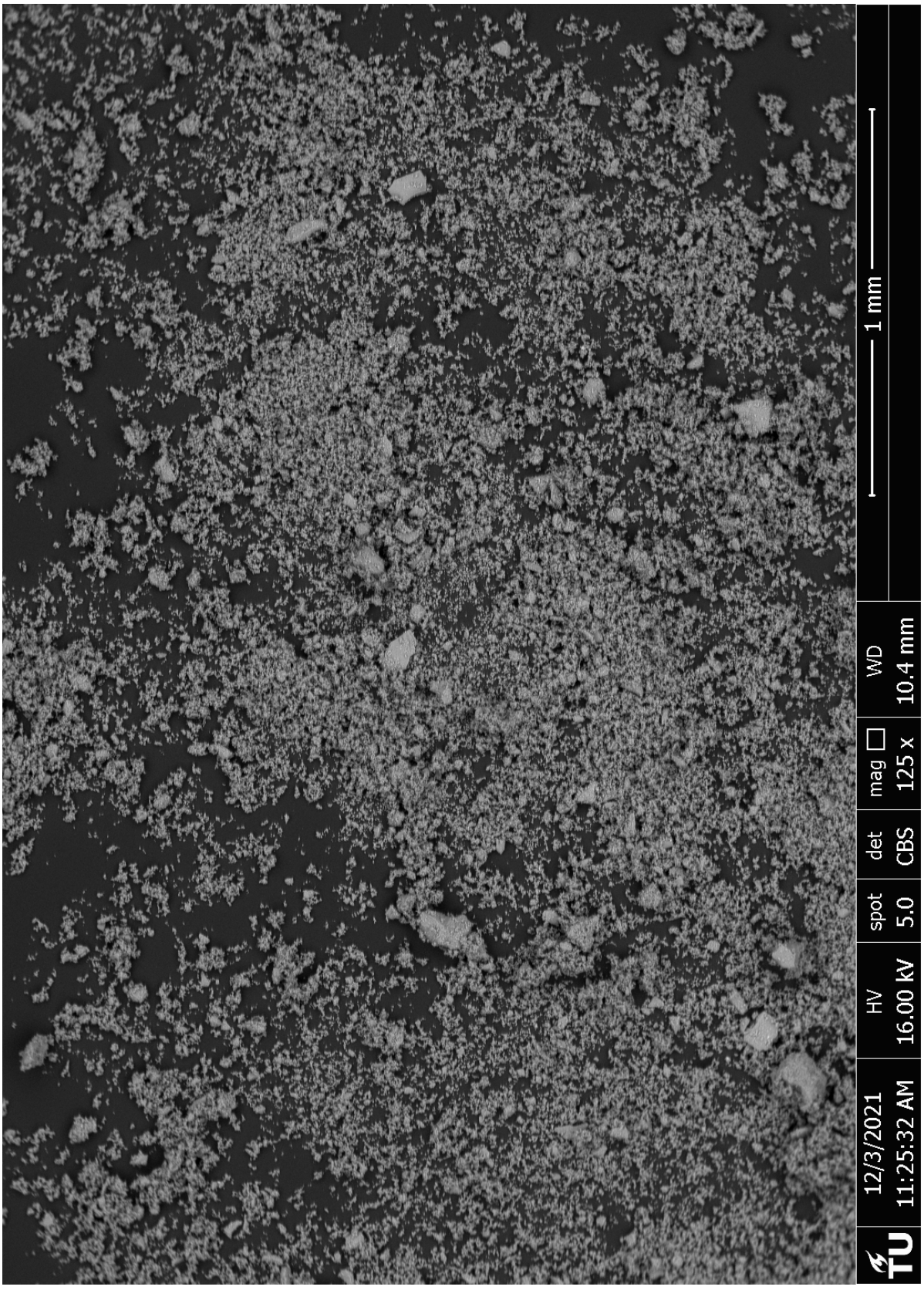

Figure D.22: Pumice ground SEM 125x magnitude

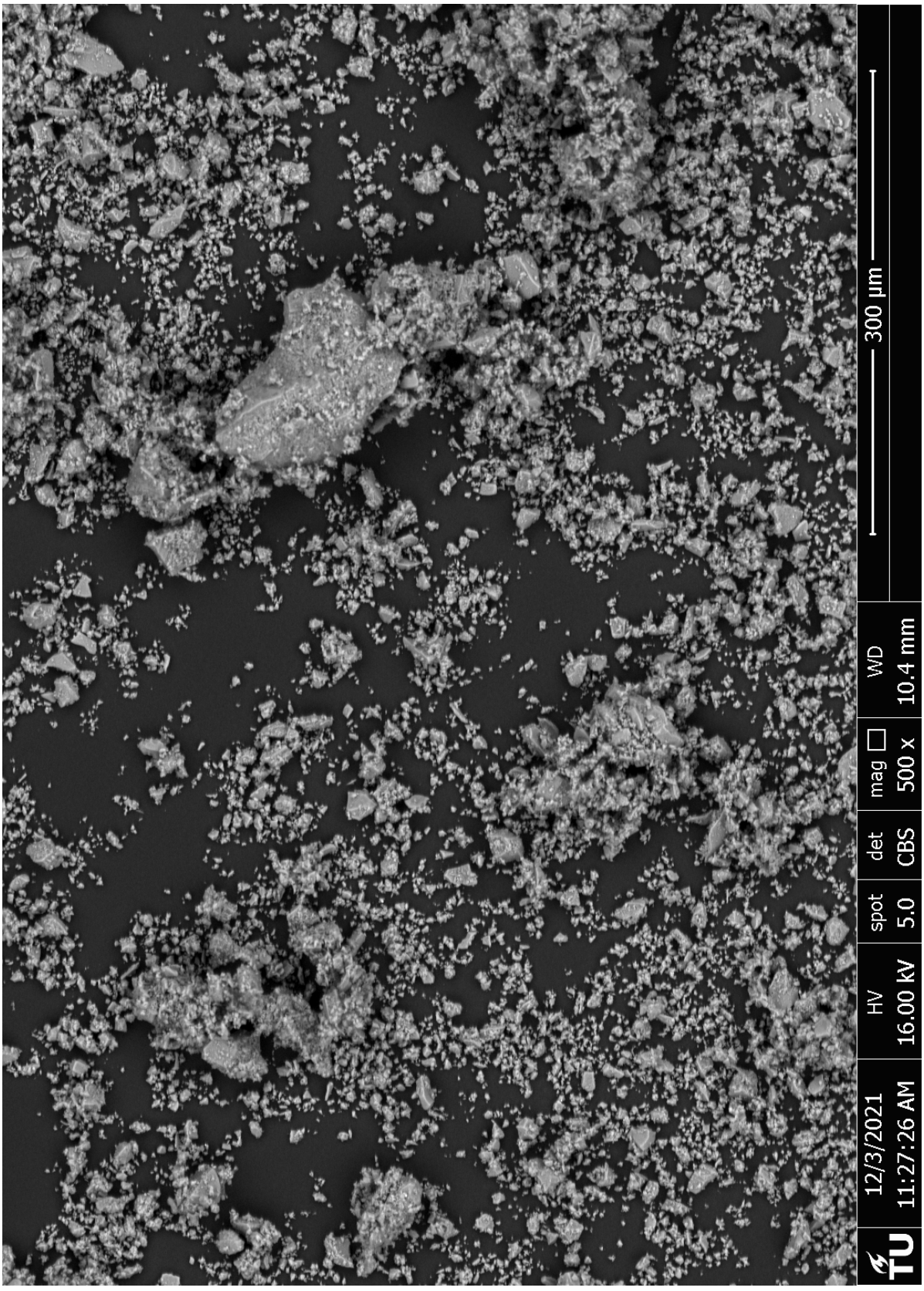

Figure D.23: Pumice ground SEM 500x magnitude

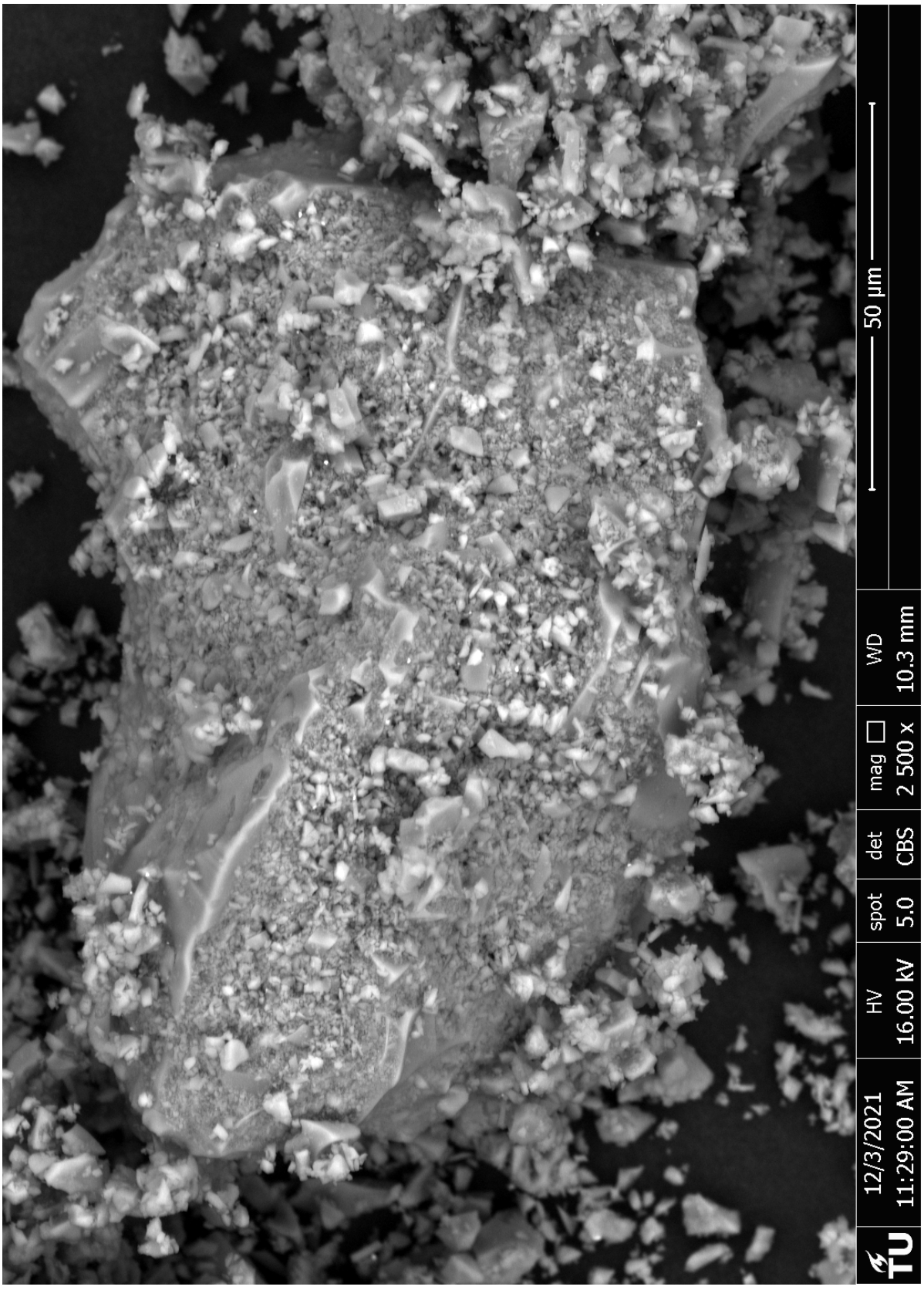

Figure D.24: Pumice ground SEM 2500x magnitude

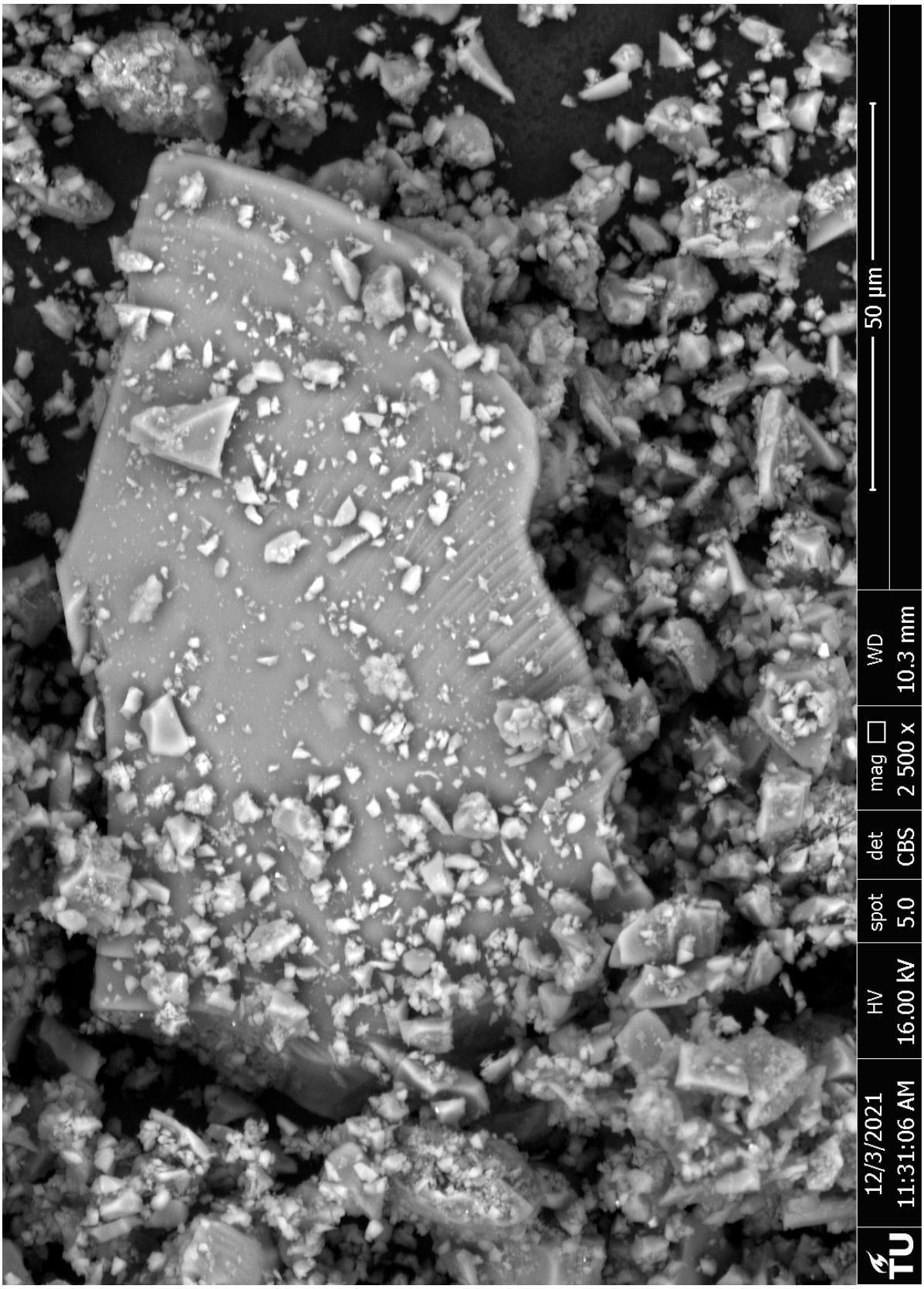

Figure D.25: Pumice ground SEM 2500x magnitude

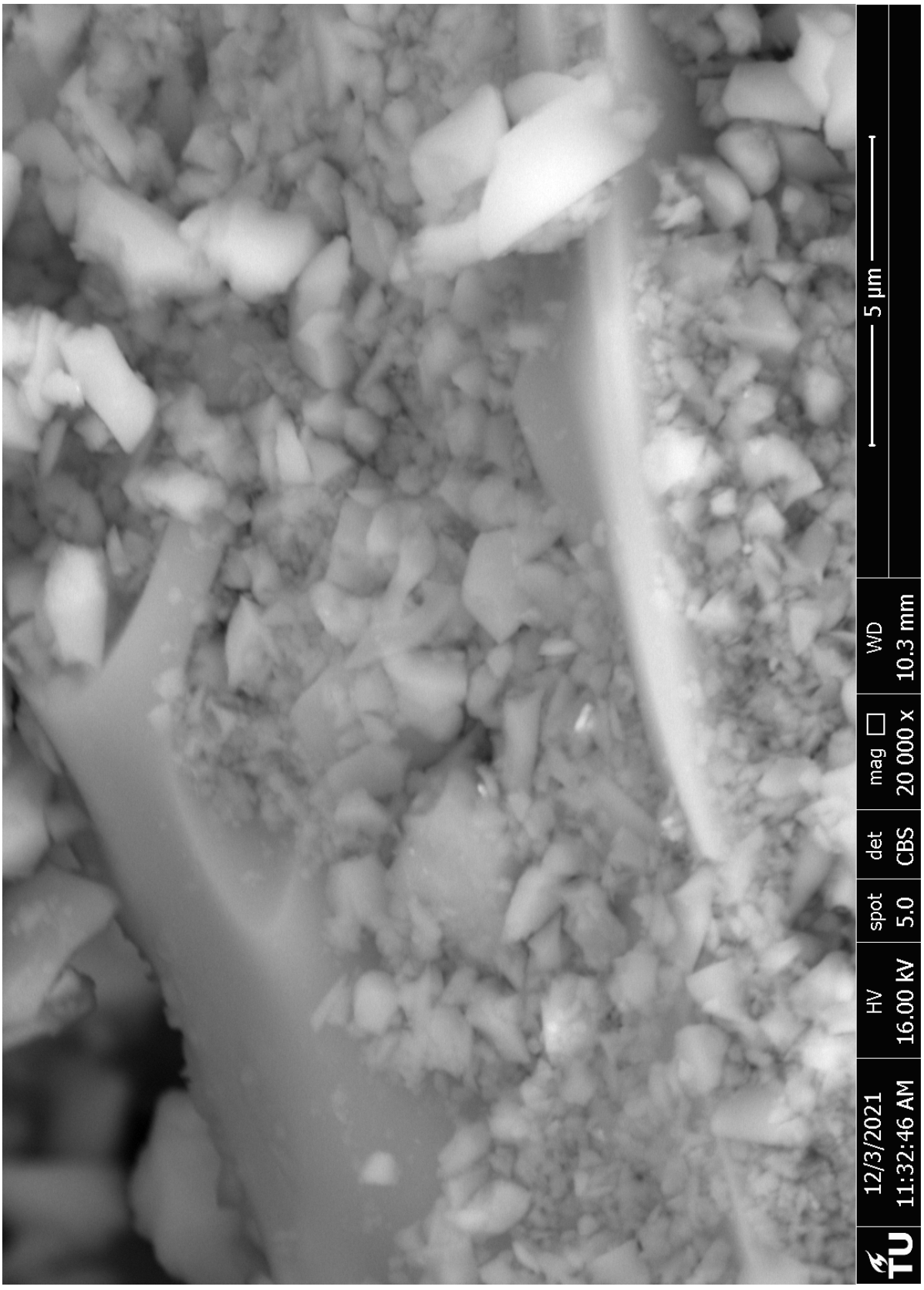

Figure D.26: Pumice ground SEM 20000x magnitude

E

XRD

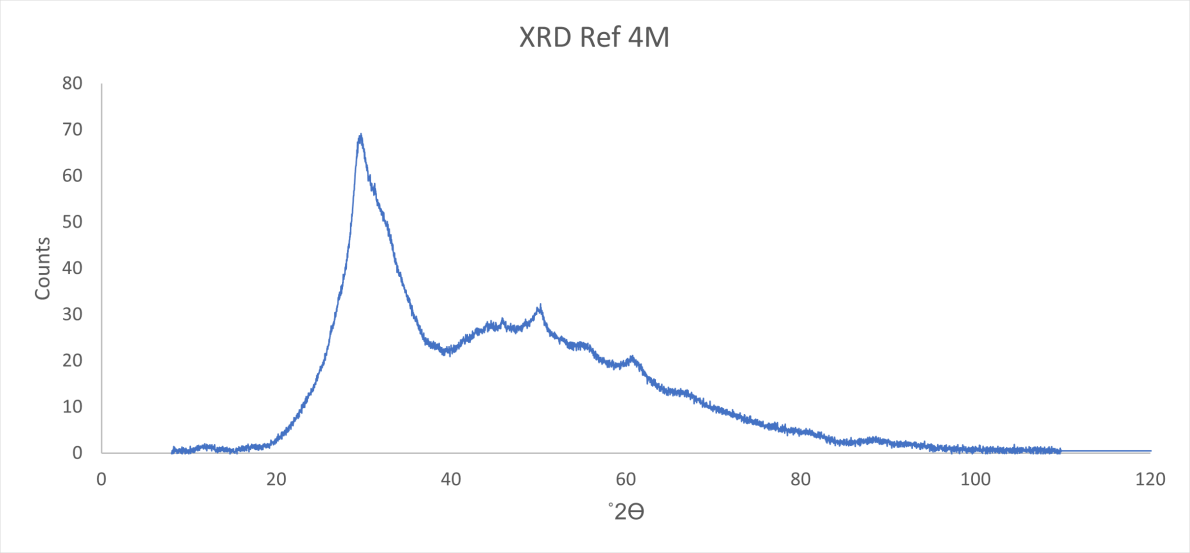

Figure E.1: XRD paste mix Ref 4M

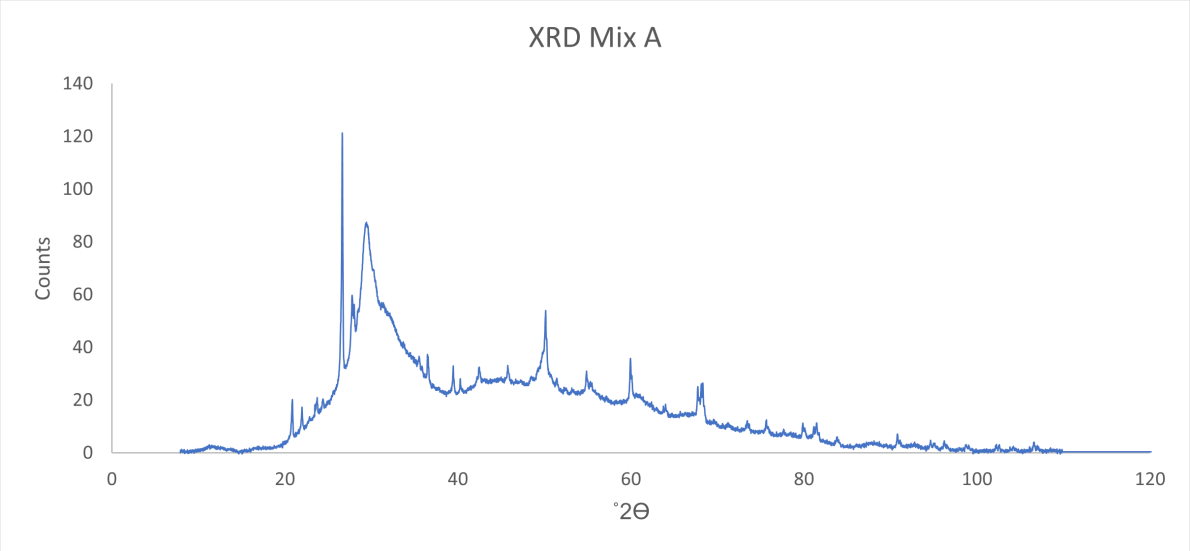

Figure E.2: XRD paste mix A

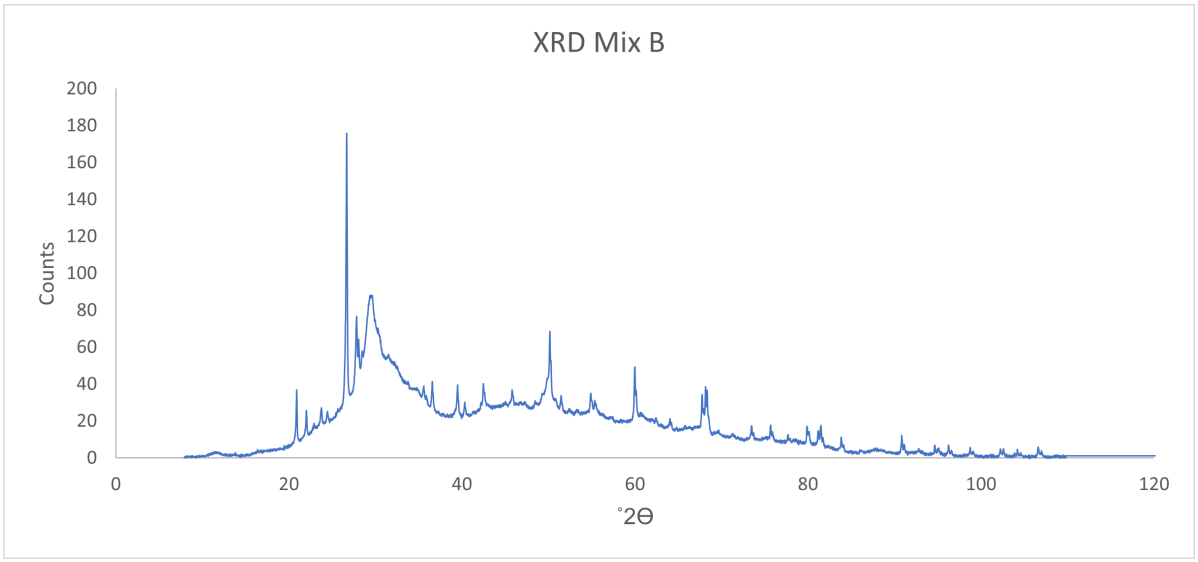

Figure E.3: XRD paste mix B

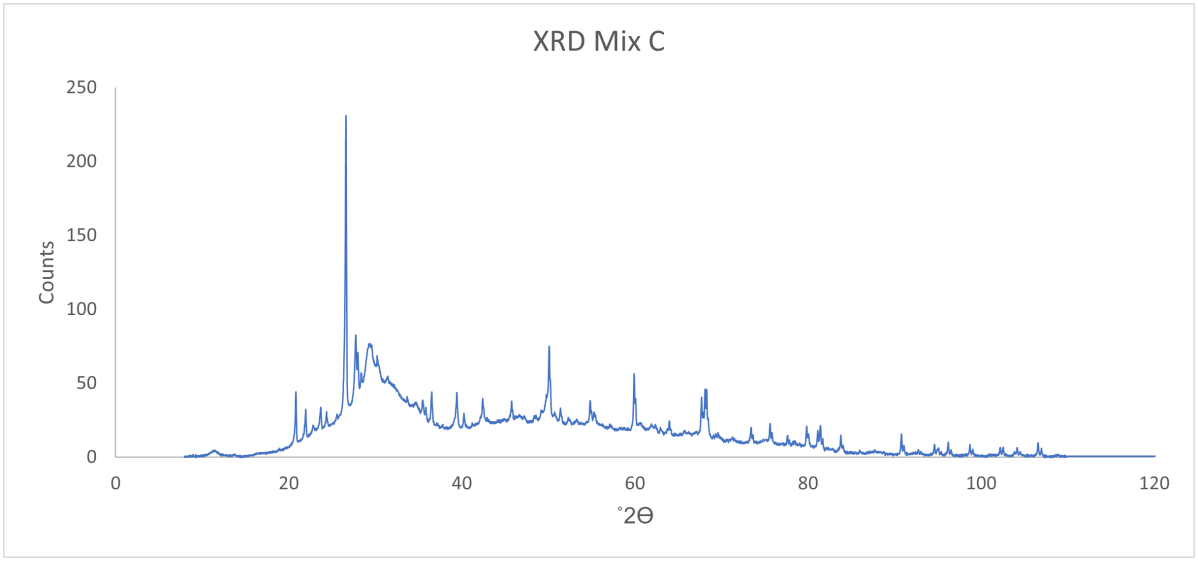

Figure E.4: XRD paste mix C

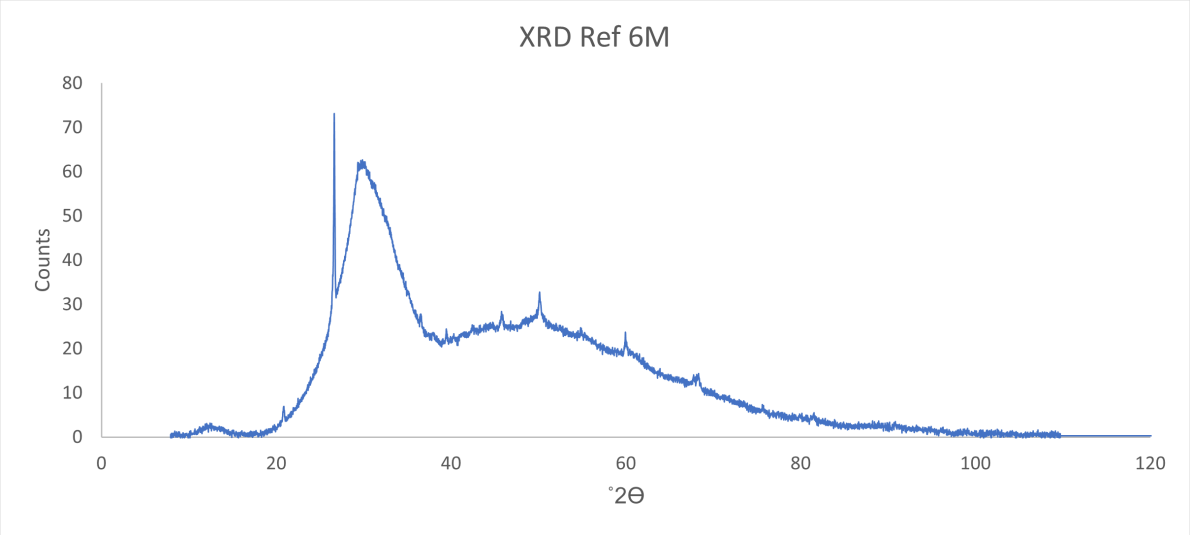

Figure E.5: XRD paste mix Ref 6M

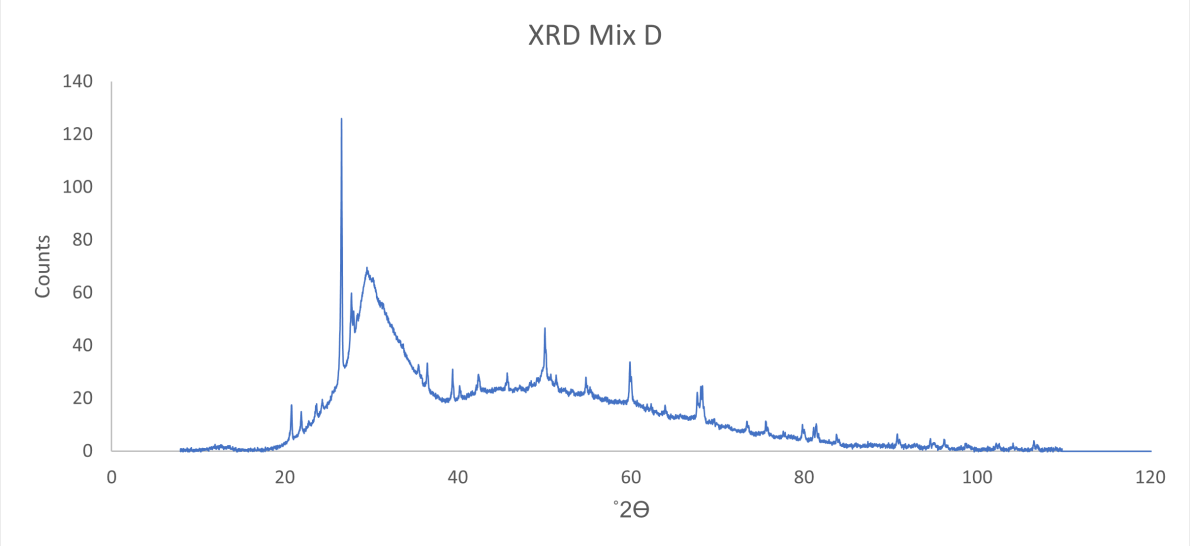

Figure E.6: XRD paste mix D

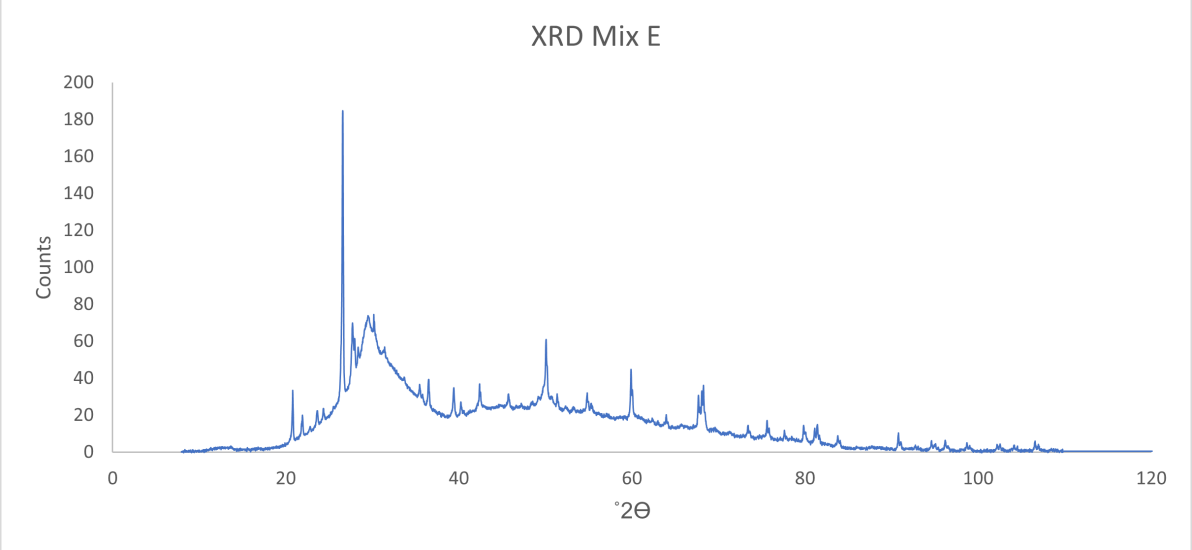

Figure E.7: XRD paste mix E

Bibliography

[1] A. M. Neville and J. J. Brooks. *Concrete Technology*. 2nd ed. Harlow: Pearson Education Limited, 2010. ISBN: 978-0-273-73219-8.

[2] J. Lehne and F. Preston. *Making Concrete Change: Innovation in Low-carbon Cement and Concrete*. London, UK.: The Royal Institute of International Affairs, 2018. ISBN: 978 1 78413 272 9.

[3] R. Snellings, G. Mertens, and J. Elsen. "Supplementary Cementitious Materials". In: *Reviews in Mineralogy and Geochemistry* 74.1 (2012), pp. 211–278. ISSN: 1529-6466. DOI: 10.2138/rmg.2012.74.6.

[4] John L. Provis and Jannie S. J. van Deventer, eds. *Alkali Activated Materials: State-of-the-art-report*. Vol. 13. Dordrecht: Springer Netherlands, 2014. ISBN: 978-94-007-7671-5. DOI: 10.1007/978-94-007-7672-2.

[5] Shahin Hajilar and Behrouz Shafei. "Assessment of structural, thermal, and mechanical properties of portlandite through molecular dynamics simulations". In: *Journal of Solid State Chemistry* 244 (2016), pp. 164–174. ISSN: 00224596. DOI: 10.1016/j.jssc.2016.09.026.

[6] Ali Hasanbeigi, Lynn Price, and Elina Lin. "Emerging energy-efficiency and CO2 emission-reduction technologies for cement and concrete production: A technical review". In: *Renewable and Sustainable Energy Reviews* 16.8 (2012), pp. 6220–6238. ISSN: 13640321. DOI: 10.1016/j.rser.2012.07.019.

[7] John L. Provis. "Alkali-activated materials". In: *Cement and Concrete Research* 114 (2018), pp. 40–48. ISSN: 00088846. DOI: 10.1016/j.cemconres.2017.02.009.

[8] Peter Duxson and John L. Provis. "Designing Precursors for Geopolymer Cements". In: *Journal of the American Ceramic Society* 91.12 (2008), pp. 3864–3869. ISSN: 00027820. DOI: 10.1111/j.1551-2916.2008.02787.x.

[9] Rafael Robayo-Salazar et al. "Life cycle assessment (LCA) of an alkali-activated binary concrete based on natural volcanic pozzolan: A comparative analysis to OPC concrete". In: *Construction and Building Materials* 176 (2018), pp. 103–111. ISSN: 09500618. DOI: 10.1016/j.conbuildmat.2018.05.017.

[10] V. Krabbendam. "Tekort aan grondstoffen en stijgende prijzen raken betonindustrie". In: *Infrasite.nl* (2021). URL: https://www.infrasite.nl/ondernemen/2021/09/20/tekort-aan-grondstoffen-en-stijgende-prijzen-voor-betonindustrie/?gdpr=accept.

[11] S. Alberici et al. *Fly ash and Blast Furnace Slag for Cement Manufacturing: BEIS research paper no.19*. London, UK., 2017. URL: https://assets.publishing.service.gov.uk/government/uploads/system/uploads/attachment_data/file/660888/fly-ash-blast-furnace-slag-cement-manufacturing.pdf.

[12] W. Mann. "Concrete shortage looms for major projects". In: *New Civil Engineer* (2014). URL: https://www.newcivilengineer.com/archive/concrete-shortage-looms-for-major-projects-29-07-2014/.

[13] Jørgen Skibsted and Ruben Snellings. "Reactivity of supplementary cementitious materials (SCMs) in cement blends". In: *Cement and Concrete Research* 124 (2019), p. 105799. ISSN: 00088846. DOI: 10.1016/j.cemconres.2019.105799.

[14] Harisankar Sreenivasan et al. "Towards designing reactive glasses for alkali activation: Understanding the origins of alkaline reactivity of Na-Mg aluminosilicate glasses". In: *PloS one* 15.12 (2020), e0244621. DOI: 10.1371/journal.pone.0244621.

[15] Alireza Joshaghani, Alireza Moazenian, and Richard Abubakar Shuaibu. "Experimental Study on the Use of Trass as a Supplementary Cementitious Material in Pervious Concrete". In: *Journal of Environmental Science and Engineering A* 6.1 (2017). ISSN: 21625298. DOI: 10.17265/2162-5298/2017.01.005.

[16] S. K. Haldar and Josip Tišljar. "Igneous Rocks". In: *Introduction to Mineralogy and Petrology*. Elsevier, 2014, pp. 93–120. ISBN: 9780124081338. DOI: 10.1016/B978-0-12-408133-8.00004-3.

[17] Serhat Çelikten, Mustafa Sarıdemir, and Kubilay Akçaözoğlu. “Effect of calcined perlite content on elevated temperature behaviour of alkali activated slag mortars”. In: *Journal of Building Engineering* 32 (2020), p. 101717. ISSN: 23527102. DOI: 10.1016/j.jobe.2020.101717.

[18] Saamiya Seraj et al. “The role of particle size on the performance of pumice as a supplementary cementitious material”. In: *Cement and Concrete Composites* 80 (2017), pp. 135–142. ISSN: 09589465. DOI: 10.1016/j.cemconcomp.2017.03.009.

[19] Nick Winter. *Understand Cement: An introduction to cement production, cement hydration and deleterious processes in concrete*. Woodbridge, UK: WHD Microanalysis Consultants Ltd, 2009.

[20] P. Kumar Mehta et al. *Concrete: Microstructure, properties, and materials*. 4th ed. Blacklick: McGraw-Hill Publishing, 2013. ISBN: 978-0-07-179788-7.

[21] H. Manzano et al. “Mechanical properties of crystalline calcium-silicate-hydrates: comparison with cementitious C-S-H gels”. In: *physica status solidi (a)* 204.6 (2007), pp. 1775–1780. ISSN: 18626300. DOI: 10.1002/pssa.200675359.

[22] R. Snellings. “Assessing, Understanding and Unlocking Supplementary Cementitious Materials”. In: *RILEM Technical Letters* 1 (2016), p. 50. DOI: 10.21809/rilemtechlett.2016.12.

[23] Peter Duxson et al. “The role of inorganic polymer technology in the development of ‘green concrete’”. In: *Cement and Concrete Research* 37.12 (2007), pp. 1590–1597. ISSN: 00088846. DOI: 10.1016/j.cemconres.2007.08.018.

[24] Xuerun Li et al. “Reactivity tests for supplementary cementitious materials: RILEM TC 267-TRM phase 1”. In: *Materials and Structures* 51.6 (2018). ISSN: 1359-5997. DOI: 10.1617/s11527-018-1269-x.

[25] Eric H. Oelkers. “General kinetic description of multioxide silicate mineral and glass dissolution”. In: *Geochimica et Cosmochimica Acta* 65.21 (2001), pp. 3703–3719. ISSN: 00167037. DOI: 10.1016/S0016-7037(01)00710-4.

[26] K. Sagoe-Crentsil and L. Weng. “Dissolution processes, hydrolysis and condensation reactions during geopolymer synthesis: Part II. High Si/Al ratio systems”. In: *Journal of Materials Science* 42.9 (2007), pp. 3007–3014. ISSN: 0022-2461. DOI: 10.1007/s10853-006-0818-9.

[27] L. Weng and K. Sagoe-Crentsil. “Dissolution processes, hydrolysis and condensation reactions during geopolymer synthesis: Part I—Low Si/Al ratio systems”. In: *Journal of Materials Science* 42.9 (2007), pp. 2997–3006. ISSN: 0022-2461. DOI: 10.1007/s10853-006-0820-2.

[28] Rupert J. Myers et al. “Generalized structural description of calcium-sodium aluminosilicate hydrate gels: the cross-linked substituted tobermorite model”. In: *Langmuir : the ACS journal of surfaces and colloids* 29.17 (2013), pp. 5294–5306. DOI: 10.1021/la4000473.

[29] Shao-Dong Wang and Karen L. Scrivener. “Hydration products of alkali activated slag cement”. In: *Cement and Concrete Research* 25.3 (1995), pp. 561–571. ISSN: 00088846. DOI: 10.1016/0008-8846(95)00045-E.

[30] Ana Fernández-Jiménez et al. “Structure of Calcium Silicate Hydrates Formed in Alkaline-Activated Slag: Influence of the Type of Alkaline Activator”. In: *Journal of the American Ceramic Society* 86.8 (2003), pp. 1389–1394. ISSN: 00027820. DOI: 10.1111/j.1151-2916.2003.tb03481.x.

[31] A. Fernández-Jiménez and A. Palomo. “Composition and microstructure of alkali activated fly ash binder: Effect of the activator”. In: *Cement and Concrete Research* 35.10 (2005), pp. 1984–1992. ISSN: 00088846. DOI: 10.1016/j.cemconres.2005.03.003.

[32] Ines García-Lodeiro et al. “Effect of Calcium Additions on N-A-S-H Cementitious Gels”. In: *Journal of the American Ceramic Society* (2010). ISSN: 00027820. DOI: 10.1111/j.1551-2916.2010.03668.x.

[33] Mary Bagley. *Properties of Matter: Solids*. 2014. URL: https://www.livescience.com/46946-solids.html.

[34] M. M. Tashima et al. “Assessment of pozzolanic/hydraulic reactivity of vitreous calcium aluminosilicate (VCAS)”. In: *Materials & Design* 96 (2016), pp. 424–430. ISSN: 02641275. DOI: 10.1016/j.matdes.2016.02.036.

[35] B. Rand. “Calcination”. In: *Concise Encyclopedia of Advanced Ceramic Materials*. Elsevier, 1991, pp. 49–51. ISBN: 9780080347202. DOI: 10.1016/B978-0-08-034720-2.50023-X.

[36] Prannoy Suraneni and Jason Weiss. “Examining the pozzolanicity of supplementary cementitious materials using isothermal calorimetry and thermogravimetric analysis”. In: *Cement and Concrete Composites* 83 (2017), pp. 273–278. ISSN: 09589465. DOI: 10.1016/j.cemconcomp.2017.07.009.

[37] Shao-Dong Wang, Karen L. Scrivener, and P. L. Pratt. “Factors affecting the strength of alkali-activated slag”. In: *Cement and Concrete Research* 24.6 (1994), pp. 1033–1043. ISSN: 00088846. DOI: 10.1016/0008-8846(94)90026-4.

[38] A. Dwivedi and J. Manish. “Fly ash - waste management and overview: A Review”. In: *Recent Research in Science and Technology* 6.1 (2014), pp. 30–35.

[39] M. Ahmaruzzaman. “A review on the utilization of fly ash”. In: *Progress in Energy and Combustion Science* 36.3 (2010), pp. 327–363. ISSN: 03601285. DOI: 10.1016/j.pecs.2009.11.003.

[40] Marius Gheorghe Miricioiu and Violeta-Carolina Niculescu. “Fly Ash, from Recycling to Potential Raw Material for Mesoporous Silica Synthesis”. In: *Nanomaterials (Basel, Switzerland)* 10.3 (2020). ISSN: 2079-4991. DOI: 10.3390/nano10030474.

[41] Isa Yuksel. “Blast-furnace slag”. In: *Waste and Supplementary Cementitious Materials in Concrete*. Elsevier, 2018, pp. 361–415. ISBN: 9780081021569. DOI: 10.1016/B978-0-08-102156-9.00012-2.

[42] S.C Pal, A. Mukherjee, and S.R Pathak. “Investigation of hydraulic activity of ground granulated blast furnace slag in concrete”. In: *Cement and Concrete Research* 33.9 (2003), pp. 1481–1486. ISSN: 00088846. DOI: 10.1016/S0008-8846(03)00062-0.

[43] Erdoğan Özbay, Mustafa Erdemir, and Halil İbrahim Durmuş. “Utilization and efficiency of ground granulated blast furnace slag on concrete properties – A review”. In: *Construction and Building Materials* 105 (2016), pp. 423–434. ISSN: 09500618. DOI: 10.1016/j.conbuildmat.2015.12.153.

[44] Ki-Yeon Moon et al. “Characteristics of Hydraulic Lime using Low-grade Dolomitic Limestone”. In: *Journal of the Korean Ceramic Society* 53.2 (2016), pp. 206–214. ISSN: 1229-7801. DOI: 10.4191/kcers.2016.53.2.206.

[45] B. I. Djon Li Ndjock, Antoine Elimbi, and Martin Cyr. “Rational utilization of volcanic ashes based on factors affecting their alkaline activation”. In: *Journal of Non-Crystalline Solids* 463 (2017), pp. 31–39. ISSN: 00223093. DOI: 10.1016/j.jnoncrysol.2017.02.024.

[46] Peter Duxson et al. “Understanding the relationship between geopolymer composition, microstructure and mechanical properties”. In: *Colloids and Surfaces A: Physicochemical and Engineering Aspects* 269.1-3 (2005), pp. 47–58. ISSN: 09277757. DOI: 10.1016/j.colsurfa.2005.06.060.

[47] V. Indrawati and A. Manaf. “Mechanical Strength of Trass as Supplementary Cementing Material”. In: *Journal of Physical Science* 19.2 (2008), pp. 51–59.

[48] Puput Risdanareni, Januarti Jaya Ekaputri, and Triwulan. “The Influence of Alkali Activator Concentration to Mechanical Properties of Geopolymer Concrete with Trass as a Filler”. In: *Materials Science Forum* 803 (2014), pp. 125–134. DOI: 10.4028/www.scientific.net/MSF.803.125.

[49] Trasswerke Meurin. *Techincal Data Sheet*. 2020.

[50] T. G. Nijland and Rob P. J. van Hees. “Volcanic foundation of Dutch architecture: Use of Rhenish tuff and trass in the Netherlands in the past two millennia”. In: *Heron* 61.2 (2016), pp. 69–98.

[51] Elie Kamseu et al. “Dependence of the geopolymerization process and end-products to the nature of solid precursors: Challenge of the sustainability”. In: *Journal of Cleaner Production* 278 (2021), p. 123587. ISSN: 09596526. DOI: 10.1016/j.jclepro.2020.123587.

[52] F. Hauri. “Natural zeolite from southern Germany: Applications in concrete”. In: *Zeolite ’06*. Ed. by Robert Bowman and Susan Delap. Socorro, New Mexico, USA, 2006, pp. 130–131.

[53] Joachim R. R. Ritter and Ulrich R. Christensen, eds. *Mantle plumes: A multidisciplinary approach / Joachim R.R. Ritter, Ulrich R. Christensen (editors)*. Berlin and New York: Springer, 2007. ISBN: 978-3-540-68045-1.

[54] Cornelius Kirsche. *Phonolite: Product Datasheet*. Neuwied, Germany, 2020.

[55] *PERLIET info*. 2021.

[56] G. Mulder. *Perlite CO2 footprint*. Ed. by D. Heimovaara. 2022.

[57] Vít Petranek et al. “Perlite Concrete Based on Alkali Activated Cements”. In: *Advanced Materials Research* 897 (2014), pp. 280–283. DOI: 10.4028/www.scientific.net/AMR.897.280.

[58] Joseph Davidovits. “Properties of Geopolymer Cements”. In: *Proceedings First Internation Conference on Alkaline Cements and Concretes*. Ed. by Pavel Krivenko. Vol. 1. Kiev, Ukraine: VIPOL Stock Company, 1994, pp. 131–149. URL: https://www.geopolymer.org/wp-content/uploads/KIEV.pdf.

[59] T. K. Erdem et al. “Use of perlite as a pozzolanic addition in producing blended cements”. In: *Cement and Concrete Composites* 29.1 (2007), pp. 13–21. ISSN: 09589465. DOI: 10.1016/j.cemconcomp.2006.07.018.

[60] Dif Fodil and Mouli Mohamed. “Compressive strength and corrosion evaluation of concretes containing pozzolana and perlite immersed in aggressive environments”. In: *Construction and Building Materials* 179 (2018), pp. 25–34. ISSN: 09500618. DOI: 10.1016/j.conbuildmat.2018.05.190.

[61] A. A. Ramezanianpour et al. “Effects of calcined perlite powder as a SCM on the strength and permeability of concrete”. In: *Construction and Building Materials* 66 (2014), pp. 222–228. ISSN: 09500618. DOI: 10.1016/j.conbuildmat.2014.05.086.

[62] L.-H Yu, H. Ou, and L.-L Lee. “Investigation on pozzolanic effect of perlite powder in concrete”. In: *Cement and Concrete Research* 33.1 (2003), pp. 73–76. ISSN: 00088846. DOI: 10.1016/S0008-8846(02)00924-9.

[63] S. T. Erdogan. “Properties of Ground Perlite Geopolymer Mortars”. In: *Journal of Materials in Civil Engineering* 27.7 (2015), p. 04014210. ISSN: 0899-1561. DOI: 10.1061/(ASCE)MT.1943-5533.0001172.

[64] G. M. Tsaousi, I. Douni, and D. Panias. “Characterization of the properties of perlite geopolymer pastes”. In: *Materiales de Construcción* 66.324 (2016), p. 102. ISSN: 0465-2746. DOI: 10.3989/mc.2016.10415.

[65] F. Bektas, L. Turanli, and P.J.M. Monteiro. “Use of perlite powder to suppress the alkali–silica reaction”. In: *Cement and Concrete Research* 35.10 (2005), pp. 2014–2017. ISSN: 00088846. DOI: 10.1016/j.cemconres.2004.10.029.

[66] Zrar Safari et al. “Mechanical characteristics of pumice-based geopolymer paste”. In: *Resources, Conservation and Recycling* 162 (2020), p. 105055. ISSN: 09213449. DOI: 10.1016/j.resconrec.2020.105055.

[67] K.M.A. Hossain, S. Ahmed, and M. Lachemi. “Lightweight concrete incorporating pumice based blended cement and aggregate: Mechanical and durability characteristics”. In: *Construction and Building Materials* 25.3 (2011), pp. 1186–1195. ISSN: 09500618. DOI: 10.1016/j.conbuildmat.2010.09.036.

[68] Khandaker M. Anwar Hossain. “Properties of volcanic pumice based cement and lightweight concrete”. In: *Cement and Concrete Research* 34.2 (2004), pp. 283–291. ISSN: 00088846. DOI: 10.1016/j.cemconres.2003.08.004.

[69] Roberta Occhipinti et al. “Alkali activated materials using pumice from the Aeolian Islands (Sicily, Italy) and their potentiality for cultural heritage applications: Preliminary study”. In: *Construction and Building Materials* 259 (2020), p. 120391. ISSN: 09500618. DOI: 10.1016/j.conbuildmat.2020.120391.

[70] Bilal Balun and Mehmet Karataş. “Influence of curing conditions on pumice-based alkali activated composites incorporating Portland cement”. In: *Journal of Building Engineering* 43 (2021), p. 102605. ISSN: 23527102. DOI: 10.1016/j.jobe.2021.102605.

[71] Aylin Özodabaş and Kemalettin Yılmaz. “Improvement of the performance of alkali activated blast furnace slag mortars with very finely ground pumice”. In: *Construction and Building Materials* 48 (2013), pp. 26–34. ISSN: 09500618. DOI: 10.1016/j.conbuildmat.2013.06.047.

[72] zaludj. “Alahverdi_suda_16_hž.qxp”. In: ().

[73] Karen Scrivener, Ruben Snellings, and Barbara Lothenbach, eds. *A Practical Guide to Microstructural Analysis of Cementitious Materials*. New York NY: CRC Press, 2016. ISBN: 978-1-4987-3867-5.

[74] David Barthelmy. *Mineralogy Database*. 2021. URL: webmineral.com.

[75] Prannoy Suraneni et al. “New insights from reactivity testing of supplementary cementitious materials”. In: *Cement and Concrete Composites* 103 (2019), pp. 331–338. ISSN: 09589465. DOI: 10.1016/j.cemconcomp.2019.05.017.

[76] Sivakumar Ramanathan, Michael Croly, and Prannoy Suraneni. “Comparison of the effects that supplementary cementitious materials replacement levels have on cementitious paste properties”. In: *Cement and Concrete Composites* 112 (2020), p. 103678. ISSN: 09589465. DOI: 10.1016/j.cemconcomp.2020.103678.

[77] Z. Tan, G. de Schutter, and G. Ye, eds. *The effect of limestone powder addition on strength of slag blended cement*. 2013. ISBN: 978-2-35158-124-7.

[78] M. Atkins et al. “A thermodynamic model for blended cements”. In: *Cement and Concrete Research* 22.2-3 (1992), pp. 497–502. ISSN: 00088846. DOI: 10.1016/0008-8846(92)90093-B.

[79] Caijun Shi. “On the state and role of alkalis during the activation of alkali-activated slag cement”. In: *Proceedings of the 11th International Congress on the Chemistry of Cement, Durban, South Africa*. Vol. 2003. 2003.

[80] A. Fernández-Jiménez and F. Puertas. “The alkali–silica reaction in alkali-activated granulated slag mortars with reactive aggregate”. In: *Cement and Concrete Research* 32.7 (2002), pp. 1019–1024. ISSN: 00088846. DOI: 10.1016/S0008-8846(01)00745-1.

[81] X Pu and C Yang. “Study on alkali-silica reaction of alkali-slag concrete”. In: *1st International Conference on Alkaline Cements and Concretes, Kiev, Ukraine*. Vol. 2. 1994, pp. 897–906.

[82] N.F.J. Vonk. *Product Information Sheet: Ground granulated blast furnace slag*. Moerdijk, 2022.

[83] John L. Provis et al. “RILEM TC 247-DTA round robin test: mix design and reproducibility of compressive strength of alkali-activated concretes”. In: *Materials and Structures* 52.5 (2019). ISSN: 1359-5997. DOI: 10.1617/s11527-019-1396-z.

[84] Mohammed Nadeem Qureshi and Somnath Ghosh. “Effect of Silicate Content on the Properties of Alkali-Activated Blast Furnace Slag Paste”. In: *Arabian Journal for Science and Engineering* 39.8 (2014), pp. 5905–5916. ISSN: 1319-8025. DOI: 10.1007/s13369-014-1172-x.

[85] Raquel P. Batista et al. “Silica Fume as Precursor in the Development of Sustainable and High-Performance MK-Based Alkali-Activated Materials Reinforced With Short PVA Fibers”. In: *Frontiers in Materials* 6 (2019). DOI: 10.3389/fmats.2019.00077.

[86] I. Rouseková, A. Bajza, and V. Zivica. “Silica Fume - Basic Blast Furnace Slag Systems Activated by an Alkali Silica Fume activator”. In: *Cement and Concrete Research* 27.12 (1997), pp. 1825–1828. ISSN: 00088846.

[87] Susan A. Bernal et al. “Activation of Metakaolin/Slag Blends Using Alkaline Solutions Based on Chemically Modified Silica Fume and Rice Husk Ash”. In: *Waste and Biomass Valorization* 3.1 (2012), pp. 99–108. ISSN: 1877-2641. DOI: 10.1007/s12649-011-9093-3.

[88] Vladimír Živica. “High effective silica fume alkali activator”. In: *Bulletin of Materials Science* 27.2 (2004), pp. 179–182. ISSN: 0250-4707. DOI: 10.1007/BF02708502.

[89] Tero Luukkonen et al. “Influence of sodium silicate powder silica modulus for mechanical and chemical properties of dry-mix alkali-activated slag mortar”. In: *Construction and Building Materials* 233 (2020), p. 117354. ISSN: 09500618. DOI: 10.1016/j.conbuildmat.2019.117354.

[90] Kushal Ghosh and Parta Ghosh. “Effect of Na2O/Al2O3, SiO2/Al2O3 and W/B Ratio on Setting Time and Workability of Fly Ash based Geopolymer”. In: *International Journal of Engineering Research and Applications* 2.4 (2012), pp. 2142–2147.

[91] Partha Sarathi Deb, Pradip Nath, and Prabir Kumar Sarker. “The effects of ground granulated blast-furnace slag blending with fly ash and activator content on the workability and strength properties of geopolymer concrete cured at ambient temperature”. In: *Materials & Design (1980-2015)* 62 (2014), pp. 32–39. ISSN: 02613069. DOI: 10.1016/j.matdes.2014.05.001.

[92] J.J Chang. “A study on the setting characteristics of sodium silicate-activated slag pastes”. In: *Cement and Concrete Research* 33.7 (2003), pp. 1005–1011. ISSN: 00088846. DOI: 10.1016/S0008-8846(02)01096-7.

[93] Catherine A. Rees et al. “The mechanism of geopolymer gel formation investigated through seeded nucleation”. In: *Colloids and Surfaces A: Physicochemical and Engineering Aspects* 318.1-3 (2008), pp. 97–105. ISSN: 09277757. DOI: 10.1016/j.colsurfa.2007.12.019.

[94] Ricarda Tänzer, Yu Jin, and Dietmar Stephan. "Alkali activated slag binder: effect of cations from silicate activators". In: *Materials and Structures* 50.1 (2017). ISSN: 1359-5997. DOI: 10.1617/s11527-016-0961-y.

[95] Mohammad I. M. Alzeer et al. "Alkali-Activation of Synthetic Aluminosilicate Glass With Basaltic Composition". In: *Frontiers in chemistry* 9 (2021), p. 715052. ISSN: 2296-2646. DOI: 10.3389/fchem.2021.715052.

[96] A.R Brough and A. Atkinson. "Sodium silicate-based, alkali-activated slag mortars". In: *Cement and Concrete Research* 32.6 (2002), pp. 865–879. ISSN: 00088846. DOI: 10.1016/S0008-8846(02)00717-2.

[97] Pooria Ghadir et al. "Shear strength and life cycle assessment of volcanic ash-based geopolymer and cement stabilized soil: A comparative study". In: *Transportation Geotechnics* 31 (2021), p. 100639. ISSN: 22143912. DOI: 10.1016/j.trgeo.2021.100639.

[98] Rafael Andres Robayo-Salazar and Ruby Mejía de Gutiérrez. "Natural volcanic pozzolans as an available raw material for alkali-activated materials in the foreseeable future: A review". In: *Construction and Building Materials* 189 (2018), pp. 109–118. ISSN: 09500618. DOI: 10.1016/j.conbuildmat.2018.08.174.

[99] T. Dijkstra. "Experimental design of an alkali-activated slag concrete railway sleeper". MSc. Delft: TU Delft, 2021.

[100] Susan A. Bernal et al. "Evolution of binder structure in sodium silicate-activated slag-metakaolin blends". In: *Cement and Concrete Composites* 33.1 (2011), pp. 46–54. ISSN: 09589465. DOI: 10.1016/j.cemconcomp.2010.09.004.

[101] Gert Jan Weltje and Rik Tjallingii. "Calibration of XRF core scanners for quantitative geochemical logging of sediment cores: Theory and application". In: *Earth and Planetary Science Letters* 274.3-4 (2008), pp. 423–438. ISSN: 0012821X. DOI: 10.1016/j.epsl.2008.07.054.

[102] Temitope D. Timothy Oyedotun. "X-ray fluorescence (XRF) in the investigation of the composition of earth materials: a review and an overview". In: *Geology, Ecology, and Landscapes* 2.2 (2018), pp. 148–154. DOI: 10.1080/24749508.2018.1452459.

[103] Ron Jenkins. *X-Ray Fluorescence Spectrometry*. Newtown Square PA, 2001. DOI: 10.1002/9783527618323.ch23.

[104] Eva Marguí, Ignasi Queralt, and Rene van Grieken. "Sample Preparation for X-Ray Fluorescence Analysis". In: *Encyclopedia of Analytical Chemistry*. Ed. by Robert A. Meyers. Chichester, UK: John Wiley & Sons, Ltd, 2006, pp. 1–25. ISBN: 9780470027318. DOI: 10.1002/9780470027318.a6806m.pub3.

[105] Scott. A. Speakman. *Introduction to X-Ray Powder Diffraction Data Analysis*. 2018. URL: http://prism.mit.edu/xray/documents/1%20Basics%20of%20X-Ray%20Powder%20Diffraction.pdf.

[106] M. A. G. Aranda*, A. G. de La Torre, and L. Leon-Reina. "Rietveld Quantitative Phase Analysis of OPC Clinkers, Cements and Hydration Products". In: *Reviews in Mineralogy and Geochemistry* 74.1 (2012), pp. 169–209. ISSN: 1529-6466. DOI: 10.2138/rmg.2012.74.5.

[107] Simon J. Blott et al. "Particle size analysis by laser diffraction". In: *Geological Society, London, Special Publications* 232.1 (2004), pp. 63–73. ISSN: 0305-8719. DOI: 10.1144/GSL.SP.2004.232.01.08.

[108] G. Eshel et al. "Critical Evaluation of the Use of Laser Diffraction for Particle-Size Distribution Analysis". In: *Soil Science Society of America Journal* 68.3 (2004), pp. 736–743. ISSN: 03615995. DOI: 10.2136/sssaj2004.7360.

[109] Simon J. Blott and Kenneth Pye. "Particle size distribution analysis of sand-sized particles by laser diffraction: an experimental investigation of instrument sensitivity and the effects of particle shape". In: *Sedimentology* 53.3 (2006), pp. 671–685. ISSN: 00370746. DOI: 10.1111/j.1365-3091.2006.00786.x.

[110] ISO International Organization for Standardization. *Plastics-Thermogravimetri (TG) of Polymers: Part 1 - General Principles*. 2014.

[111] Sravanthi Loganathan et al. “Thermogravimetric Analysis for Characterization of Nanomaterials”. In: *Thermal and Rheological Measurement Techniques for Nanomaterials Characterization*. Elsevier, 2017, pp. 67–108. ISBN: 9780323461399. DOI: 10.1016/B978-0-323-46139-9.00004-9.